Petrographic analysis of eleven samples from the upper Tertiary-age Navarin basin, Nancy Well #1 (API: 55460000030000), 1986

Amoco Oil Co.

GMC DATA REPORT 450

This GMC data report from the Amoco Heritage collection has been made available through funding from the FY2018 USGS National Geological and Geophysical Data Preservation Program, Grant Number G18AP00054. This project report is presented in its original format and has not been reviewed for technical content or for conformity to the editorial standards of DGGS. It should not be used or cited as reviewed data.

2019
State of Alaska
Department of Natural Resources
Division of Geological & Geophysical Surveys
GEOLOGIC MATERIALS CENTER

PETROGRAPHIC ANALYSIS
OF ELEVEN SAMPLES FROM THE
UPPER TERTIARY-AGE NAVARIN BASIN
for
AMOCO PRODUCTION COMPANY
Denver, Colorado

55-460-00663-00

AMOCO PRODUCTION COMPANY
Nancy No. 1, OCS-Y-0719 Well
Navarin Basin Field
Offshore, Alaska

10703 East Bethany Drive, Aurora, Colorado 80014, 303/751-9334

February 13, 1986

CORE LABORATORIES, INC.

Amoco Production Company
1670 Broadway
Denver, CO. 80202

Petrographic Services

Attention: Mr. Randy Billingsley

Subject:
Petrographic Analysis of the Upper Tertiary-Age Navarin Basin samples from the Amoco Production Company Nancy No. 1 O.C.S. Y-0719 Well, Navarin Basin Field, Offshore, Alaska. File Numbers: PD-85066, PD-85074 and PD-85077

Gentlemen:

The complete petrographic analysis performed on the eleven sidewall core samples from the referenced well consists of three routines: 1) X-ray diffraction analysis of bulk mineralogy and detailed clay mineralogy; 2) examination by scanning electron microscopy; and 3) examination by thin section petrography. The results of this analysis, integrating data from these three routines, are presented in the accompanying report. Samples received for analysis will be stored by Core Laboratories for six months following completion of this report. After this time, the samples will be discarded if no instructions are received regarding their disposition.

A listing of the Cation Exchange Capacity (CEC) measurements for the eleven samples is included in Table IV of this report.

It has been a pleasure to perform this study for Amoco Production Company. If you have any questions about the data presented in the accompanying report or if we can be of any further service, please do not hesitate to contact us at (303)751-9334.

Very truly yours,

CORE LABORATORIES, Inc.

Robert C. Bond
Petrologist

Richard C. Heathcote
Supervisor of Reservoir Geology
and Petrographic Services

RCB:RCH:tb
Enclosure

TABLE OF CONTENTS

SCANNING ELECTRON MICROSCOPE PHOTOMICROGRAPHS

TABLE OF CONTENTS (Continued)

AMOCO PRODUCTION COMPANY
Nancy No. 1 O.C.S. Y-0719 Well

File Number: PD-85066
File Number: PD-85074
File Number: PD-85077

SUMMARY

Petrographic analyses were completed for eleven samples of the Upper Tertiary-Age Navarin Basin sediments. The samples were received from selected depths of the sidewall cores from the following well:

AMOCO PRODUCTION COMPANY
Nancy No. 1 O.C.S. Y-0719 Well
Navarin Basin Field
Offshore, Alaska

PD-85066: 2462, 2950, 3212, 3742, 4104 feet depth.
PD-85074: 4232, 5164, 6652 feet depth.
PD-85077: 7229, 7413, 8051 feet depth.

The samples are marine siltstone (2462, 2950, 3742, 4104 feet depth), sandy siltstone (3212, 6652, 7229 feet depth), silty sandstone (4232, 5164 feet depth), and sandstone (7413, 8051 feet depth).

The sand/silt-size fraction of these samples is composed of 3 normative percent to 41 normative percent quartz, 11 normative percent to 58 normative percent feldspars, and 16 normative percent to 84 normative percent rock fragments (combined volcanic, plutonic, metamorphic, and sedimentary rock fragments, chert, skeletal fossil fragments, and detrital accessory minerals). The samples are classified as litharenite (2950, 3212, 7413, 8051 feet depth), feldspathic litharenite (2462, 3742, 4104 feet depth), and lithic arkose (4232, 5164, 6652, 7229 feet depth) by the nomenclature system of Pettijohn, et al. (1972); refer to Figure I of this report.

Minor percentages of visible porosity are apparent in these samples. Trace occurrences of visible intergranular porosity are distributed randomly throughout the samples, and are associated frequently with the bioturbated regions of these samples. A large percentage of the visible intergranular porosity occurs as ineffective microporosity among aggregates of clay minerals. Visible intraskeletal porosity is common to rare with increasing depth of the diatomaceous samples (2462 through 4104 feet depth). Trace to minor intragranular porosity occurs due to dissolution of framework grain constituents (dominantly, feldspars and volcanic rock fragments). This secondary dissolution porosity and the visible intraskeletal porosity have not contributed significantly to the effective porosity due to restricted interconnection of pore pathways and partial occlusion of the pore areas by authigenic minerals. These samples are considered to have limited development of total effective porosity.

SUMMARY (Continued)

Minor to extensive occlusion of visible porosity is caused by authigenic clay minerals, pyrite, sodic plagioclase, potassium feldspar, zeolite, carbonate (calcite or aragonite), gypsum, and cristobalite. Microporous aggregates of intergrown smectite (Plate 22B) or mixed-layer illite-smectite (Plates 14A, 14B, 16B), crystal-coatings of illite (Plates 4B, 6B, 14A, 18A), vermiform aggregates of chlorite crystals (Plates 22A, 22B, 32A, 32B), euhedral pyrite crystals and crystal aggregates (Plates 6B, 14A, 23B, 25B, 26B), euhedral crystals of sodic plagioclase (Plates 12B, 20B), euhedral crystals of potassium feldspar (Plate 14A), pore-lining crystals of zeolite (Plates 17B, 18B, 28B), pore-bridging crystals of carbonate (Plate 10B), void- or fissure-filling gypsum (Plates 17B, 18A, 18B), and pore-lining cristobalite lepispheres (Plate 12B) reduce the intergranular, intragranular, and intraskeletal pore volumes, and cause geometric complexity and high tortuosity of pore pathways.

Partial dissolution or disaggregation of authigenic minerals may cause formation damage in these samples. Dissolution of ferroan chlorite (as inferred from EDS analysis) or pyrite could initiate precipitation of pore-occluding iron oxide or hydroxide. High or unsteady fluid flow rates and high or rapid transient fluid pressure changes could cause disaggregation and migration of pore-blocking, fine crystals and crystal fragments of smectite or mixed-layer illite-smectite, chlorite, and illite clay minerals.

Potassium chloride or oil-based drilling fluid systems should be used to inhibit swelling (volumetric expansion) of smectite or mixed-layer illite-smectite clay minerals. Iron chelating or oxygen scavenging agents should be introduced during acid treatment of chlorite- or pyrite-rich formations. Steady, low pressure fluid flow rates with low transient pressure changes, and use of a clay stabilizing agent in the downhole fluid should inhibit migration of fine clay constituents.

The authigenic clay minerals and pyrite constituents of these samples may cause minor variations of the responses from the wireline logging techniques. Smectite, mixed-layer illite-smectite, and illite will retard the spontaneous potential (SP) response and can yield anomalously high gamma-ray (GR) responses, which will cause sandstones to appear more shale-rich. These effective clay minerals can cause abnormally low apparent density calculations, which could be interpreted as high total porosity. Ferroan chlorite will not affect the SP technique; chlorite-rich formations could appear as "clean sandstones" on the SP log. Ferroan chlorite and pyrite can cause abnormally high apparent density calculations, which could

SUMMARY (Continued)

be interpreted as low total porosity from the density log. All clay minerals and pyrite can cause lower apparent resistivity (Ro) and erroneously high calculations of water saturation (Sw) from the resistivity log. In addition, the clay minerals and pyrite will cause anomalously high apparent porosity calculations from the neutron logging technique.

DISCUSSION

Introduction

Eleven samples of the Upper Tertiary-Age Navarin Basin sediments were received for petrographic analysis from selected depths of the sidewall cores from the following well:

AMOCO PRODUCTION COMPANY
Nancy No. 1 O.C.S. Y-0719 Well
Navarin Basin Field
Offshore, Alaska
PD-85066: 2462, 2950, 3212, 3742, 4104 feet depth.
PD-85074: 4232, 5164, 6652 feet depth.
PD-85077: 7229, 7413, 8051 feet depth.

The samples are marine siltstone (2462, 2950, 3742, 4104 feet depth), sandy siltstone (3212, 6652, 7229 feet depth), silty sandstone (4232, 5164 feet depth), and sandstone (7413, 8051 feet depth). The samples vary in texture and composition from massive, bioturbated and diatomaceous, to fine planar- or wavy-laminated and volcaniclastic with increasing depth. The sand-size framework grains have a random or chaotic distribution in the massive and bioturbated samples, and exhibit a poorly developed size grading in the planar- or wavy-laminated samples.

The client requested a study to delineate the compositional and textural character of the detrital and diagenetic mineral constituents, and to evaluate the reservoir fluid sensitivity and the potential for causing formation damage of the diagenetic minerals. In addition, the client requested a determination of the cation exchange capacity of these samples.

Complete petrographic analyses were performed on the samples. These analyses consist of: 1) determination of whole-rock mineralogy with detailed analysis of the clay mineralogy by X-ray diffraction (XRD); 2) examination of the rock texture and grain composition by scanning electron microscope with attached energy dispersive spectrometer (SEM/EDS); and 3) determination of the relative abundance, textural habit, and intergranular relationships of the various detrital and authigenic constituents by optical microscopy of thin sections.

Details of sample preparation and analytical techniques are presented in Appendix A of this report. A compilation of the X-ray diffraction analyses is given in Table I. A summary of the thin section petrographic analyses is

DISCUSSION (Continued)

presented in Table II. A compilation of the reservoir fluid sensitive, diagenetic minerals is given in Table III. A listing of the cation exchange capacity measurements is included in Table IV.

X-ray Diffractometry

Eleven sidewall core samples were analyzed by X-ray diffraction. These samples are composed dominantly of quartz, feldspars, accessory minerals, pyrite, and clay minerals. Erratic occurrences of zeolites, gypsum, barite, cristobalite, calcite, and opal A or opal CT were detected in some samples.

Quartz is the principal mineral component and forms 24 to 42 weight percent of the samples. Feldspars, as combined plagioclase and potassium feldspar, compose 22 to 51 weight percent of these samples. Plagioclase is approximately 6 to 51 times (average: 21 times) more abundant than potassium feldspar.

Micas, hornblende, and pyrite, which are the prominent accessory mineral constituents, range from nil to 7 weight percent, nil to 2 weight percent, and nil to 5 weight percent, respectively. Measurable quantities of zeolites (1 to 6 weight percent), barite (2 weight percent), and of calcite (1 weight percent) are present in these samples. Gypsum, cristobalite, opal A and opal CT occur in trace quantities, only.

Clay minerals form 17 to 44 weight percent of these samples. Analysis of the clay-size fraction indicates the presence of five clay minerals. Smectite and mixed-layer illite-smectite, which (combined) form 48 to 75 normative percent of the clay fraction, are approximately 1 to 3 times more abundant than the combined percentages of kaolinite, chlorite, and illite. Chlorite constitutes 15 to 42 normative percent of the clay minerals. Illite and kaolinite form nil to 32 normative percent and nil to 5 normative percent of the clay minerals, respectively. Smectite and mixed-layer illite-smectite do not occur in significant concentrations in the same sample. These two clays alternate as the principal mineral constituent of the clay fraction of these samples.

Scanning Electron Microscopy/Energy Dispersive Spectrometry

Examination of the eleven sidewall core samples with the scanning electron microscope indicates that the clay mineral constituents are detrital and authigenic in origin.

DISCUSSION (Continued)

Randomly oriented, plate-like crystals and stacked crystal aggregates of chlorite form a moderate (2462, 2950, 3212, 3742, 4104, 4232, 7229, 7413 feet depth) to large (5164, 6652, 8051 feet depth) percentage of the clay-size fraction in these samples. Chlorite is iron-rich (as inferred from EDS analysis; see: Spectra 1, 8) and exhibits abundant detrital (e.g. Plates 1B, 2B, 4B) and rare authigenic (e.g. Plates 20A, 22A, 22B) textural morphologies.

Irregular, matted to sponge-like intergrowths of iron-rich smectite crystals (Spectrum 10) are abundant in the samples from 2462, 2950, 3212, 3942, 4104, and 8051 feet depth. Smectite crystals form a massive, blanket-like coating over the framework grains (e.g. Plates 4A, 4B, 8B, 10B, 22B) and partially block intercrystalline spaces between chlorite crystal aggregates (Plate 6B). Smectite crystals and crystal aggregates are detrital in most locations of these samples. Partial replacement of inter-and intragranular pore areas by intergrowths of authigenic smectite crystals is evident in rare locations.

Flake-like crystals and sponge-like crystal intergrowths of authigenic mixed-layer illite-smectite (Spectrum 6) form mat-like coatings on framework grains, chlorite, framboidal pyrite, gypsum, and authigenic feldspars (Plates 14A, 14B, 16B, 17B, 18A, 18B, 20B). Illite-smectite bridges intergranular pore areas and partially occludes intragranular pore spaces. Illite-smectite crystals inhibit growth of authigenic feldspars (Plates 14A, 20B).

Fine, hair- or wire-like fibers of illite project into pore areas from the margins of framework grains, chlorite, smectite, mixed-layer illite-smectite, pyrite, and authigenic feldspars (Plates 2B, 4A, 4B, 6A, 6B, 8B, 10B, 12A, 14A, 14B, 16A, 16B, 18A, 20B, 22A). Illite occurs with greater frequency in regions of prominent, partially dissolved feldspar framework grains.

Pore-lining to pore-occluding, euhedral crystals and/or framboidal aggregates of pyrite (Spectrum 3) occur sporadically throughout these samples (Plates 6B, 10A, 14A, 14B). Pyrite framboids have formed over detrital framework grains and detrital chlorite and smectite clays. Euhedral pyrite crystals and crystal aggregates have nucleated over authigenic chlorite, smectite, mixed-layer illite-smectite, and occur in pore areas of partially dissolved feldspars, and in micropores of the diatom fragments. Pyrite framboids exhibit coatings of the authigenic clays. Pyrite crystals host coatings of illite, only (refer to Plate 6B).

DISCUSSION (Continued)

Euhedral crystals of sodic plagioclase (Spectrum 9) occur along pore walls adjacent to, or as overgrowths of, detrital feldspar grains (Plates 12B, 20B). Authigenic plagioclase crystallized as a result of minor to extensive dissolution of detrital calcic (Spectrum 4) or antiperthitic plagioclase (e.g. Plates 10B, 12A, 21B, 22B). Sodic plagioclase was formed after the crystallization of illite.

Euhedral crystals of potassium feldspar (Spectrum 2) occur along pore walls in rare locations (Plate 14A). Mixed-layer illite-smectite partially inhibited crystallization of authigenic potassium feldspar. Pyrite crystals have nucleated over the authigenic potassium feldspar in some locations.

Euhedral gypsum crystals and crystal aggregates are present in the sample from 7229 feet depth (identified by X-ray diffraction analysis; inferred composition from EDS analysis, see: Spectrum 7). Gypsum exhibits partial dissolution, and hosts crystal coatings of authigenic illite-smectite, illite, and zeolite (Plates 17B, 18A, 18B). Gypsum may have originated as a void- or fissure-occluding cement.

Pore-lining to pore-bridging cristobalite lepispheres occur in the sample from 4232 feet depth (Plate 12B). Authigenic cristobalite forms coatings on authigenic plagioclase and mixed-layer illite-smectite. Cristobalite lepispheres do not host other authigenic mineral constituents.

Pore-lining to pore-bridging, euhedral crystals of aragonite occur in or adjacent to partially dissolved feldspar grains (Plate 10B). Authigenic aragonite crystals do not host other authigenic mineral constituents. Aragonite growth may have occurred contemporaneously with authigenic plagioclase.

Pore-lining to pore-bridging authigenic zeolite crystals (var.: heulandite; Spectrum 5) occur in partially dissolved gypsum (Plates 17B, 18B) and in partially dissolved feldspar grains. Authigenic zeolite crystals do not host other authigenic mineral constituents.

Trace to minor occurrences of kaolinite and of barite were located in these samples by X-ray diffraction. The textural nature and occurrence of kaolinite or barite could not be documented by SEM/EDS analysis.

The apparent porosity of these samples has been reduced significantly by the authigenic mineral constituents. Intergranular pore regions average 10 to 20

DISCUSSION (Continued)

microns in diameter, and contain multiple pore throats that range up to 5 microns in diameter. Intragranular pore areas average approximately 6 microns in diameter. Inter- and intragranular pore regions exhibit complex geometry and have pore pathways with high tortuosity. Intraskeletal porosity of the diatom fragments could not be evaluated by scanning electron microscopy. The total visible porosity is considered low in these samples.

Thin Section Petrography

The eleven sidewall core samples from the Nancy No. 1 O.C.S. Y-0719 Well are classified by the following nomenclature systems:

1. Modal grain-size distribution and prominent detrital component as applicable (Picard, 1971). Diatomaceous siltstone (2462, 2950, 3742, 4104 feet depth), diatomaceous sandy siltstone (3212 feet depth), sandy siltstone (6652 feet depth), volcaniclastic sandy siltstone (7229 feet depth), silty sandstone (4232, 5164 feet depth), and volcaniclastic sandstone (7413, 8051 feet depth).

2. Normative composition of sand/silt-size fraction (Pettijohn, et al., 1972). Litharenite (2950, 3212, 7413, 8051 feet depth), feldspathic litharenite (2462, 3742, 4104 feet depth), and lithic arkose (4232, 5164, 6652, 7229 feet depth). The modal percentages of skeletal fragments are included in the plotted sample location points of this ternary classification system (refer to Figure I, this report).

The samples have random (un-sorted) to poorly sorted textures, and are composed of angular to rounded, medium silt-size to granule-size (average: subangular and coarse silt-size or very fine sand-size) framework grains. The framework grains exhibit trace to minor crystal straining (undulose extinction), and have point (common to abundant) to concavo-convex (trace to rare) intergranular contacts. The samples are poorly to moderately compacted and indurated. Clay-size matrix constituents range from common to rare with increasing depth of these samples.

The eleven samples may be divided into three groups based on textural and compositional similarities (Figure I, and Table II). The samples from 2462, 2950, 3212, 3742, and 4104 feet depth have progressively decreasing percentages of skeletal diatom fragments, and exhibit decreasing apparent disruption of the rock matrix due to bioturbation. The sample from 4232 feet depth contains rare skeletal diatom fragments; the inversion/recrystalliza-

AMOCO PRODUCTION COMPANY
Nancy No. 1 O.C.S. Y-0719

File Number: PD-85066
File Number: PD-85074
File Number: PD-85077

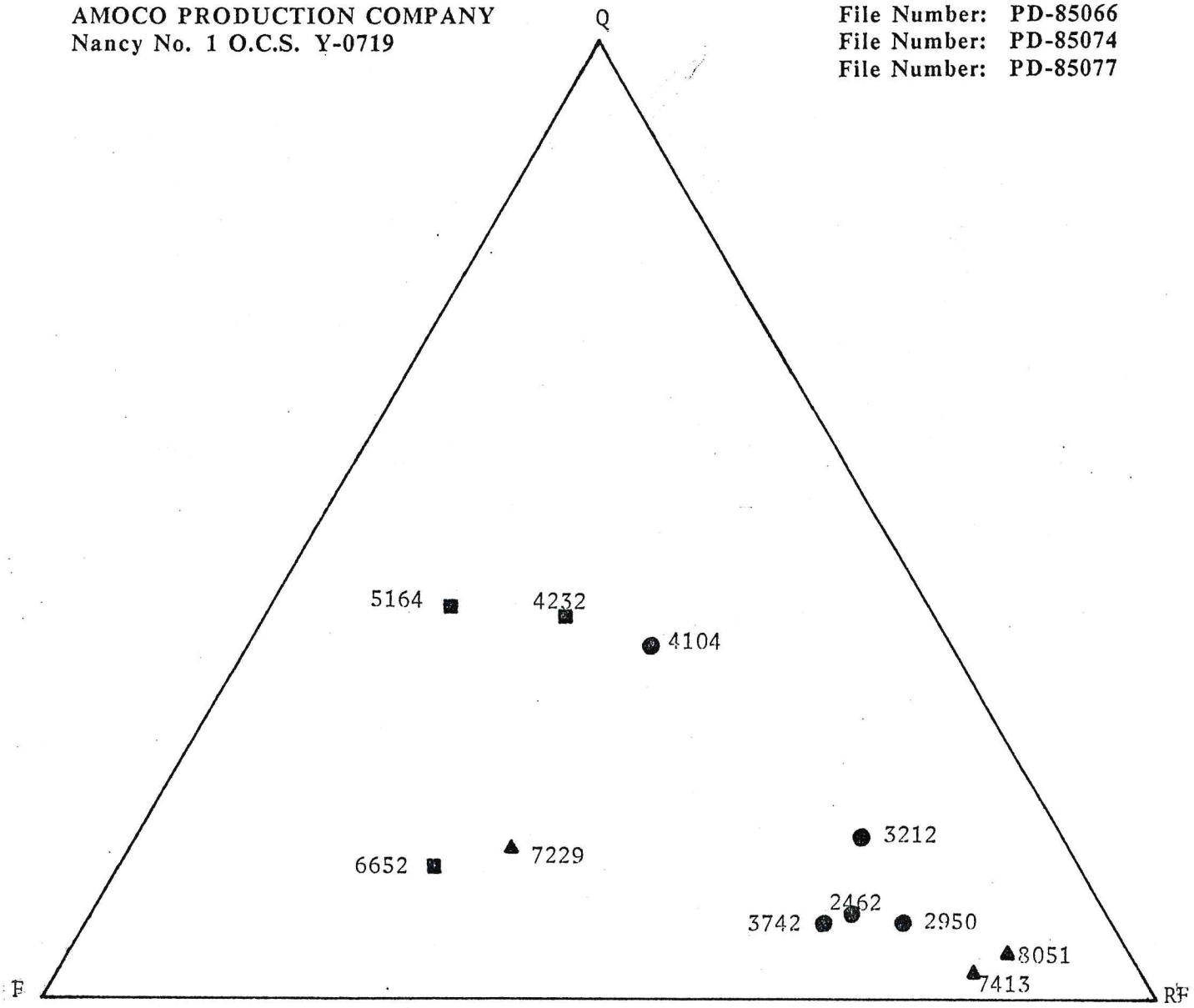

FIGURE 1

Ternary Diagram of Sandstone Compositions
(modified from: Pettijohn, et al., 1972)

Q = Quartz F = Feldspars RF = Rock Fragments (including chert and mica)

● PD-85066; 2462, 2950, 3212, 3742, 4104 feet

■ PD-85074; 4232, 5164, 6652 feet

▲ PD-85077; 7229, 7413, 8051 feet

DISCUSSION (Continued)

tion of the opaline skeletal tests to cristobalite or other silica minerals is near completion at this depth (Isaacs, 1981).

The samples from 4232, 5164, 6652, and 7229 feet depth have minor localized occurrences of bioturbation, and have rare to prominent development of wavy or planar laminations of the rock fabric. The samples from 7229, 7413, and 8051 feet depth contain moderate to abundant percentages of volcanic rock fragments, and trace to extensive development of pseudomatrix due to compaction and deformation of these lithic constituents.

Detrital Components

Quartz: Angular to subangular, equant to elongate grains. Some of the detrital quartz grains exhibit strain (as undulose extinction) that ranges from nil to 15° of extinction sweep, and averages 5° to 7° of extinction sweep. Inclusions are rare to common; fluid-filled vacuole trails, tourmaline, apatite, muscovite, and rutile have been noted.

Feldspars: Angular to subangular, elongate to equant grains of plagioclase (approximate composition: andesine to labradorite), potassium feldspar (microcline), and antiperthitic plagioclase (approximate composition: oligoclase to andesine with exsolution intergrowths of microcline or orthoclase). Frequently, plagioclase grains exhibit normal zonation, and contain inclusions of apatite. Myrmekitic intergrowths of quartz in plagioclase occur in rare locations. Feldspar have traces of clay, zeolite, or calcite replacement (Plates 28B, 30B, 31A). Myrmekitic and antiperthitic feldspars do not exhibit visible alteration. Partial dissolution of plagioclase (rare to common) and of antiperthitic plagioclase (trace) has contributed to total visible porosity in some locations (Plates 26A, 26B, 27B, 28B, 30B, 32A, 33A, 33B).

Rock Fragments: Angular to rounded, equant to ellipsoidal grains that have trace to abundant plastic grain deformation due to compaction (frequency of grain deformation increases with depth). Five types of rock fragments occur in these samples: 1) volcanic rock fragments; 2) plutonic rock fragments; 3) metamorphic rock fragments; 4) sedimentary rock fragments; and 5) chert.

The volcanic rock fragments are composed of (in order of decreasing abundance):

DISCUSSION (Continued)

a. Porphyritic dacite/rhyodacite: Prominent phenocrysts of plagioclase, and traces of microlitic potassium feldspar and iron oxides. Brown to green clay-replaced groundmass.

b. Porphyritic andesite: Prominent to abundant phenocrysts of plagioclase in a dark brown clay- and iron oxide-replaced groundmass. Trace to abundant pyrite.

c. Microlitic quartz latite: Prominent to abundant microlites of quartz and potassium feldspar, and traces of plagioclase and iron oxide microlites in a green clay- and chert-replaced groundmass.

d. Rhyolitic crystal tuff: Siliceous (devitrified) crystal tuff. Microlites of potassium feldspar and/or quartz in chert-replaced groundmass. Traces of green clay(s) in the groundmass.

e. Andesitic lithic tuff: Compaction-deformed and devitrified volcanic fragments of probably andesite to dacite composition. Traces of plagioclase microlites are planar-aligned due to compaction. Rock fragments exhibit quenched and healed margins. Groundmass of the lithic fragments is replaced by dark brown clay and traces of iron oxides.

f. Amygdular andesite: Trace occurrences of microlitic plagioclase in a dark brown clay- and iron oxide-replaced groundmass. Amygdules are composed of concentrically ringed chert or quartz. Possible occurrences of light brown clay and zeolite.

g. Devitrified glass: Trace occurrences of light brown clay- and/or silica-replaced, concentrically ringed glass fragments. Probably are eroded fragments of amygdules.

The volcanic rock fragments increase in abundance with increasing depth of these samples. The volcanic rock fragments range from trace or minor (2462, 2950, 3212, 3742, 4104, 4232, 5164 feet depth) to moderate (6652 feet depth), common (7229 feet depth), and abundant (7413, 8051 feet depth) percentages of the detrital constituents (refer to Table II of this report).

Minor to abundant intragranular porosity is developed locally in the volcanic rock fragments due to partial or complete dissolution of the devitrified groundmass (Plate 31A). Trace to minor dissolution of feldspar phenocrysts occurs in some locations. Authigenic clays and pyrite have partially occluded intragranular porosity of the volcanic rock fragments.

DISCUSSION (Continued)

The plutonic rock fragments are dominantly porphyritic granodiorite or quartz monzonite. Subhedral phenocrysts of calcic plagioclase (approximate composition: labradorite) and potassium feldspar (microcline) are surrounded by interstice-fillings of quartz, chlorite-replaced biotite or (rarely) hornblende, and trace quantities of antiperthitic plagioclase or myrmekitic plagioclase. Calcic plagioclase phenocrysts are frequently zoned and contain euhedral crystals of apatite.

The plutonic rock fragments have irregular to poorly developed mosaic textures which may reflect partial recrystallization. Minor to moderate clay replacement of the calcic plagioclase and potassium feldspar components is visible in some locations. Generally, the plutonic rock fragments have tight intercrystalline contacts and no visible porosity.

The metamorphic rock fragments are composed exclusively of quartzite that has a well developed mosaic and/or strain-lineated texture. Trace occurrences of muscovite are parallel to foliation of some rock fragments. The highly schistose fragments may have been sheared. The metamorphic rock fragments have tight intercrystalline contacts and no apparent intragranular porosity.

Trace to rare occurrences of arkosic sandstone, lithic sandstone, and sandy siltstone or mudstone are present in these samples. Arkosic sandstone has a poorly developed mosaic texture, and exhibits partial dissolution and authigenic clay and pyrite replacement of the plagioclase framework grains (Plate 31B). The lithic sandstone contains trace to minor percentages of volcanic and sedimentary rock fragments. The lithic sandstone and sandy siltstone or mudstone fragments exhibit trace to moderate, compaction-related grain deformation. Traces of visible intragranular porosity are present in some arkosic sandstone fragments.

Trace occurrences of chert are present in this sample. Most chert grains have an even, microcrystalline texture. Some chert grains exhibit an irregular crystal size distribution and have a prominent, strain-related crystal lineation. Traces of intercrystalline porosity in the chert fragments were visible in rare locations.

Skeletal Constituents: Trace to abundant percentages of skeletal diatom fragments are present in the samples from 2462 through 4232 feet depth. Pennate and centric varieties of skeletal diatoms are visible in Plates 23B, 24A, 24B, 25A, 25B, 26A, 26B, 27A, and 27B. The taxonomic identification was not attempted for these skeletal fragments.

DISCUSSION (Continued)

Other Detrital Constituents: Trace to minor occurrences of micas (principally biotite; lesser muscovite) and hornblende are present in all eleven samples. Trace to minor percentages of glauconite are present in the samples from 2462 feet through 7229 feet depth. Trace occurrences of zircon, tourmaline, apatite, anatase, and magnetite or ilmenite are present in random locations.

Authigenic Components

The principal authigenic constituents of these samples are pyrite, calcite, clay minerals, and zeolite. Traces of sericite and chert occur as a replacement of the detrital rock fragments.

Euhedral crystals and irregular crystal aggregates of pyrite partially occlude intergranular, intragranular, and intraskeletal pore areas in these samples. Frequently, pyrite forms void- or fissure-fillings along the margins of the bioturbated regions of the diatomaceous samples (Plates 23A, 24A, 25A, 26A, 27A). The apparent intergranular porosity of the bioturbated regions has been reduced by authigenic pyrite. Intraskeletal pore-fillings of pyrite are common (Plates 23B, 24B, 25B, 26B). Intragranular (dissolution) pore areas exhibit minor (Plates 26A, 27B, 28B, 31B) to abundant (Plate 31B) occlusion by authigenic pyrite.

Rare, anhedral to euhedral crystals of calcite partially occlude intragranular pore areas. Calcite forms in or adjacent to partially dissolved framework grains of feldspar and rock fragments (particularly, volcanic and plutonic rock fragments). Frequently, calcite is associated with authigenic clay minerals in the dissolution pore regions.

Framework grain- and detrital clay-coating, and pore-lining to pore-filling authigenic clay minerals occur in trace to minor percentages of these samples. Irregular-shaped aggregates of smectite or mixed-layer illite-smectite crystals form coatings on detrital chlorite, and partially to totally fill intergranular (Plates 31A, 31B, 33B) and intragranular (Plates 28B, 30B, 31A, 31B, 32B) pore areas. Vermiform aggregates of chlorite crystals project into pore areas from the margins of framework grains (Plates 32A, 32B). The clay minerals partially replace unstable framework grains (dominantly biotite, feldspars, and volcanic rock fragments). Authigenic clays form delicate pore bridges and constricted, highly irregular pore throats and pore channels in the open pore regions.

DISCUSSION (Continued)

Trace occurrences of subhedral to euhedral zeolite (heulandite and/or analcite) partially occlude intragranular pore regions (e.g. Plate 28B). Generally, zeolite is associated with authigenic clay minerals in dissolution cavities of detrital feldspars and volcanic rock fragments.

Comparison of X-Ray Diffraction and Point Count Modal Analyses

Compositional variances occur between the point count modal analyses and the bulk mineralogy analyses (from X-ray diffraction) for these samples (Tables II and I, respectively). These compositional variances result from mineral partitioning of quartz and feldspars into detrital rock fragments. Minor to moderate compositional variance of the clay-size fraction analyses may be attributed to the presence of skeletal diatom fragments as a matrix constituent of some samples, and to partial replacement of feldspars and rock fragments by authigenic clay minerals.

The relative abundances of both volcanic and plutonic rock fragments increase with depth in these samples. Approximately nil to 80 modal percent of the plagioclase and of the potassium feldspar occur in volcanic rock fragments (as discrete crystals and normative feldspar components of the devitrified groundmass). The volcanic rock fragments exhibit an indistinct composition trend that becomes more mafic and, therefore, plagioclase component-enriched with increasing depth. Approximately 10 to 20 modal percent of the plagioclase and of the potassium feldspar, and all (100 modal percent) of the antiperthitic plagioclase occur in plutonic rock fragments. Trace quantities of plagioclase or potassium feldspar are present in some sedimentary (arkosic sandstone) and, possibly, metamorphic rock fragments. The combined modal percentages of discrete feldspar grains and rock fragment feldspar constituents is comparable to the bulk weight percentages and relative abundance trends of the feldspars from X-ray diffraction analysis.

Quartz is partitioned into volcanic, sedimentary, and metamorphic rock fragments, and chert as well as discrete quartz framework grains. Frequently, the felsic to intermediate composition volcanic rock fragments are silicified (chert-replaced) and contain approximately 70 to 80 normative percent quartz. Traces of sandstone fragments (sedimentary rock fragments), strain-lineated quartzite (metamorphic rock fragments), and of chert grains are present in these samples. The combined modal percentages of discrete quartz grains and of quartz constituents in rock fragments is comparable to the total weight percent quartz from X-ray diffraction analysis.

DISCUSSION (continued)

Skeletal diatom fragments occur in the matrix of the samples from 2462, 2950, 3212, 3742, and 4104 feet depth. Although the total weight percentage of opaline minerals (as combined opal A and opal CT) in these skeletal fragments is low to unmeasurable, the large spatial distribution of these fragments in the matrix causes a moderate to large reduction of the modal percentages of clay minerals of the point count analyses. Many detrital feldspar grains and rock fragments (especially, volcanic rock fragments) exhibited trace to extensive (average: minor to moderate) replacement by authigenic clay minerals. The point count analyses reflect the host framework grains, which causes a decrease of the modal abundances of clay minerals in the sample.

Diagenetic History

Petrographic and SEM/EDS analyses of the authigenic constituents indicate that diagenesis occurred in stages of single mineral and, possibly, of multiple mineral species due to local fluctuations of pore fluid composition and intergranular physical and chemical conditions. Textural relationships of the authigenic constituents indicate that crystallization of some mineral species occurred in localized areas and, consequently, may not be characteristic of the regional diagenetic sequence.

A representative sequence of authigenic mineral crystallization and associated diagenetic events for these samples follows (from oldest to youngest):

1. Precipitation of framboidal aggregates of pyrite. Growth of pyrite framboids resulted from bio-degradation of trapped organic material during sediment lithification.

2. Crystallization of void- or fissure-filling gypsum cement. Gypsum precipitation occurred in rare locations of the sample from 7229 feet depth.

3. Framework grain-coating, and pore-lining to pore-filling intergrowths of smectite crystals. Smectite forms an irregular blanket-like coating on detrital clays, framboidal pyrite, and detrital mineral constituents. Smectite growth partially occluded intercrystalline pore spaces among deposits of detrital clays.

DISCUSSION (Continued)

4. Crystallization of euhedral potassium feldspar crystals. Growth of authigenic potassium feldspar may have resulted from partial dissolution of detrital feldspars and/or unstable lithic fragments. Illite-smectite formed interpenetrative embayments in the potassium feldspar crystals prior to completion of crystallization.

5. Detrital grain- and clay-coating, and pore-lining to pore-filling intergrowths of mixed-layer illite-smectite crystals. Illite-smectite coats detrital smectite and chlorite clays, and framework grain constituents. Illite-smectite inhibited crystallization of authigenic potassium feldspar crystals.

6. Crystallization of euhedral pyrite crystals and crystal aggregates. Pyrite crystals nucleated over authigenic smectite and illite-smectite clays, and authigenic potassium feldspar. Pyrite crystals exhibit coatings of illite in some locations. Pyrite crystals partially occlude intraskeletal pore areas.

7. Pore-lining and crystal-coating illite clay. Hair- or wire-like fibers and matted crystal aggregates of illite protrude into pore areas from the margins of the authigenic constituents of stages 1 through 6.

8. Dissolution of detrital feldspars (in particular, calcic plagioclase), and of unstable lithic fragments (principally, volcanic rock fragments). Dissolution of gypsum may have occurred during this stage of diagenesis.

9. Intragranular pore-lining, euhedral sodic plagioclase crystal overgrowths of partially dissolved detrital feldspars, and of partially dissolved feldspar constituents in lithic fragments. Authigenic plagioclase crystals host crystals of authigenic chlorite in rare locations.

10. Crystallization of euhedral chlorite crystals and vermicular crystal intergrowths. Pore-lining and grain-coating aggregates of authigenic chlorite partially occlude dissolution pore areas in feldspars and rock fragments. Authigenic chlorite crystals do not host other authigenic constituents.

11. Pore-lining to pore-bridging euhedral crystals of zeolite and aragonite. The two minerals were not viewed in textural association. These authigenic constituents may have crystallized as a result

DISCUSSION (Continued)

of calcic feldspar dissolution. The two minerals may be considered time contemporaneous in these samples.

12. Crystallization of intragranular pore-lining, cristobalite lepispheres. Authigenic cristobalite formed as a result of recrystallization/inversion of opal CT from the skeletal diatom fragments (Isaacs, 1981). Cristobalite does not host other authigenic mineral constituents. Cristobalite lepispheres nucleated over authigenic sodic plagioclase. Cristobalite was not viewed in association with authigenic zeolites or aragonite.

This generalized diagenetic sequence is representative of the eleven samples of this study. Local variations of this sequence may occur.

Apparent Porosity and Reservoir Potential

The reservoir potential of the Upper Tertiary samples from the Nancy No. 1 O.C.S. Y-0719 Well was investigated through scanning electron microscopy and thin section petrography.

The major percentage of the visible porosity occurs in the samples from 2462 feet to 4104 feet depth. Intraskeletal porosity is common to rare with increasing depth of these diatomaceous samples (e.g. Plates 23B, 24B, 25B, 26B). The visible intraskeletal pore areas exhibit complex internal geometries and have poor interconnection of pore pathways.

Trace to minor percentages of visible intergranular porosity are developed in the bioturbated regions of these samples (e.g. Plates 23A, 25A, 27A, 28A). Intergranular pores are small, sporadic in occurrence, and have highly tortuous pathways with complex internal geometries.

Trace to minor intragranular porosity occurs due to dissolution of framework grains. Relict detrital feldspars and rock fragments, which exhibit minor (plagioclase grain at B-C5.5, Plate 32A) to extensive (volcanic rock fragment at C6, Plate 31A) dissolution, are rare to common in the samples from 2462 feet to 6652 feet depth and are common to abundant in the samples from 7229 feet to 8051 feet depth.

The visible intergranular porosity is limited to ineffective microporosity among deposits of authigenic and, possibly, detrital clay mineral constituents. The secondary dissolution porosity of the framework grain constituents and the visible intraskeletal porosity have not contributed

DISCUSSION (continued)

significantly to total effective porosity due to restricted interconnection of pore pathways and partial occlusion of the pore areas by authigenic minerals. These samples are considered to have minor development of total visible porosity.

The reservoir potential of the Upper Tertiary Navarin Basin sediments from the Nancy No. 1 O.C.S. Y-0719 Well is inferred from analysis of the apparent porosity of the petrographic sections. The reservoir potential is considered to be limited by the poorly developed intergranular porosity, the minor development of microporous, secondary dissolution porosity, and the prominent pore-occluding, authigenic mineral constituents. Detailed analysis of the reservoir potential of these sediments should include the measured physical parameters of conventional core analysis and other techniques. That data was not available for this petrographic compilation and discussion.

Potential Formation Damage from Authigenic Minerals

Several authigenic minerals that occur in the Upper Tertiary samples of the Navarin Basin could cause problems with the use of downhole fluids and in reservoir development programs. These problems are summarized for each mineral in the following paragraphs. Table III indicates the relative potential for causing formation damage by the authigenic minerals in these samples, and lists general procedures to avoid or correct formation damage.

Chlorite

Chlorite is a clay mineral that contains variable amounts of magnesium, iron, and aluminum in a hydrated silicate framework. Chlorite is sensitive to acidic and oxygen-rich water. Acid treatment of chlorite-bearing formations can release iron from chlorite, and can cause precipitation of insoluble ferric oxide or hydroxide in pore areas. An iron-chelating agent and an oxygen scavenger should be introduced with acid treatments of chlorite bearing zones to inhibit this problem.

Chlorite exhibits a vermicular morphology of stacked, plate-like crystals. These vermiform crystal aggregates project into pore areas, and may be loosely attached to the substrate. Fluctuating fluid flow pressures and flow rates can cause mechanical breakage of these clay aggregates. Clay to silt-size particles can migrate along pore pathways and form pore-bridging clogs at pore throats. Low fluid flow pressures and flow rates should be maintained during formation treatment and production to avoid this situation.

DISCUSSION (continued)

Smectitic Clay Minerals

Under equilibrium conditions in a reservoir (i.e. prior to penetration by drilling), smectitic clay minerals occur as irregular, matted or boxwork-shaped intergrowths of fibrous and sheet-like crystals. If the clay/pore fluid stability system in a formation is disturbed by introduction of water that is less saline than the ambient pore fluid, smectitic clays will adsorb water into the crystal lattice which will cause swelling and a corresponding increase in clay volume. Clay swelling will reduce porosity and permeability of the rock.

Pure smectite exhibits the greatest expandability; the expandability decreases in mixed-layer clay structures due to the presence of non-expandable illite or chlorite. The expandability of mixed-layer clay minerals is proportional to the percentages of expandable and non-expandable components in the clay structure. Mixed-layer clays, that contain low percentages of non-expandable clays, will have properties similar to a pure smectite (high expandability). Mixed-layer clays, that contain high percentages of non-expandable clays, will have properties similar to the interlayered clay species.

The mixed-layer illite-smectite of these samples contains 80 percent expandable interlayers in the clay structure. This mixed-layer clay contains a low percentage of non-expandable illite, which will increase the volumetric change of the clay structure during expansion (water adsorption).

Illite-smectite of this sample is considered to have high expandability, and a corresponding high potential for reduction of porosity and permeability.

Smectite clays will disaggregate in the presence of alkaline fluids. Migration of fine particulate, smectitic clay crystals could cause clogging of pore throats. Clays are dissolved and flushed from the formation during acid treatments. Low fluid flow pressures and flow rates are less likely to cause clogging of pore throats by migrating fine particles during the acidizing operations. Formation damage from smectitic clays can be prevented by potassium chloride or oil-based drilling fluid systems which inhibit swelling of these minerals. Clay stabilizing agents (e.g. polymers) will inhibit migration of fine clay particles.

DISCUSSION (Continued)

Illite

Illite is a clay mineral that occurs as hair- or wire-shaped fibers and acicular lath-shaped crystals or aggregates of crystals. Commonly, illite forms bundles of randomly oriented crystals that project from pore walls into pore spaces. Alkaline fluids cause physical and chemical changes on the surface of illite crystals which disperse the crystal aggregates. These clay particles can migrate through pore areas and clog pore throats. Clay stabilizing agents can cause in-situ collapse of clay bundles into a microporous network or matte of crystals. These pore wall-coating, matted clay crystals are ineffective for the transmission of liquids. Illite is removed by weak hydrochloric acid treatment of the formation.

Pyrite

Iron released from pyrite during reaction with acidic or oxygenated fluid can cause insoluble iron oxide or hydroxide to precipitate in pores. An iron-chelating agent and an oxygen-scavenging agent should be used during acid stimulations to avoid this problem.

Mineralogical Influence of Wireline Log Response

The authigenic minerals that occur in these siltstone and sandstone samples can interact with induced physical and chemical effects, which can change the responses of wireline logs. It may be impossible to quantify a log response as the sum of component mineral properties. However, the presence of certain minerals in significant concentrations (5 weight percent or greater) can alter a logging tool response from the reference standards of an ideal sandstone lithology. These effects are outlined in the following paragraphs. Additional discussions of this topic may be found in Hilchie (1982a, b), SPWLA (1982), and Helander (1983).

Resistivity

The presence of the effective clay minerals, smectite, illite, and mixed-layer species (those with high cation exchange capacity; Johnson and Linke, 1977), will cause a lower apparent total resistivity (Rt) in oil-bearing zones. This effect will result in erroneously high calculations of water saturation (Sw). In water-bearing zones, effective clays will cause variable calculations of apparent resistivity. These calculations are dependent on the measured value of water resistivity (Rw).

DISCUSSION (Continued)

The non-effective clay minerals, chlorite and kaolinite (op.cit.), have minor effects on apparent resistivity of sandstones or siltstones. These minerals can cause erroneously high calculations of Sw due to their microporous morphology in aggregate forms. Ferroan chlorite has a lower resistivity than the magnesian chlorite, which can reduce Rt if this mineral occurs in high concentrations.

Pyrite has an effect on the resistivity log that varies with the frequency of the electric field as well as with the amount and distribution of pyrite in the stratum. Higher frequency techniques (modern induction logs and shallow-sensing tools) are much more sensitive than the lower frequency techniques (deep-sensing tools) to the affects caused by pyrite that occurs disseminated uniformly throughout a stratum. If a layer of pyrite exists along a stylolite, fracture, burrowed region, or other such textural feature, all resistivity tools will detect extremely high conductance of the layer. The presence of pyrite in a formation will cause a lower apparent resistivity of the log responses.

Spontaneous Potential

The effective clay minerals will reduce the amplitude of the SP response, which will cause a pure sandstone to appear more shaly. The non-effective clay minerals have no affect on the SP technique. Consequently, a chlorite-rich sandstone may appear as a "clean sandstone" on this log.

Disseminated pyrite has no effect on the SP technique. Concentrations of pyrite (as in layers, fracture fillings, stylolites, etc.) will cause a positive shift of the SP response.

Gamma-Ray

Effective clay minerals yield high gamma-ray readings that are similar to the responses from a "shaly" zone. Non-effective clay minerals have no detectable effect on the gamma-ray log.

Density

Hydrated smectitic clay minerals have densities that are much lower than the framework grain constituents of common sandstones. Consequently, an erroneously high porosity may be calculated for a sandstone that contains a high percentage of these clay minerals.

DISCUSSION (Continued)

Illite has a variable density that may be higher or lower than the framework grain constituents of common sandstones. The net effect of illite on calculations of porosity is not consistent.

Chlorite has an average density of 2.74 g/cc, which is higher than the average density of common sandstone framework minerals. Varieties of chlorite, that have high iron and silicon contents, can have densities approaching 3.3 g/cc. Chlorites, that have high magnesium and aluminum contents, can have densities as low as 2.6 g/cc. The ferroan chlorite of these samples may cause erroneously high apparent density calculations, which can be interpreted as low total porosity.

Kaolinite has approximately the same density as the quartz and feldspar framework grains of the sandstone, and is not detectable on density logs.

The density of pyrite (5.0 g/cc) is nearly twice the density of an ideal sandstone. Significant errors could be made during calculations of total porosity of low porosity formations if the apparent formation density is not corrected for the high density effect of pyrite.

Neutron

All clays cause erroneously high apparent porosity calculations from the neutron log. Kaolinite, which is invisible on all other logs, may be detected by the neutron technique. Modern logging techniques will record an erroneously high apparent porosity in the presence of pyrite.

Acoustic

All clay minerals are detected in a similar manner by the acoustic logging technique. Clays, that occur in discrete layers or as clasts in the sandstone framework grain fraction, will be recorded as a lower velocity material. Clays of this textural occurrence cause erroneously high calculations of porosity. Clay minerals, that are dispersed throughout a sandstone stratum as coatings on framework grains and as linings in pore regions, will not be detected by acoustic logging techniques.

TABLE I
X-RAY DIFFRACTION ANALYSES
Whole-rock Composition (weight percent)

Sample Depth (feet)	2462	2950	3212	3742	4104
Quartz	29	32	27	28	24
Plagioclase	25	21	25	34	24
Potassium Feldspar	03	01	02	03	01
Mica	04	06	07	05	02
Hornblende	02	01	01	01	01
Pyrite	03	04	03	04	tr
Heulandite	-	-	-	-	04
Zeolite (undifferentiated)	01	-	-	-	-
Gypsum	-	-	-	-	-
Barite	-	tr	02	tr	tr
Calcite	-	-	-	-	-
Opal A	tr	tr	tr	-	-
Opal CT	-	-	-	tr	tr
Cristobalite	-	-	-	-	-
Clay Minerals	33	35	33	25	44
TOTAL	100	100	100	100	100

Clay Fraction Composition (normalized to 100 percent)

Kaolinite	04	05	01	03	01
Chlorite	19	15	20	22	21
Illite	21	32	19	10	08
Smectite	56	45	59	65	70
Mixed-layer Illite-smectite*	tr	03	01	-	-
TOTAL	100	100	100	100	100

* Mixed-layer illite-smectite contains approximately 80 percent expandable interlayers.

TABLE I (Continued)
X-RAY DIFFRACTION ANALYSES
Whole-rock Composition (weight percent)

Sample Depth (feet)	4232	5164	6652	7229	7413	8051
Quartz	33	42	35	37	29	25
Plagioclase	31	32	31	26	51	49
Potassium Feldspar	03	01	05	03	-	-
Mica	01	03	01	01	-	tr
Hornblende	-	-	-	01	02	01
Pyrite	03	02	03	05	-	-
Heulandite	06	tr	-	-	-	-
Zeolite (undifferentiated)	-	-	-	-	-	03
Gypsum	-	-	-	tr	-	-
Barite	-	-	-	-	-	-
Calcite	-	-	-	-	01	-
Opal A	-	-	-	-	-	-
Opal CT	-	-	-	-	-	-
Cristobalite	tr	-	-	-	-	-
Clay Minerals	23	20	25	27	17	22
TOTAL	100	100	100	100	100	100

Clay Fraction Composition (normalized to 100 percent)

Kaolinite	01	03	01	tr	-	-
Chlorite	19	37	35	25	25	42
Illite	11	07	04	06	-	-
Smectite	tr	tr	tr	-	-	58
Mixed-layer Illite-smectite*	69	53	60	69	75	tr
TOTAL	100	100	100	100	100	100

* Mixed-layer illite-smectite contains approximately 80 percent expandable interlayers.

TABLE II
THIN SECTION ANALYSIS DATA

Sample Depth (feet)	2462	2950	3212	3742
Classification*	Diatomaceous Siltstone (Feldspathic litharenite)	Diatomaceous Siltstone (Litharenite)	Sandy diatomaceous siltstone (Litharenite)	Diatomaceous Siltstone (Feldspathic litharenite)
Sorting	Moderate to poor	Moderate to poor	Moderate to poor	Moderate
Induration	Moderate to poor	Moderate to poor	Moderate to poor	Moderate to poor
Texture	Indistinct wavy lamination; healed fractures; moderate bioturbation	Massive to disrupted texture; healed fractures; moderate to heavy bioturbation	Massive to disrupted texture; healed fractures; moderate to heavy bioturbation	Disrupted texture; healed fractures; moderate bioturbation
Grain Size				
min.	0.01 mm (medium silt)	0.01 mm (medium silt)	0.01 mm (medium silt)	0.01 mm (medium silt)
max.	0.28 mm (medium sand)	0.21 mm (fine sand)	0.32 mm (medium sand)	0.45 mm (medium sand)
avg.	0.05 mm (coarse silt)	0.04 mm (coarse silt)	0.06 mm (coarse silt)	0.04 mm (coarse silt)
Angularity and Grain Shape	Angular-rounded average:subangular elongate>equant	Angular-rounded average:subangular elongate>equant	Angular-rounded average:subangular elongate>equant	Angular-rounded average:subangular elongate>equant
Grain Contacts	Floating>point	Floating>point	Floating>point	Floating>point
Porosity Types	Traces of intergranular, traces of intragranular due to dissolution of feldspars and rock fragments, and prominent to abundant intraskeletal porosity	Traces of intergranular, traces of intragranular due to dissolution of feldspars and rock fragments, and minor to prominent intra-skeletal porosity	Traces of intergranular, trace to minor intra-granular due to dis-solution of feldspars and rock fragments, and minor to prominent intraskeletal porosity	Trace to minor intergranular, traces of intragranular due to dissolution of feldspars and rock fragments, and minor to prominent intra-skeletal porosity

* Classification of rock nomenclature of the sand-size fraction (in parentheses) from Pettijohn, et al., 1972.

POINT COUNT ANALYSIS
(in modal percent)

Sample Depth (feet)	2462	2950	3212	3742
Detrital Constituents	95	93	94	96
Quartz	07	06	13	07
Plagioclase	20	14	15	21
Antiperthitic Plagioclase	tr	tr	tr	tr
Potassium Feldspar	tr	tr	tr	01
Volcanic Rock Fragments	tr	tr	tr	02
Plutonic Rock Fragments	tr	tr	tr	01
Metamorphic Rock Fragments	-	-	-	tr
Sedimentary Rock Fragments	-	-	-	tr
Chert	tr	tr	tr	tr
Mica	04	02	03	03
Hornblende	03	02	01	tr
Glauconite	tr	02	tr	04
Accessory Minerals	tr	tr	tr	tr
Fossil Fragments	50	48	44	42
Clay Minerals	11	19	18	15
Authigenic Constituents	05	07	06	04
Pyrite	04	06	05	04
Calcite	01	01	01	tr
Zeolite	-	-	-	-
Clay Minerals	tr	tr	tr	tr
TOTAL	100	100	100	100

TABLE II (Continued)
THIN SECTION ANALYSIS DATA
(in normative percent)

Sample Depth (feet)	2462	2950	3212	3742
Volcanic Rock Fragments				
Porphyritic dacite/rhyodacite	-	-	-	17
Porphyritic andesite	-	-	-	17
Microlitic quartz latite	100	100	100	32
Rhyolitic crystal tuff	-	-	-	17
Andesitic lithic tuff	-	-	-	-
Amygdular andesite	-	-	-	-
Devitrified glass	-	-	-	17
TOTAL	100	100	100	100

TABLE II (Continued)
THIN SECTION ANALYSIS DATA

Sample Depth (feet)	4104	4232	5164	6652
Classification*	Diatomaceous siltstone (Feldspathic litharenite)	Silty sandstone (Lithic arkose)	Silty sandstone (Lithic arkose)	Sandy siltstone (Lithic arkose)
Sorting	Moderate to poor	Poor to very poor	Poor to moderate	Poor to moderate
Induration	Poor to moderate	Moderate to poor	Moderate to poor	Moderate to poor
Texture	Indistinct wavy laminations that are irregular and disrupted; healed fractures; moderate bioturbation	Wavy and lenticular laminations; healed fractures; minor bioturbation	Indistinct wavy laminations; healed fractures; minor bioturbation	Indistinct wavy, graded amd cross laminations; trace bioturbation
Grain Size				
min.	0.01mm(medium silt)	0.02mm(medium silt)	0.01mm(medium silt)	0.01mm(medium silt)
max.	0.24mm(fine sand)	1.18mm(v. coarse sand)	0.26mm(medium sand)	0.48mm(medium sand)
avg.	0.05mm(coarse silt)	0.16mm(fine sand)	0.06mm(v. fine sand)	0.07mm(v. fine sand)
Angularity and Grain Shape	Angular-rounded average:subangular elongate>equant	Angular-rounded average:subangular elongate≥equant	Angular-subrounded average:subangular equant>elongate	Angular-rounded average:subangular elongate>equant
Grain Contacts	Floating>point	Floating≥point	Floating>point traces of elongate	Floating>point traces of elongate
Porosity Types	Trace to minor intergranular, traces of intragranular due to dissolution of feldspars and rock fragments, and trace to minor intraskeletal porosity	Trace to minor intergranular, traces of intragranular porosity due to dissolution of feldspars and rock fragments	Trace of intergranular, trace of intragranular due to dissolution of feldspars and rock fragments, trace of moldic porosity due to dissolution of microfossils	Traces of intergranular and traces of intragranular porosity due to dissolution of feldspars and rock fragments

* Classification of rock nomenclature of the sand-size fraction (in parentheses) from Pettijohn, et al., 1972.

POINT COUNT ANALYSIS
(in modal percent)

Sample Depth (feet)	4104	4232	5164	6652
Detrital Constituents	96	93	94	92
Quartz	23	29	28	10
Plagioclase	17	24	30	36
Antiperthitic Plagioclase	tr	tr	tr	tr
Potassium Feldspar	tr	tr	tr	02
Volcanic Rock Fragments	01	02	01	06
Plutonic Rock Fragments	tr	05	02	02
Metamorphic Rock Fragments	-	tr	tr	01
Sedimentary Rock Fragments	tr	01	tr	tr
Chert	tr	01	01	tr
Mica	03	03	04	03
Hornblende	01	03	02	02
Glauconite	02	04	03	04
Accessory Minerals	tr	01	tr	tr
Fossil Fragments	15	01	-	-
Clay Minerals	34	19	23	26
Authigenic Constituents	04	07	06	08
Pyrite	02	04	04	04
Calcite	02	01	01	03
Zeolite	tr	02	01	01
Clay Minerals	tr	tr	tr	tr
TOTAL	100	100	100	100

TABLE II (Continued)
THIN SECTION ANALYSIS DATA
(in normative percent)

Sample Depth (feet)	4104	4232	5164	6652
Volcanic Rock Fragments				
Porphyritic dacite/rhyodacite	50	100	100	36
Porphyritic andesite	-	-	-	07
Microlitic quartz latite	-	-	-	29
Rhyolitic crystal tuff	50	-	-	21
Andesitic lithic tuff	-	-	-	07
Amygdular andesite	-	-	-	-
Devitrified glass	-	-	-	-
TOTAL	100	100	100	100

TABLE II (Continued)
THIN SECTION ANALYSIS DATA

Sample Depth (feet)	7229	7413	8051
Classification*	Volcaniclastic sandy siltstone (Lithic arkose)	Volcaniclastic sandstone (Litharenite)	Volcaniclastic sandstone (Litharenite)
Sorting	Poor to very poor	Very poor	Very poor
Induration	Poor to moderate	Moderate to poor	Moderate to poor
Texture	Indistinct wavy lamination, truncated planar lamination, possible cross lamination; trace bioturbation; possible pseudomatrix	Indistinct wavy and planar laminations, possible cross lamination; prominent to abundant pseudomatrix	No apparent lamination; abundant pseudomatrix
Grain Size			
min.	0.01 mm (medium silt)	0.04 mm (coarse silt)	0.04 mm (coarse silt)
max.	2.03 mm (granule)	2.74 mm (granule)	1.06 mm (v. coarse sand)
avg.	0.14 mm (fine sand)	0.43 mm (medium sand)	0.24 mm (fine sand)
Angularity and Grain Shape	Angular-rounded average: subangular Equant>elongate	Angular-rounded average: subangular-subrounded Equant>elongate	Angular-rounded average: subangular-subrounded Equant>elongate
Grain Contacts	Floating>point trace of elongate	Elongate>concavo-convex trace of point	Elongate≥concavo-convex trace of point
Porosity Types	Traces of intergranular, traces of intragranular due to dissolution of feldspars and rock fragments	Traces of intergranular, trace to minor intragranular porosity due to dissolution of feldspars and rock fragments	Traces of intergranular, and traces of intragranular porosity due to dissolution of feldspars and rock fragments

* Classification of rock nomenclature of the sand-size fraction (in parentheses) from Pettijohn, et al., 1972.

POINT COUNT ANALYSIS
(in modal percent)

Sample Depth (feet)	7229	7413	8051
Detrital Constituents	94	95	100
Quartz	10	02	03
Plagioclase	28	10	06
Antiperthitic Plagioclase	01	01	03
Potassium Feldspar	01	01	tr
Volcanic Rock Fragments	16	60	67
Plutonic Rock Fragments	tr	01	06
Metamorphic Rock Fragments	tr	tr	-
Sedimentary Rock Fragments	-	-	-
Chert	-	tr	01
Mica	02	tr	01
Hornblende	tr	tr	tr
Glauconite	02	-	-
Accessory Minerals	tr	01	tr
Fossil Fragments	-	-	-
Clay Minerals	34	19	13
Authigenic Constituents	06	05	tr
Pyrite	06	03	tr
Calcite	tr	02	tr
Zeolite	-	-	tr
Clay Minerals	tr	tr	tr
TOTAL	100	100	100

TABLE II (Continued)
THIN SECTION ANALYSIS DATA
(in normative percent)

Sample Depth (feet)	7229	7413	8051
Volcanic Rock Fragments			
Porphyritic dacite/rhyodacite	22	31	31
Porphyritic andesite	30	27	21
Microlitic quartz latite	17	19	24
Rhyolitic crystal tuff	22	12	15
Andesitic lithic tuff	07	07	06
Amygdular andesite	-	01	-
Devitrified glass	02	03	03
TOTAL	100	100	100

TABLE III

POTENTIAL FORMATION DAMAGE FROM SENSITIVE MINERALS

Estimated Potential for Damage *** great * small	Potential Substance	Problem:	Avoid Using	Use	Treatment to Eliminate
***	Smectite (including mixed-layer illite-smectite	migration of fine material (due to vermicular morphology)	high or un-steady fluid flow rates	low and steady fluid flow rates	proper pre- and post treatment flushes and clay stabilizers
**	Chlorite	iron-hydroxide precipitate	oxygenated fluid systems; high pH	acid systems with oxygen scavengers	acidize with HCl/HF and use a suitable chelating agent
*		migration of fine material (due to vermicular morphology)	high or un-steady fluid flow rates	low and steady fluid flow rates	proper pre- and post treatment flushes and clay stabilizers
*	Illite	migration of fine material	high or un-steady fluid flow rates and high transient pressures	low, steady fluid flow rates and low transient pressures	acidize with HCl/HF and use proper pre- and post-treatment flushes, and stabilizers
*	Pyrite	iron-hydroxide precipitate	oxygenated fluid systems	acid systems with oxygen scavengers	acidize with HCl/HF and use a suitable chelating agent

TABLE IV

CATION EXCHANGE CAPACITY MEASUREMENTS

Project Number	Sample Depth (in feet)	CEC (meq/100g)	Total Weight Percent Clay in Sample (from XRD)	Total Weight Percent Expandable Clays in Sample (from XRD)	Total Weight Percent Zeolite in Sample (from XRD)
PD-85066	2462	31.14	33	56	01
PD-85066	2950	45.83	35	48	-
PD-85066	3212	35.45	33	60	-
PD-85066	3742	33.58	25	65	-
PD-85066	4104	44.91	44	70	04
PD-85074	4232	30.77	23	69	06
PD-85074	5164	23.01	20	53	tr
PD-85074	6652	27.11	25	60	-
PD-85077	7229	*	27	69	-
PD-85077	7413	42.02	17	75	-
PD-85077	8051	40.49	22	58	03

* Sample was too small for accurate analysis

APPENDIX A

ANALYTICAL PROCEDURES

X-ray Diffraction: The fraction of each sample selected for XRD analysis is first weighed and disaggregated using standard techniques. The sample is then centrifugally size-fractionated in water, into a clay-size fraction (less than 4 microns) and a sand/silt-size fraction. The clay-size fraction is subsequently suspended in water and deposited onto a porous silver substrate. Each clay-size fraction is analyzed dry (under relative humidity conditions of 50%) and after treatment with ethylene glycol. The sand/silt fraction is made into a pellet using standard powder techniques.

XRD analyses are done utilizing a fully-automated Scintag Pad-V System. The weight percents of rock-forming minerals in both size fractions are determined by empirical matrix correction procedure with internal standard normalization. The detectability limit is 0.5-1.0% in the fraction analyzed. Weight percents of the various clay species were determined by peak-deconvolution/empirical peak-area-ratio method. The composition and identification of the clay minerals is determined according to procedures outlined by Weaver (1956), Jonas and Brown (1959), and Reynolds (1980). The weight percent of total clay minerals in the whole sample is estimated by determining and subtracting the total weight percent of rock-forming minerals from the total clay-size fraction. Whole-rock compositions are determined by mathematically combining and normalizing XRD data from both sand/silt and clay/size fractions.

Thin Section Petrography: The sample is vacuum-impregnated with blue-dyed epoxy, mounted on a glass slide, then cut and lapped in water to an approximate thickness of 30 microns.

Scanning Electron Microscopy/Energy Dispersive Spectrometry: The sample fraction selected for SEM/EDS is first broken to form a fresh, uncontaminated surface. The sample is then mounted on a 10mm aluminum stub and coated with a thin layer of gold. The samples are analyzed utilizing an ISI-SS60 scanning electron microscope. Photomicrographs display an alphanumeric caption which displays magnification, micron scale, accelerating voltage (KV), and micron bar. Qualitative energy dispersive spectrometry (EDS) analyses of selected minerals are made with a Tracor Northern 5400 energy dispersive system. This system utilizes a Si(Li) detector; spectra are taken with an electron-beam accelerating potential of 20kV.

REFERENCES

Bush, D. C. and Jenkins, R. E., 1977, Shaly Sand Log Analysis Using Cation Exchange Capacity Data, in: Sixth Formation Evaluation Symposium, Canadian Well Logging Society.

Helander, D. P., 1983, Fundamentals of Formation Evaluation: OGCI Publications, OGCI, Inc., Tulsa, OK p. 332.

Hilchie, D. W., 1982a, Applied Openhole Log Interpretation for Geologists and Engineers: Revised ed., D. W. Hilchie, Inc., Golden, CO.

Hilchie, D. W., 1982b, Advanced Well Log Interpretation: D. W. Hilchie, Inc., Golden, CO.

Isaacs, C. M., 1981, Porosity Reduction During Diagenesis of the Monterey Formation, Santa Barbara Coastal Area, California, in: The Monterey Formation and Related Siliceous Rocks of California: Soc. Econ. Paleontologists and Mineralogists, pp. 151-271.

Jonas, E. C., and Brown, T. E., 1959, Analysis of Interlayer Mixtures of Three Clay Mineral Types by X-ray Diffraction: Jour. Sed. Pet. 29, pp. 77-86.

Johnson, W. L., and Linke, W. A., 1977, Some Practical Applications to Improve Formation Evaluation of Sandstones in the MacKenzie Delta: Sixth Formation Eval. Symp. CWLS, Paper R, Calgary, Alberta.

Pettijohn, F. J., Potter, P. E., and Siever, R., 1972, Sand and Sandstone: Springer Verlag, New York, p. 618.

Picard, M. D., 1971, Classification of Fine-Grained Sedimentary Rocks, Journal of Sedimentary Petrology, Volume 41, pp. 179.

Reynolds, R. C., Jr., 1980, Interstratified Clay Minerals, in Brindley, W., and Brown, G. (eds), Crystal Structures of Clay Minerals and Thin X-ray Identification: Mineralogical Soc. of London Pub.

Shepard, F. P., 1954, Nomenclature Based on Sand-Silt-Clay Ratios, Journal of Sedimentary Petrology 24, pp. 151-158.

SPWLA 1982, Shaly Sand: reprint volume, W. H. Lang, Jr., Chmn.

REFERENCES (Continued)

Srodon, J., 1980, Precise Identification of Illite/Smectite Interstratification by X-ray Powder Diffraction. Clays and Clay Minerals, Vol. 28, pp. 401-411.

Weaver, C. E., 1956, The Distribution and Identification of Mixed-Layer Clays in Sedimentary Rocks: Amer. Min. 41, pp. 202-221.

AMOCO PRODUCTION COMPANY
Nancy No. 1 O.C.S. Y-0719 Well

File Number: PD-85066
File Number: PD-85074
File Number: PD-85077

SCANNING ELECTRON MICROSCOPE PHOTOMICROGRAPH SCALES

A scale bar preceded by dash marks is present in the legend at the bottom of each photomicrograph. The number of dash marks indicates the length in microns of the bar. One dash indicates the scale bar is one micron long; two dashes indicates the scale bar is ten microns long, and so forth by a factor of 10 for each scale bar.

Amoco Production Company
Nancy No. 1 O.C.S. Y-0719 Well

File Number: PD-85066

Sample Depth: 2462 feet

Plate 1A

A 40X magnification view of a poorly sorted, coarse-grained siltstone that is composed dominantly of angular quartz (e.g. F8) and plagioclase (e.g. F11.5) grains, and skeletal diatom fragments (e.g. D1, J2) in clay matrix. The apparent fracturing occurred during sample collection.

Plate 1B

A 160X magnification photomicrograph of an intergranular area in this siltstone (refer to E7, Plate 1A). Skeletal fragments of centric (e.g. C7, G-H2, H10) and pennate (A10, A13, C-D13, F3.5, G-H3.5) diatoms are abundant in this sample. A silt-size quartz grain is visible at G11 of this view.

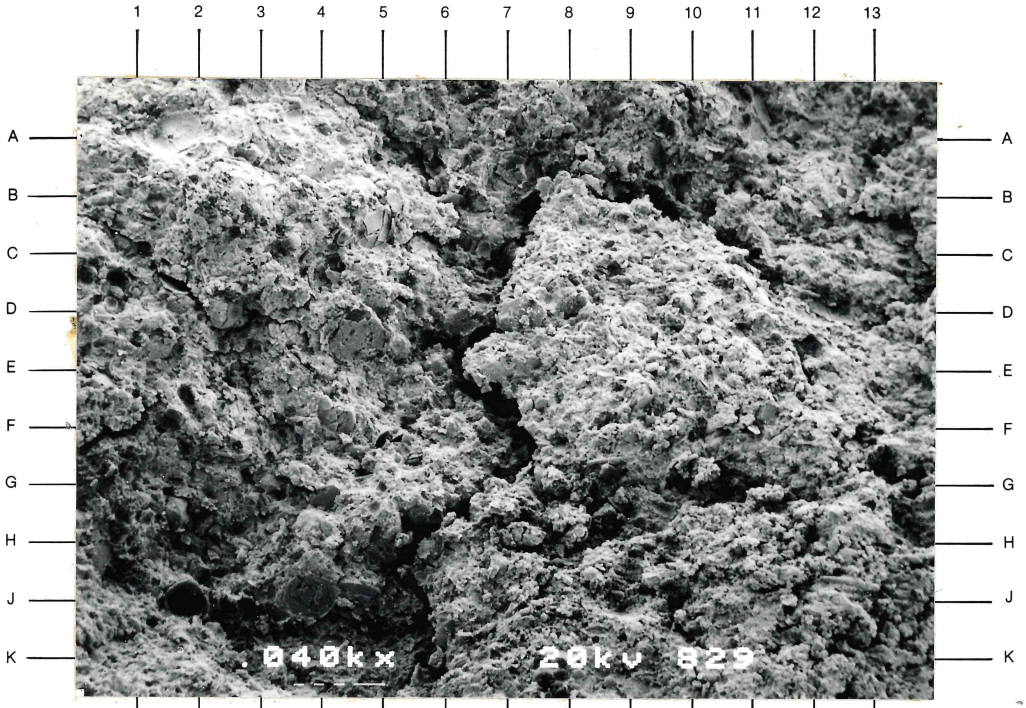
1 2 3 4 5 6 7 8 9 10 11 12 13
A B C D E F G H J K
.040kx 20kv 829

A

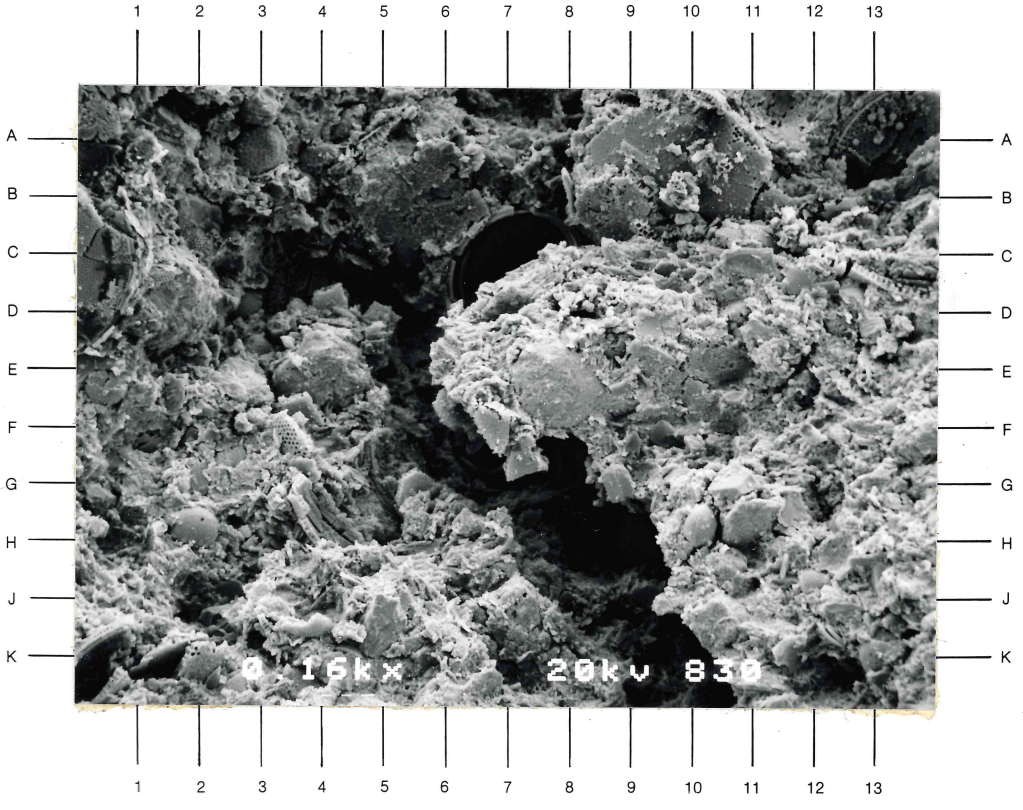
1 2 3 4 5 6 7 8 9 10 11 12 13
A B C D E F G H J K
.16kx 20kv 830

B

Amoco Production Company
Nancy No. 1 O.C.S. Y-0719 Well

File Number: PD-85066

Sample Depth: 2462 feet

Plate 2A

A 450X magnification textural view of this diatomaceous siltstone (refer to E5.5, Plate 1B). Skeletal fragments of pennate diatoms exhibit trace (H11) to moderate (J2) intraskeletal porosity. The detrital clay matrix of this sample is visible at D9.5 to F12 of this view.

Plate 2B

A 3000X magnification photomicrograph of the matrix in this diatomaceous siltstone (refer to D-E9.5, Plate 2A). Irregular stacks of detrital ferroan chlorite plates (Spectrum 1) are visible at C2.5 to G-H7 of this view. Wire- or hair-like fibers of authigenic illite form coatings on the chlorite plates and crystal aggregates (C11, E8, F9).

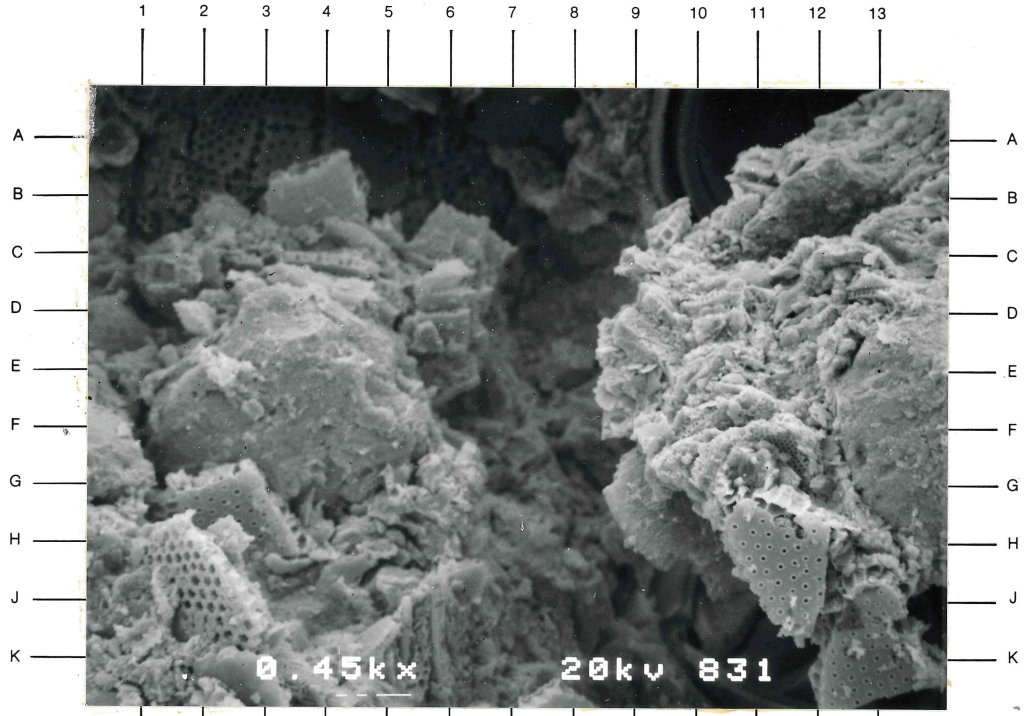
1 2 3 4 5 6 7 8 9 10 11 12 13
A B C D E F G H J K
0.45kx
20kv 831

A

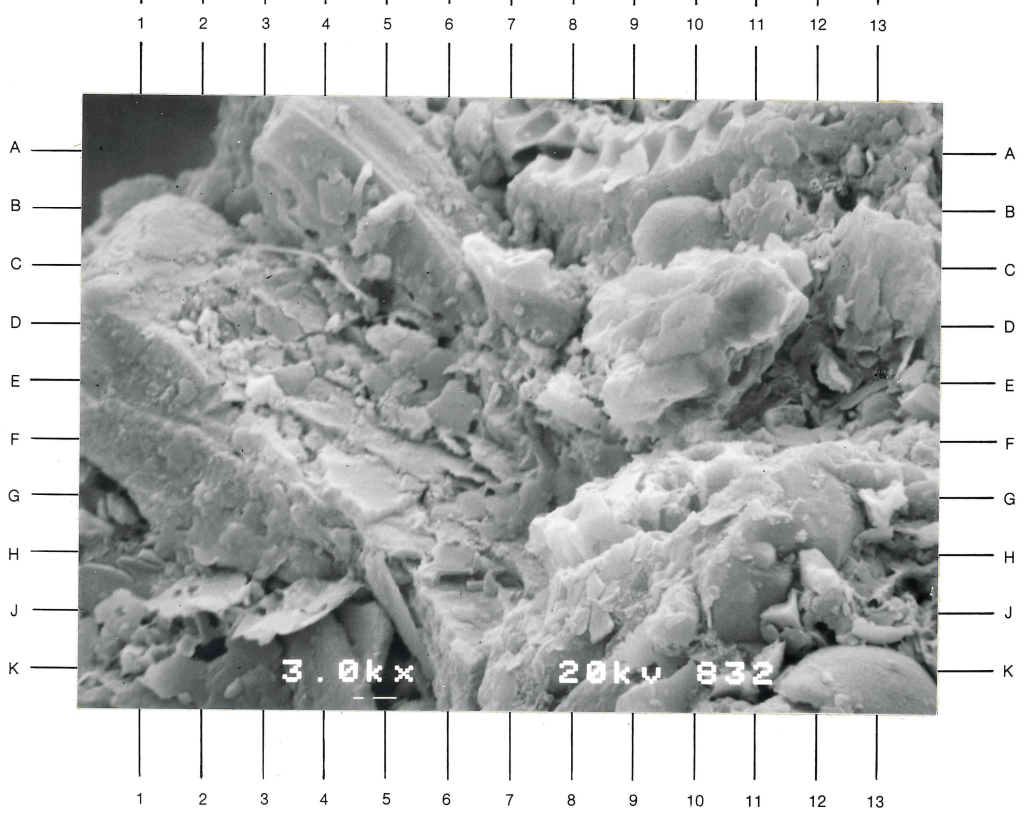
1 2 3 4 5 6 7 8 9 10 11 12 13
A B C D E F G H J K
3.0kx
20kv 832

B

Amoco Production Company
Nancy No. 1 O.C.S. Y-0719 Well

File Number: PD-85066

Sample Depth: 2950 feet

Plate 3A

A 40X magnification view of a poorly sorted, coarse-grained siltstone that contains detrital mica fragments (F6.5, F-G10.5, J2) and skeletal diatom fragments (B-C13.5, D6.5, F13, F-G4) in a detrital clay matrix. Note the intraskeletal pore area at E7 of this view.

Plate 3B

A 160X magnification photomicrograph of an intergranular area in this siltstone (refer to D8.5, Plate 3A). Detrital feldspar fragments (E1.5, J13), mica fragments (D8.5, J8), and centric diatom fragments (D5, E12, F11, G7) exhibit coatings of authigenic clays (e.g. E2, H6, J12). The intergranular matrix is composed dominantly of detrital clay minerals.

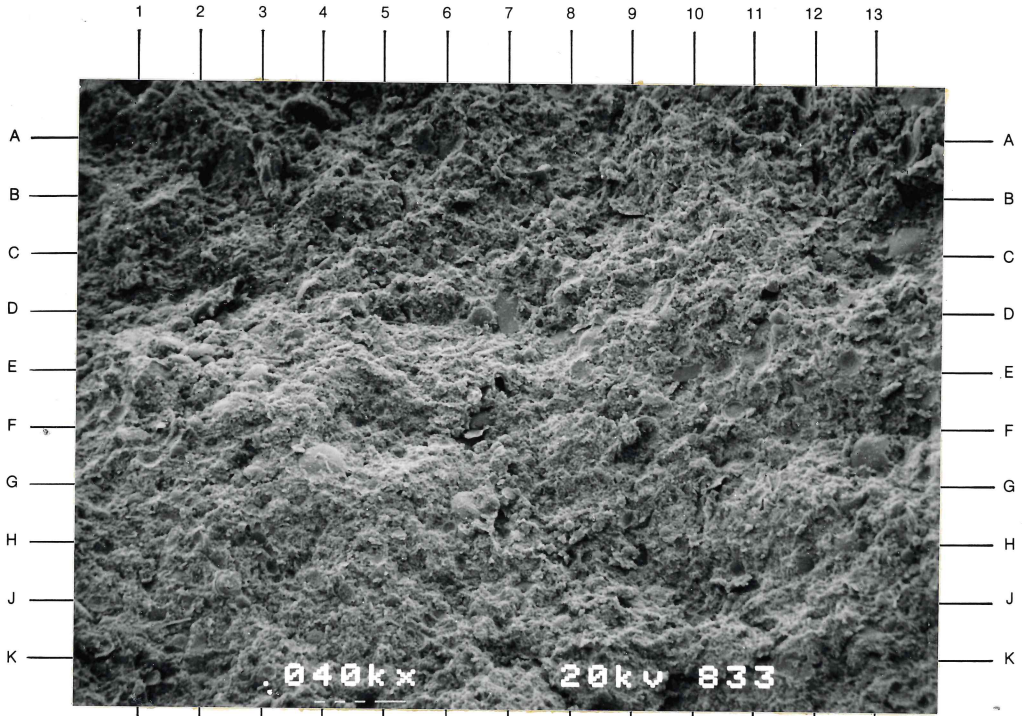

A

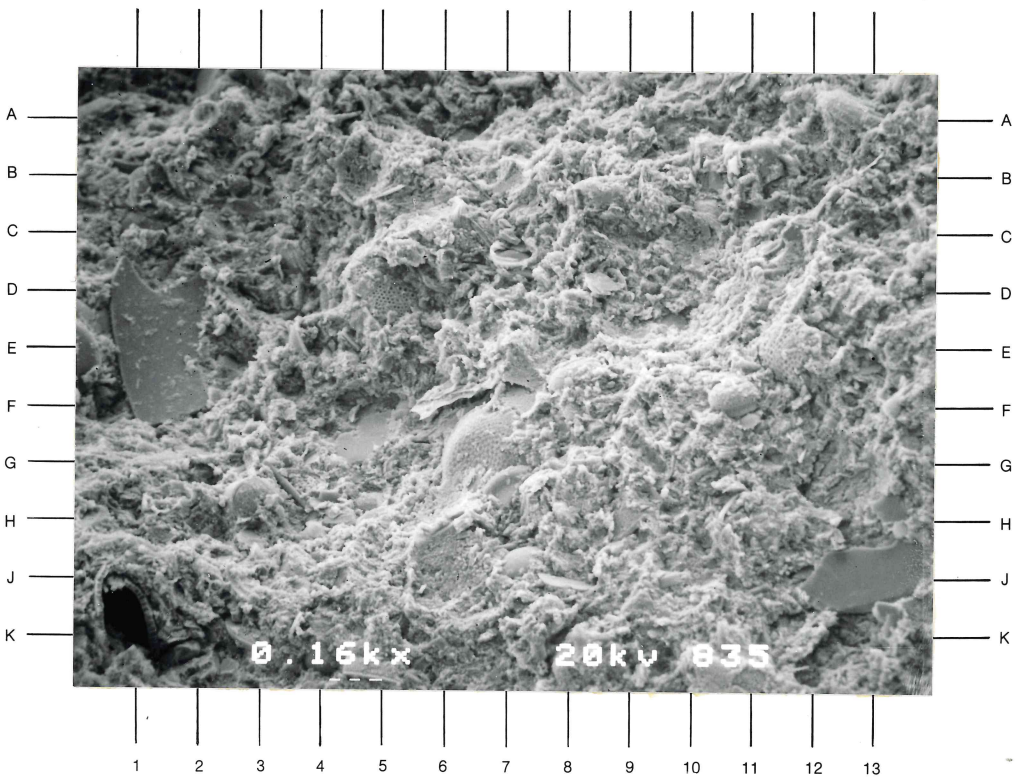

B

CORE LABORATORIES, INC.

Reservoir Geology/Petrographic Services

Amoco Production Company
Nancy No. 1 O.C.S. Y-0719 Well

File Number: PD-85066

Sample Depth: 2950 feet

Plate 4A

A 2500X magnification view of the matrix in this diatomaceous siltstone (refer to E3, Plate 3B). Flake-like crystals and crystal aggregates of detrital smectite (D-H5, D10-J9) exhibit coatings of authigenic illite (D4, H-J4.5, J6). Traces of detrital chlorite are present (C10, G-J13). Note the intraskeletal porosity in the pennate diatom fragments (A1-H3, D-F7).

Plate 4B

A 3500X magnification photomicrograph of intergranular microporosity in the detrital clay matrix of this diatomaceous siltstone (e.g. A3.5, D1.5, E8.5, E9.5, F9.5). Detrital ferroan chlorite plates are present at A-B4, A-D10, D-F1, and F-H10 of this view. Irregular flakes of detrital smectite (E-F5, D12-K13.5) were deposited after the chlorite. Authigenic illite forms coatings on the detrital clay plates and on the surface of the diatom fragment (G5, J9.5).

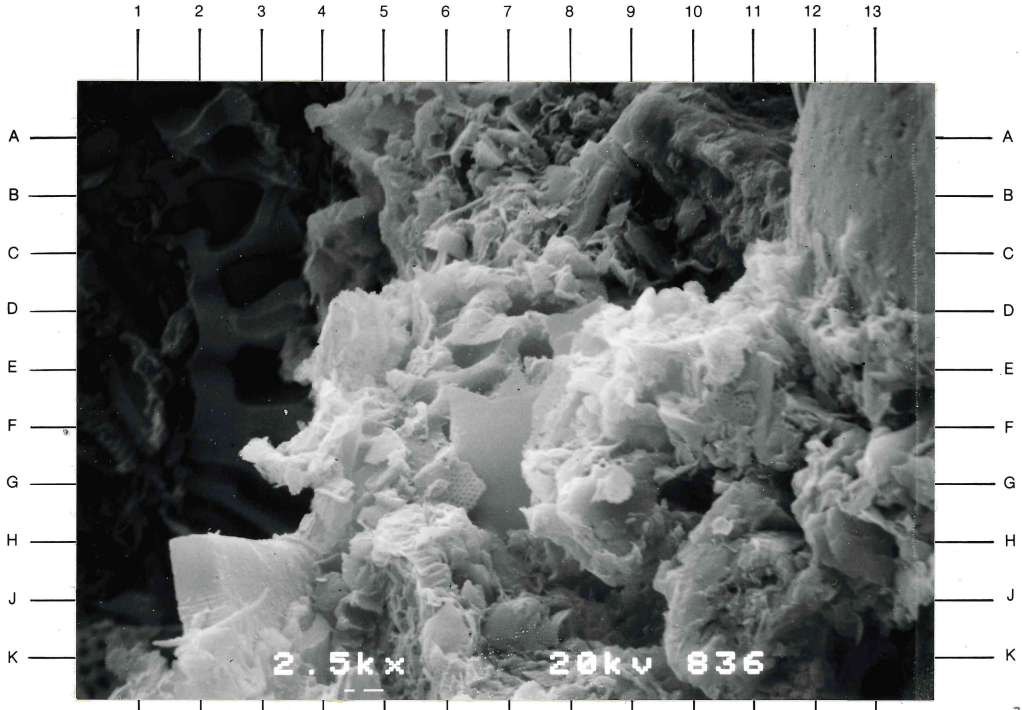

A

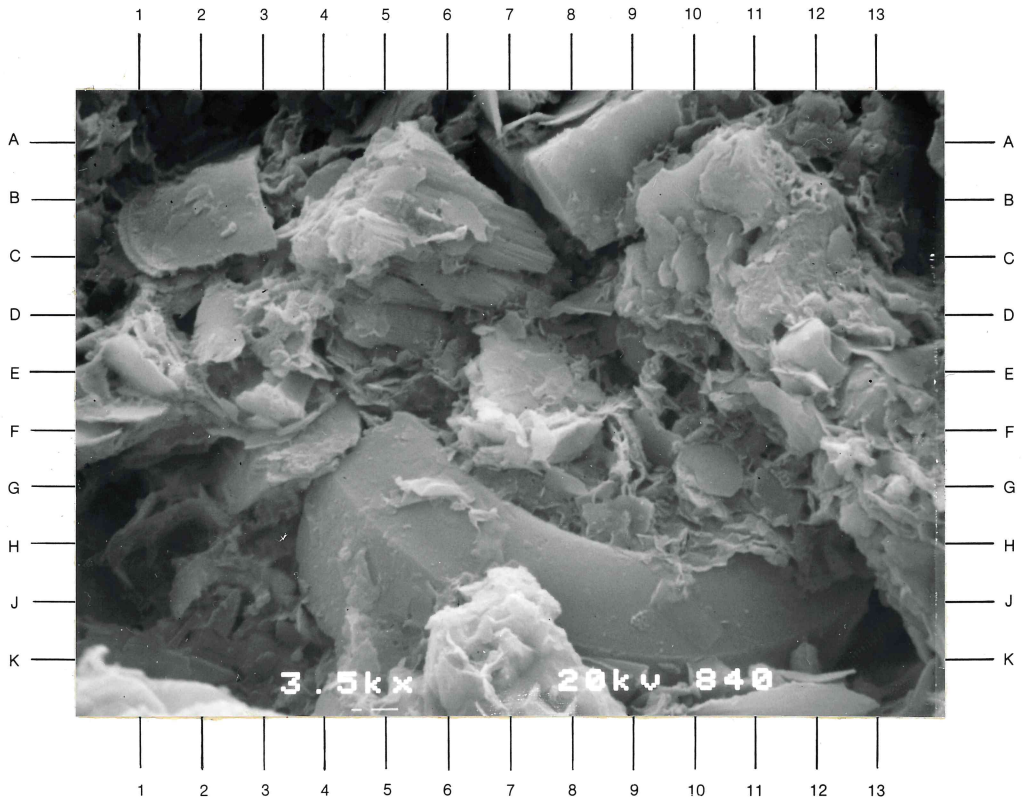

B

CORE LABORATORIES, INC.

Reservoir Geology/Petrographic Services

Amoco Production Company
Nancy No. 1 O.C.S. Y-0719 Well

File Number: PD-85066

Sample Depth: 3212 feet

Plate 5A

A 40X magnification view of a poorly to moderately sorted, coarse-grained siltstone that contains abundant skeletal diatom fragments (A11.5, A-B11, B7.5, B-C3.5, G4, G-H1.5). The matrix is composed dominantly of detrital clay. Note the mica fragments at A-B3 and H2.5.

Plate 5B

A 160X magnification photomicrograph of an intergranular region in this siltstone (refer to J2, Plate 5A). Detrital grains of plagioclase (e.g. E11.5, J-K5), mica (B7), and of skeletal diatom fragments (A0.5, A-B8.5, D4, F4, F6, G5, J9.5) occur in the microporous, detrital clay matrix of this sample.

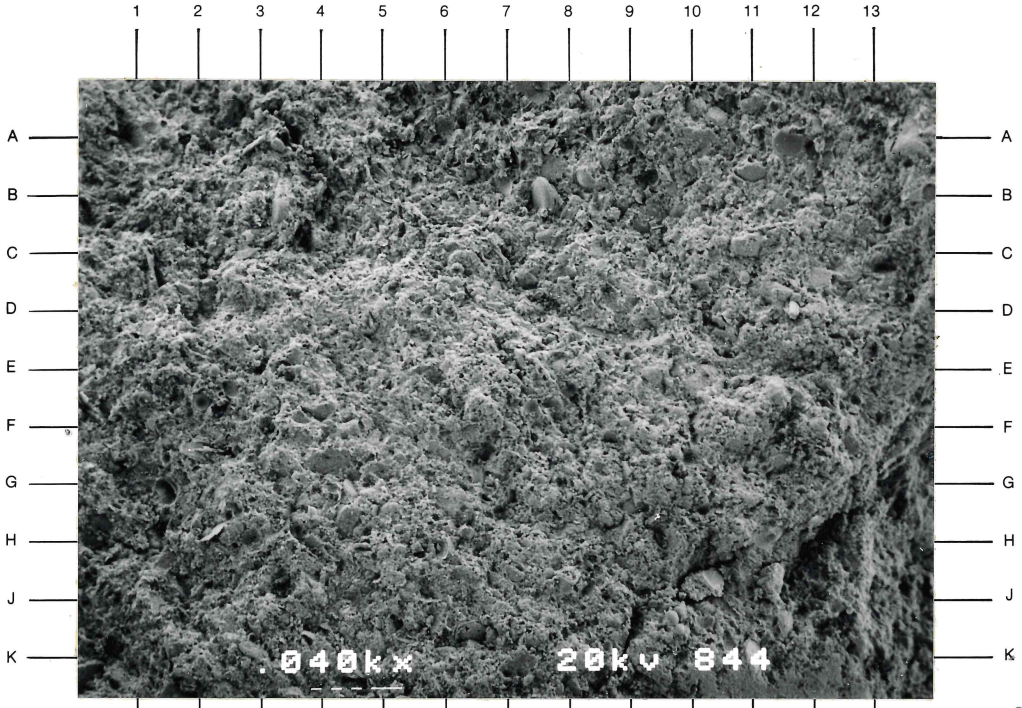
1 2 3 4 5 6 7 8 9 10 11 12 13
A B C D E F G H J K
.040kx 20kv 844

A

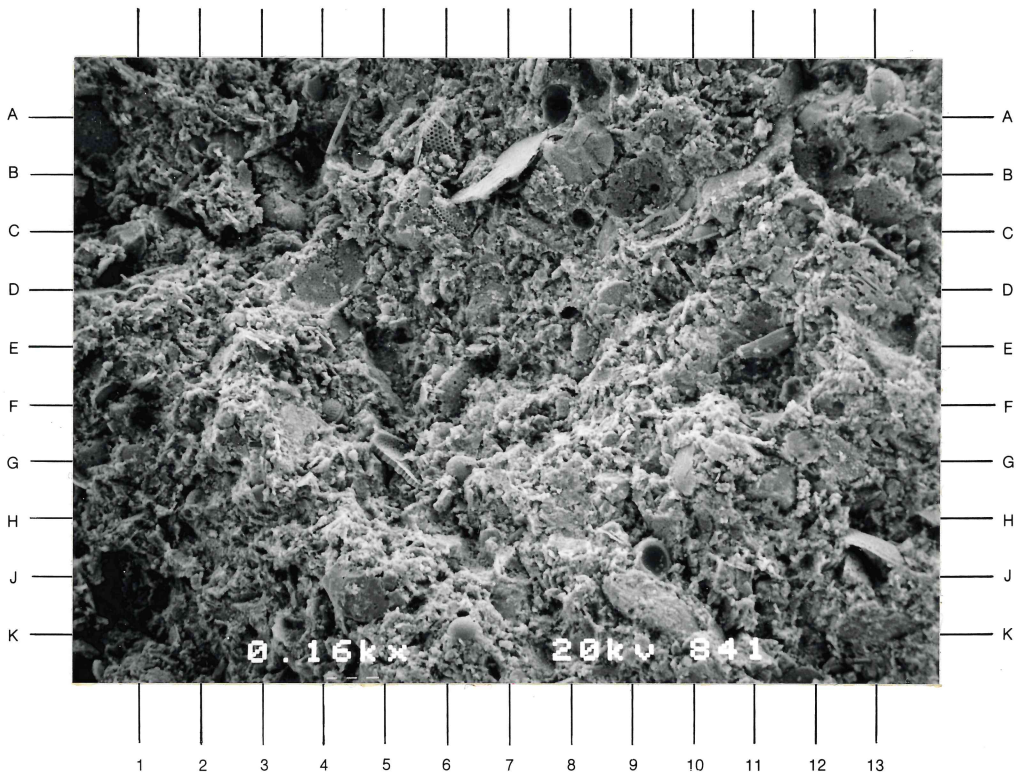
1 2 3 4 5 6 7 8 9 10 11 12 13
A B C D E F G H J K
0.16kx 20kv 841

B

Amoco Production Company
Nancy No. 1 O.C.S. Y-0719 Well

File Number: PD-85066

Sample Depth: 3212 feet

Plate 6A

A 2000X magnification view of the matrix in this diatomaceous siltstone (refer to E6.5, Plate 5B). Traces of intergranular microporosity (e.g. B1, B4, D-E10, E1, H-J8) occur in deposits of detrital chlorite (C10, F-G9) and smectite (A-D11.5, D1, G12, J9.5) clay minerals. Authigenic illite forms coatings on the detrital clays and framework grains of mica (C-D5.5) and skeletal diatom fragments (C2, C13, E-F12, F0.5, F8, F-K4). Note that intraskeletal porosity in the diatom fragment (F5.5-K0) has been occluded by authigenic illite clay.

Plate 6B

A 4000X magnification photomicrograph of an intergranular area in this siltstone. Irregular flake-like crystals and crystal aggregates of detrital smectite (A3,-D1.5, A6-D9, E9-K13.5) exhibit coatings of authigenic illite (e.g. B4, E-F1.5, G3-4, H7.5-K7, J-K9). Detrital smectite coats the framboidal aggregate of pyrite at left center of this view (A3-D3).

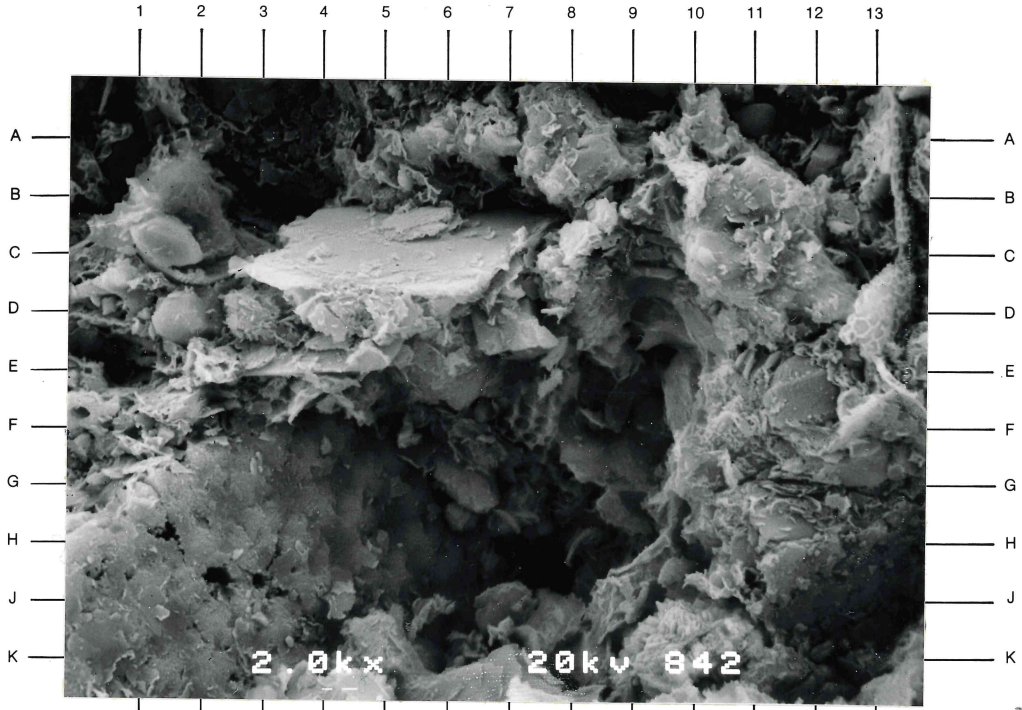

A

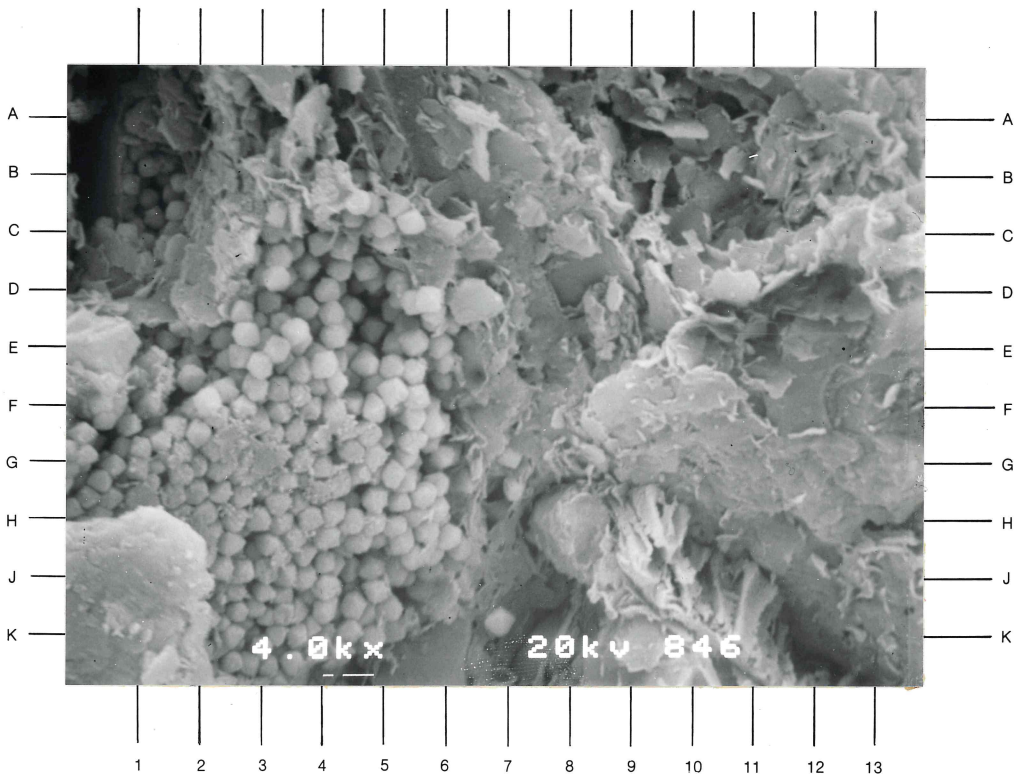

B

CORE LABORATORIES, INC.

Reservoir Geology/Petrographic Services

Amoco Production Company
Nancy No. 1 O.C.S. Y-0719 Well

File Number: PD-85066

Sample Depth: 3742 feet

Plate 7A

A 40X magnification view of a poorly sorted, coarse-grained siltstone that is composed of detrital plagioclase (F0.5), quartz (A-B8), and mica (G-H0.5) grains and skeletal diatom fragments (B-C5, D0.5, C-D8, D-E13, K5.5) in detrital clay matrix. Note the intergranular pore area in the detrital clay matrix at A5.5 of this view.

Plate 7B

A 160X magnification photomicrograph of the texture of this diatomaceous siltstone (refer to C9, Plate 7A). Detrital quartz (F8) and plagioclase (K7) grains, and skeletal diatom fragments (A4.5, A-B1.5, C2-4, C7, D5, G-H4) are angular in shape and occur in random orientations in this sample. Authigenic clay coats the detrital grains and skeletal fragments in rare locations (e.g. A4-5).

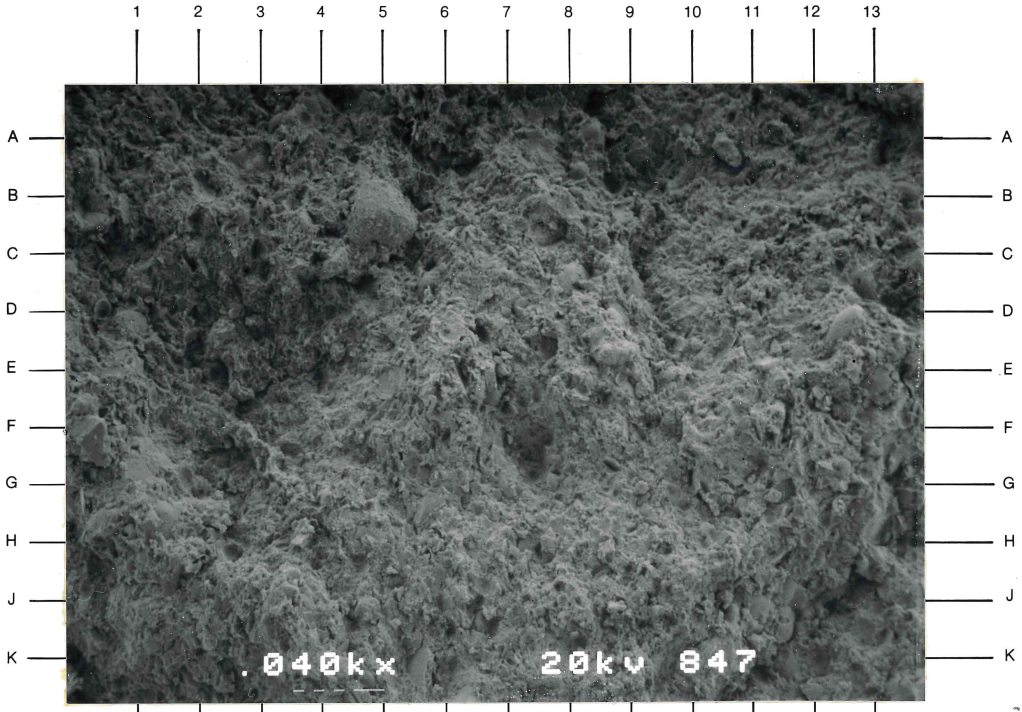

A

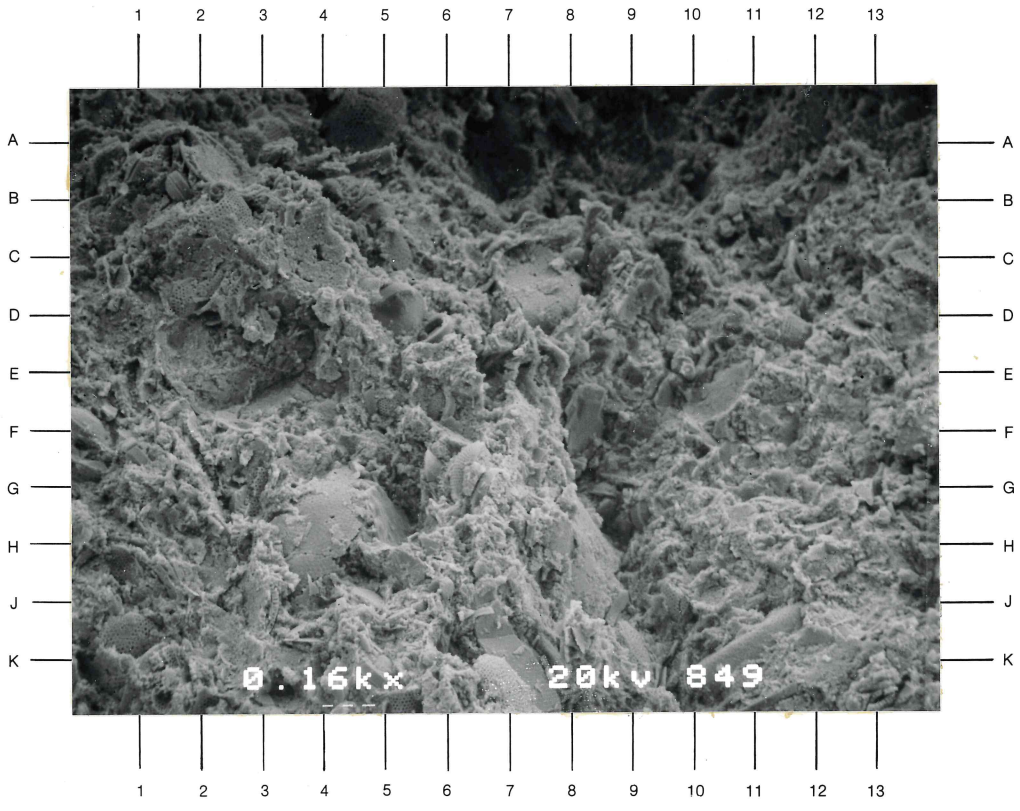

B

CORE LABORATORIES, INC.

Reservoir Geology/Petrographic Services

Amoco Production Company
Nancy No. 1 O.C.S. Y-0719 Well

File Number: PD-85066

Sample Depth: 3742 feet

Plate 8A

A 600X magnification view of an intergranular area in this diatomaceous siltstone (refer to G9.5, Plate 7B). Centric (D-E3.5, F6, J7, J-K10) and pennate (A2, E7.5) diatom fragments exhibit traces of intraskeletal porosity. Note the trace occurrences of intergranular microporosity in the detrital clay matrix.

Plate 8B

A 2000X magnification photomicrograph of the matrix in this diatomaceous siltstone (refer to K8.5, Plate 8A). Detrital aggregates of smectite crystals (e.g. A5.5-C7, A13.50-H8.5) have been deposited over detrital chlorite plates (A4.5, D5.5) in this view. The detrital clays occlude most of the effective intergranular porosity in this sample. Traces of authigenic illite form coatings on the detrital clays and skeletal diatom fragments.

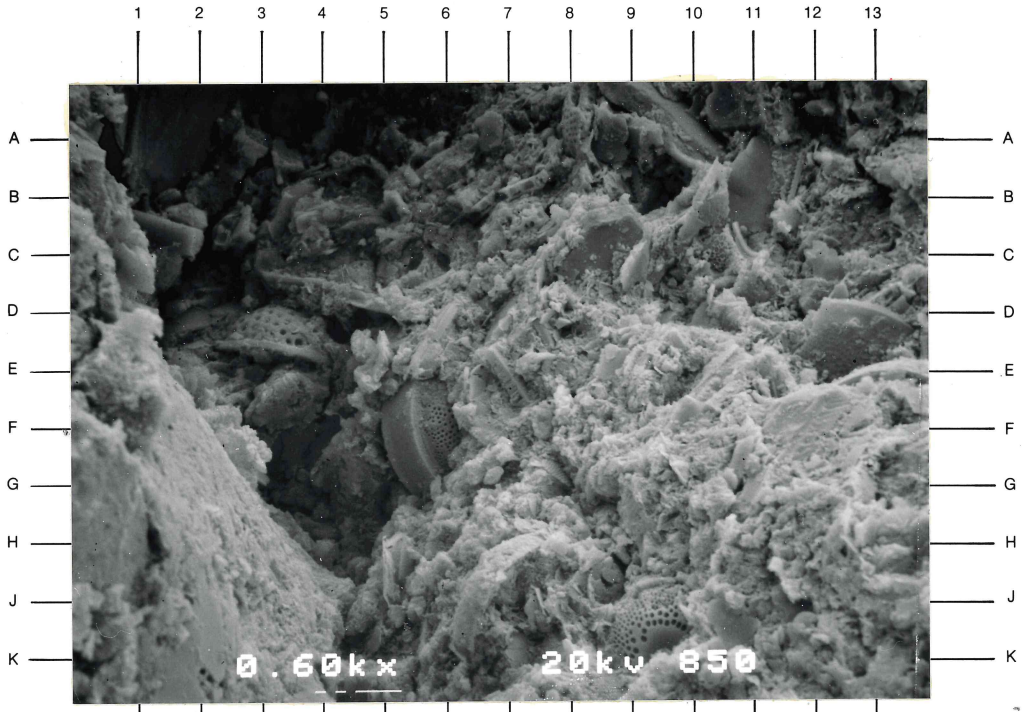
1 2 3 4 5 6 7 8 9 10 11 12 13
A B C D E F G H J K
0.60kx
20kv 850

A

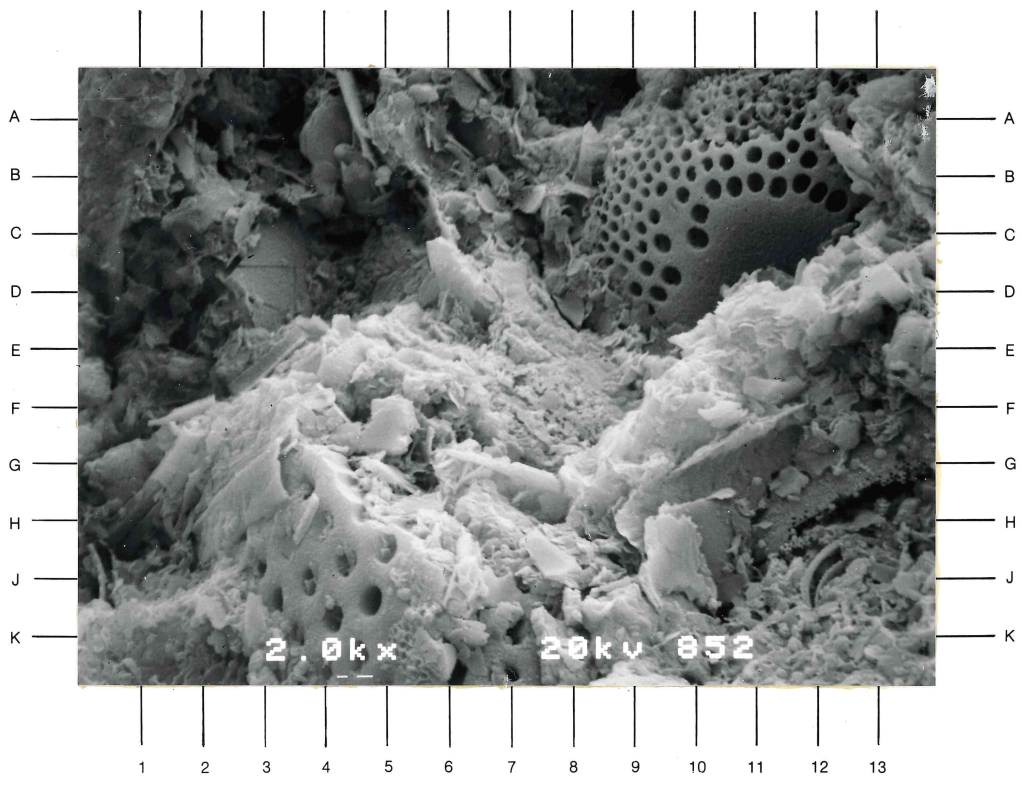
1 2 3 4 5 6 7 8 9 10 11 12 13
A B C D E F G H J K
2.0kx
20kv 852

B

Amoco Production Company
Nancy No. 1 O.C.S. Y-0719 Well

File Number: PD-85066

Sample Depth: 4104 feet

Plate 9A

A 40X magnification view of a poorly to moderately sorted, coarse-grained siltstone that has a massive texture (no apparent lamination) and is moderately indurated. A detrital plagioclase grain is visible at G-H7 of this view.

Plate 9B

A 160X magnification photomicrograph of the texture of this siltstone (refer to G-H8.5, Plate 9A). Detrital quartz (E9, F-G10.5) and plagioclase (D-E2) grains, and skeletal diatom fragments (H-J1, J10) are suspended in the clay matrix. Note the traces of intergranular porosity in the aggregates of clay minerals (e.g. E-F10, G-H9.5, K4.5).

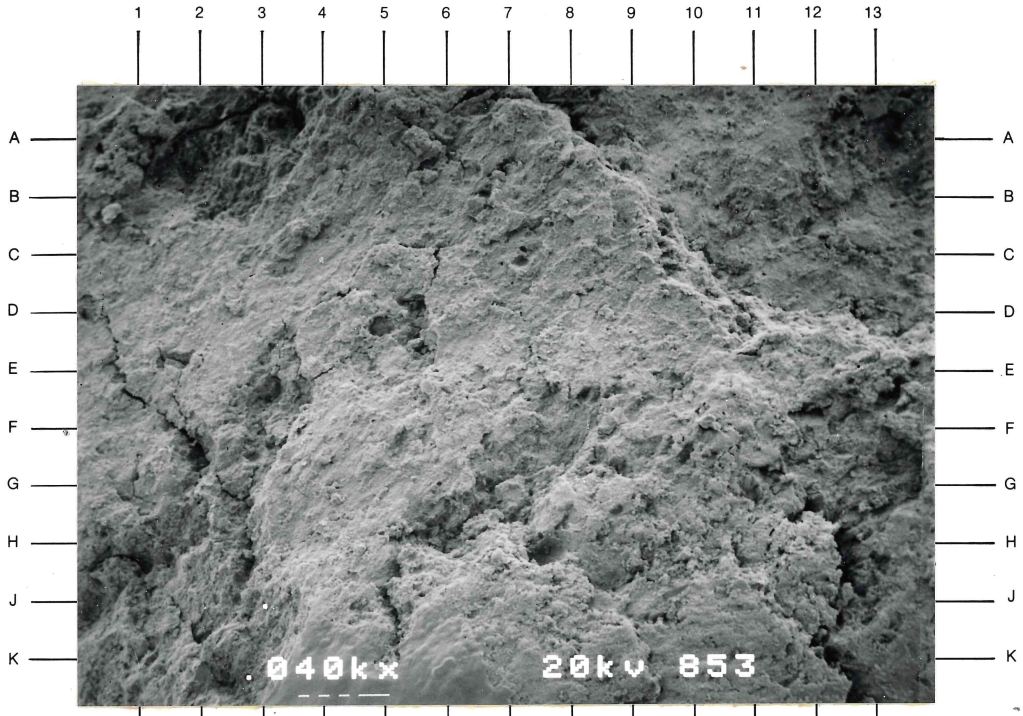

A

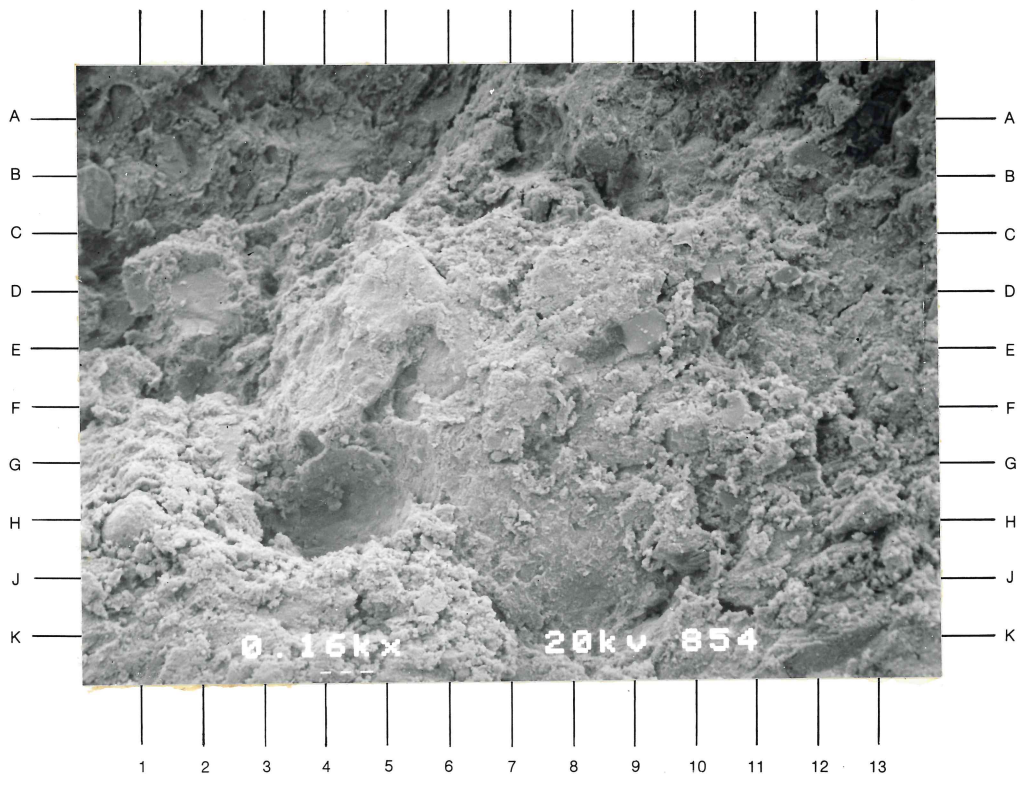

B

CORE LABORATORIES, INC.

Reservoir Geology/Petrographic Services

Amoco Production Company
Nancy No. 1 O.C.S. Y-0719 Well

File Number: PD-85066

Sample Depth: 4104 feet

Plate 10A

A 1000X magnification view of an intergranular area in this siltstone (refer to J1, Plate 9B). A framboidal aggregate of pyrite crystals (center at B-C4) is partially covered by detrital clay minerals (e.g. A-B7-9) and exhibits coatings of authigenic clay (illite or mixed-layer illite-smectite; e.g. C-D5.5). Detrital plagioclase (E-J5) has undergone partial dissolution and is replaced by authigenic clay minerals.

Plate 10B

A 1700X magnification photomicrograph of a partially dissolved, detrital plagioclase grain. Detrital, flake-like crystal aggregates of smectite (B5.5-H12) partially cover the surface of the relict plagioclase grain. Authigenic illite fibers and crystal masses form coatings on the detrital smectite (B9, D7, E6.5, H-J12.5) and the detrital plagioclase (H4, H-J3.5, J-K9). Plagioclase has been replaced by rod-like crystals of aragonite (H4, J7), and elongate crystals of authigenic plagioclase (A-B3, C2.5). Note that fine crystalline quartz intergrowths (possible cristobalite lepispheres) have nucleated in this dissolution pore area (B-C3.5, F2, H5-J4.5).

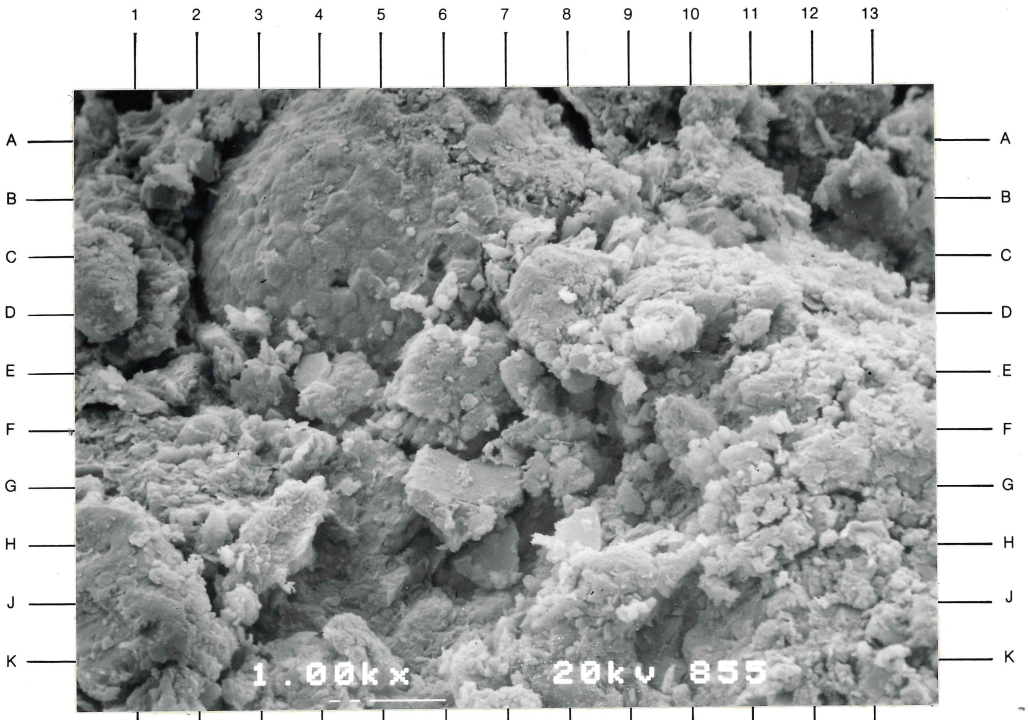
1 2 3 4 5 6 7 8 9 10 11 12 13
A B C D E F G H J K
1.00kx 20kv 855

A

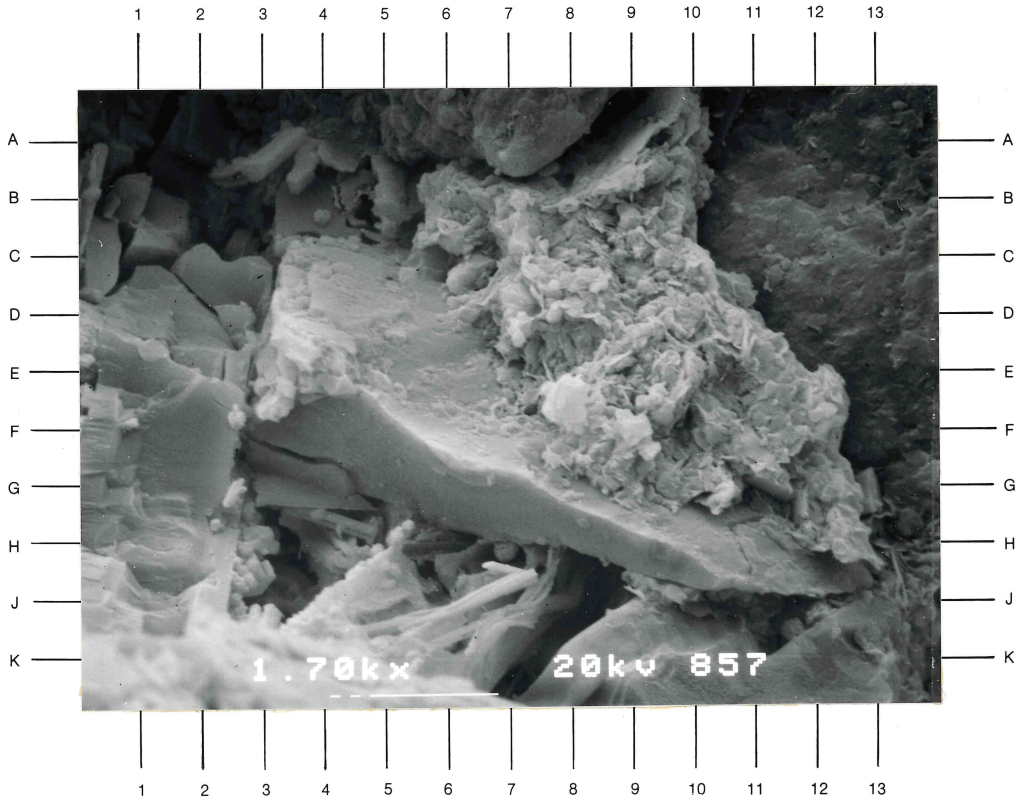
1 2 3 4 5 6 7 8 9 10 11 12 13
A B C D E F G H J K
1.70kx 20kv 857

B

Amoco Production Company
Nancy No. 1 O.C.S. Y-0719 Well

File Number: PD-85074

Sample Depth: 4232 feet

Plate 11A

A 40X magnification view of a poorly to very poorly sorted, fine-grained sandstone or silty sandstone that exhibits an indistinct planar lamination (F0-3, G5.5-7.5). Angular grains of quartz (A10, E-F10) and plagioclase (A6, F-G9.5, G-H2) are visible in the clay matrix of this sample.

Plate 11B

A 160X magnification photomicrograph of the matrix of this sandstone (refer to E-F6.5, Plate 11A). Detrital clay minerals have occluded intergranular porosity in this sample. Partial dissolution of plagioclase grains has developed traces of secondary intragranular porosity (D8, H9). Skeletal diatom fragments are very rare in this sample (G11). A detrital mica fragment is visible at G8 of this view.

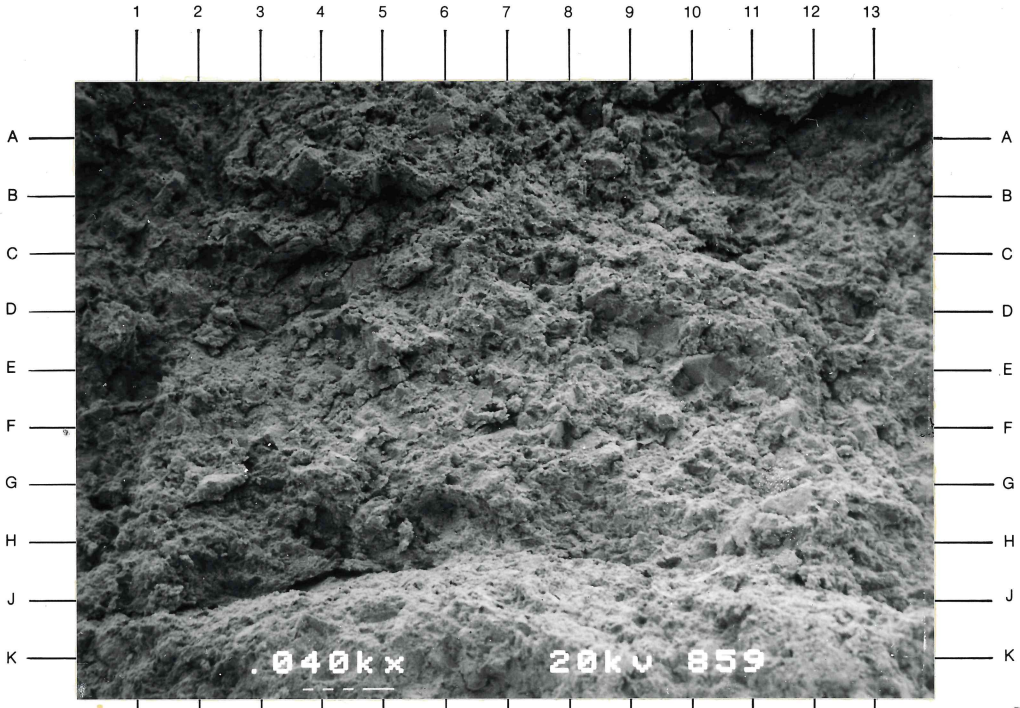

A

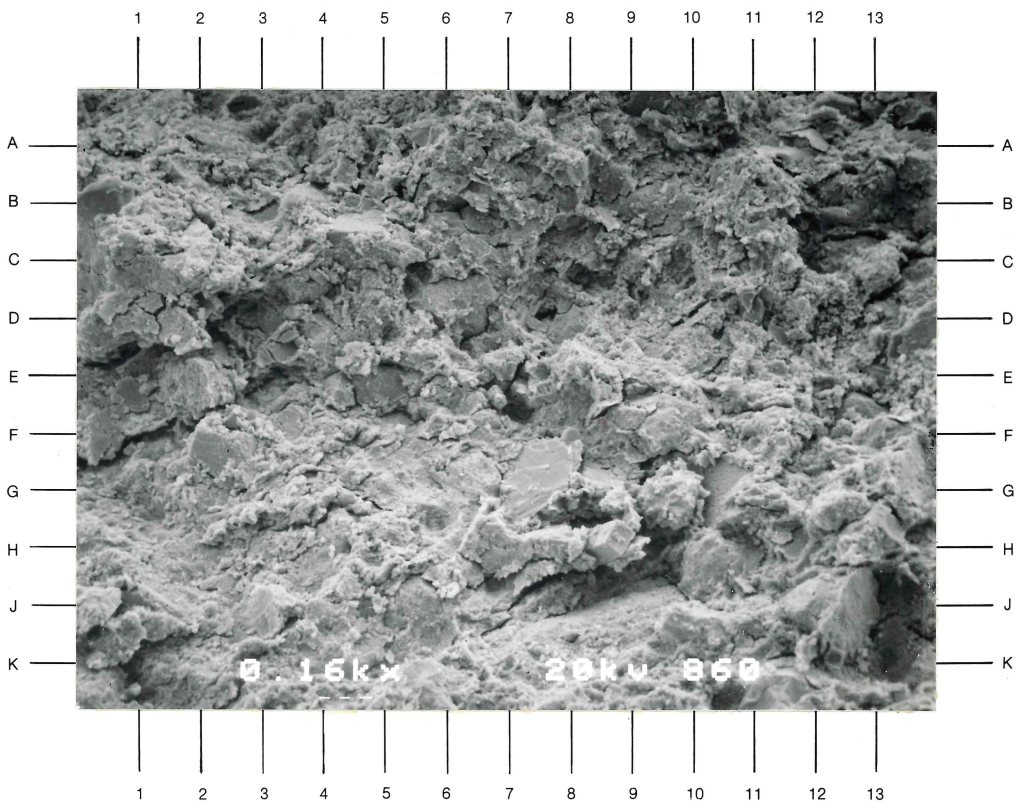

B

CORE LABORATORIES, INC.

Reservoir Geology/Petrographic Services

Amoco Production Company
Nancy No. 1 O.C.S. Y-0719 Well

File Number: PD-85074

Sample Depth: 4232 feet

Plate 12A

A 1250X magnification view of an intragranular pore region in this sandstone sample (refer to H9, Plate 11B). Relict crystals of calcic plagioclase (Spectrum 4; Centers at C10.5, F8, H-J10) have undergone moderate to extensive dissolution, and exhibit partial replacement by authigenic illite (A7.5, D8, G12.5) and crystals of calcite or aragonite (e.g. E1-4, E4-H2.5). Authigenic sodic plagioclase crystals (Spectrum 9) occur along the margins of the pore region (e.g. A5). Note that the calcic plagioclase may have formed phenocrysts in a relict volcanic rock fragment.

Plate 12B

A 2000X magnification photomicrograph of intragranular (dissolution) porosity in this sandstone sample. Authigenic sodic plagioclase crystals form intergrowths at all orientations in a partially dissolved calcic plagioclase grain (relict fragment at E3.5 of this view). The pore-lining to pore-bridging albite crystals cause pore pathways to have complex geometries. Pore throats are very small (approximately 5 to 8 microns in diameter). Fine spheroidal intergrowths of cristobalite crystals (cristobalite lepispheres) have nucleated over authigenic plagioclase in the intragranular pore areas at this location.

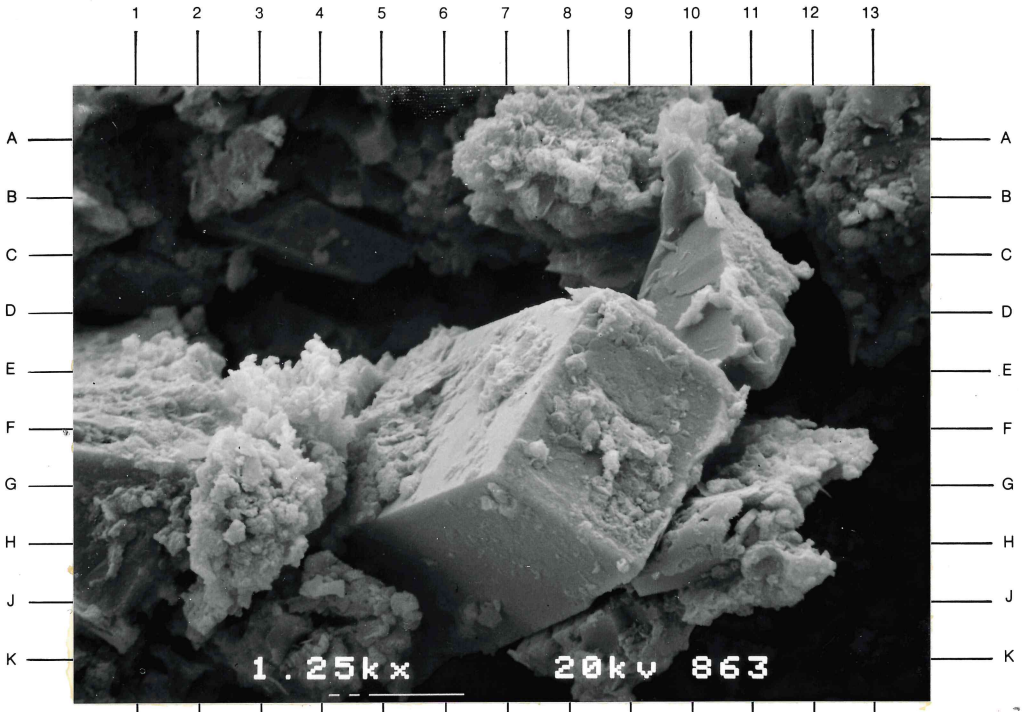
1 2 3 4 5 6 7 8 9 10 11 12 13
A B C D E F G H J K
1.25kx 20kv 863

A

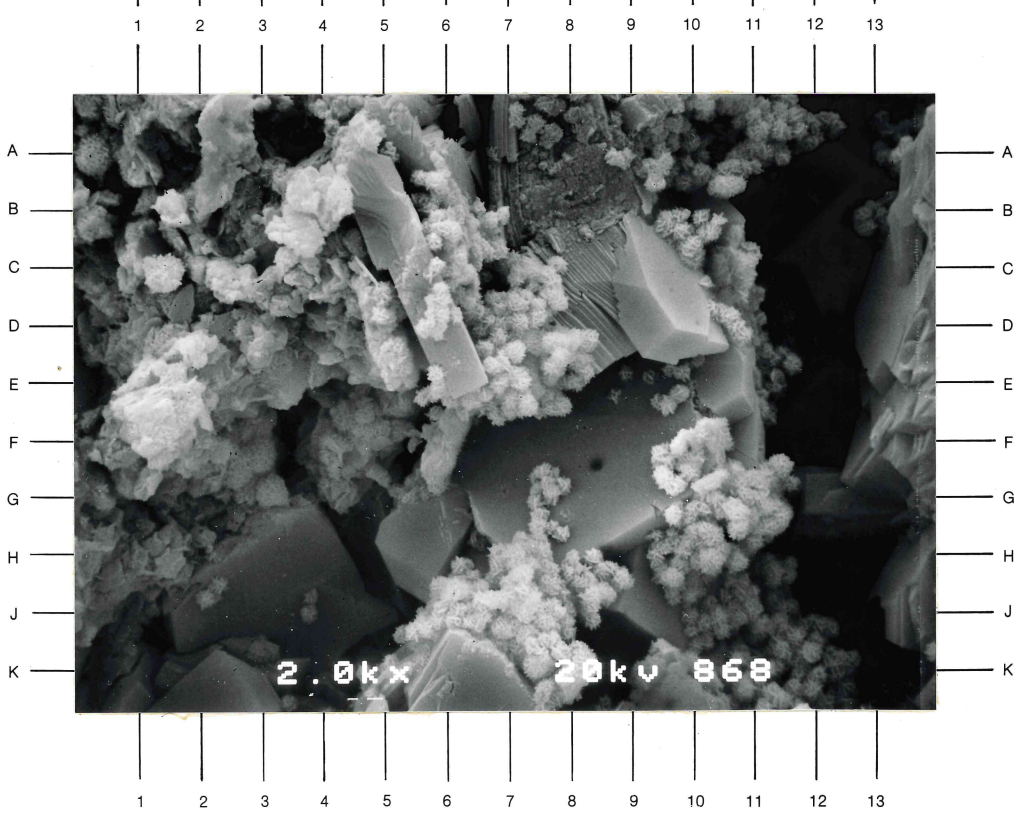
1 2 3 4 5 6 7 8 9 10 11 12 13
A B C D E F G H J K
2.0kx 20kv 868

B

Amoco Production Company
Nancy No. 1 O.C.S. Y-0719 Well

File Number: PD-85074

Sample Depth: 5164 feet

Plate 13A

A 40X magnification view of a poorly to moderately sorted, very fine-grained sandstone or silty sandstone. An indistinct wavy lamination is visible in some locations of this sample (E0.5-D4). Detrital plagioclase (D-E11, H13.5) and quartz (B6, F9, K13) and possible lithic fragments (F11.5) exhibit angular grain shapes and occur in random orientations.

Plate 13B

A 160X magnification photomicrograph of the texture of this sandstone (refer to E3.5, Plate 13A). The irregular wavy lamination of this sample is highlighted by the detrital clay minerals (A8.5-E0, C9-G3). Note the broad range of framework grain sizes of the detrital rock fragment (center at B-C13, F-G7), detrital plagioclase (C10, E10.5), and detrital quartz (C11.5, D11, K9) grains. Detrital clay minerals form the matrix of this sample.

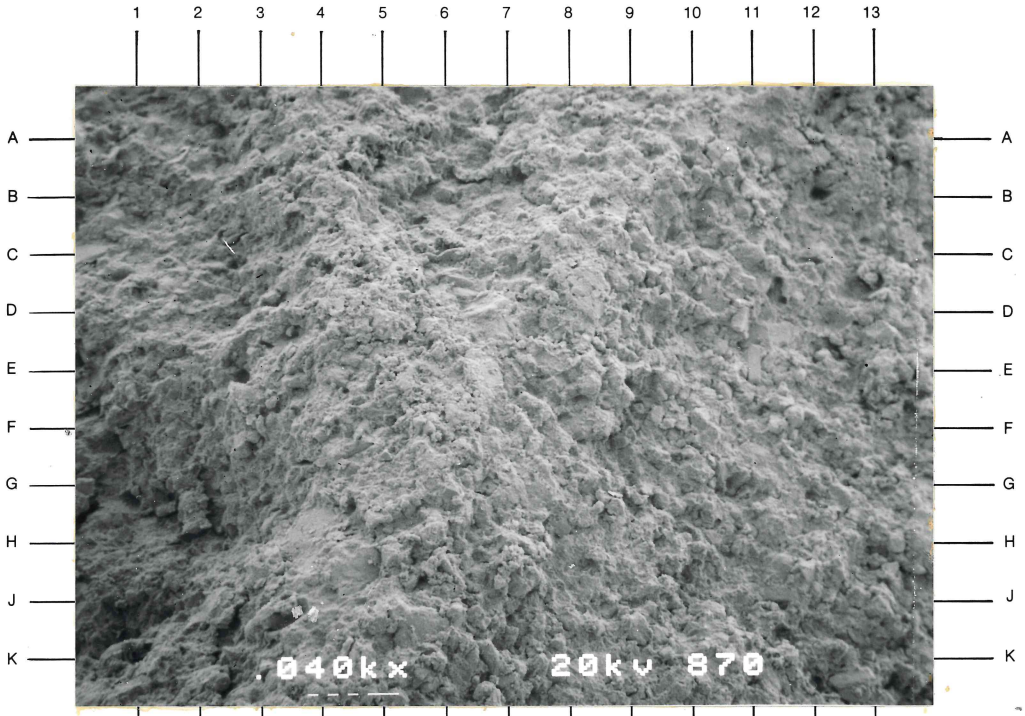

A

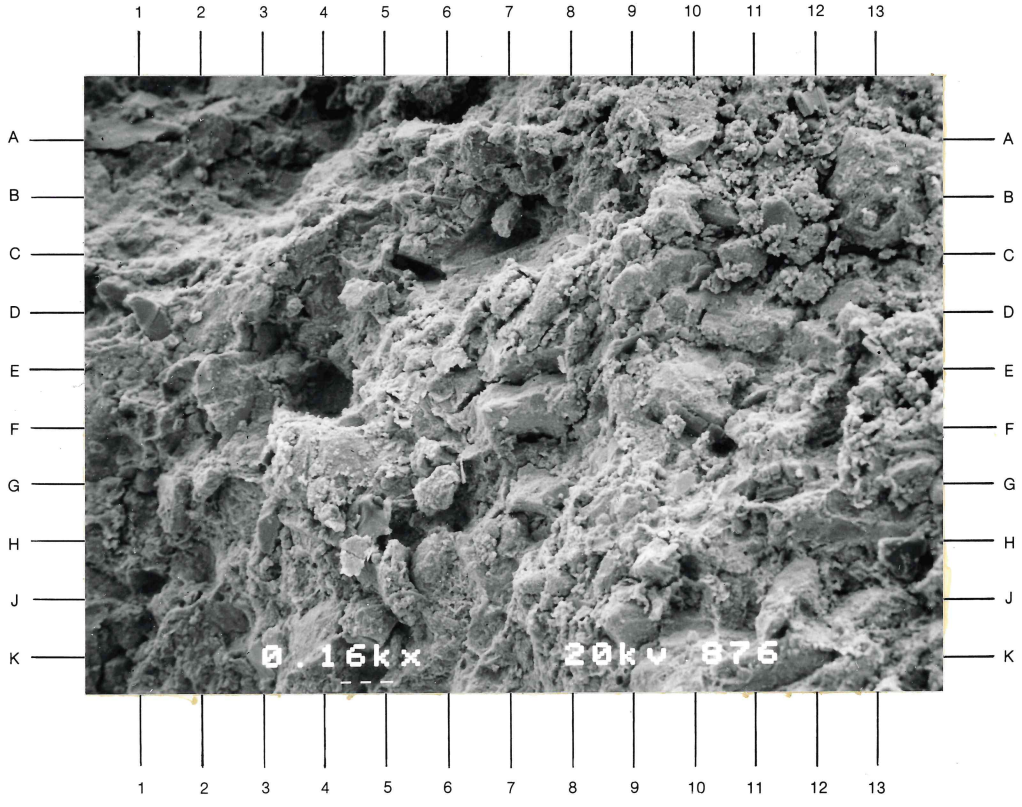

B

CORE LABORATORIES, INC.

Reservoir Geology/Petrographic Services

Amoco Production Company
Nancy No. 1 O.C.S. Y-0719 Well

File Number: PD-85074

Sample Depth: 5164 feet

Plate 14A

A 2000X magnification view of an intergranular area in this sandstone (refer to F-G5, Plate 13B). Irregular flake-like crystals and crystal aggregates of authigenic, mixed-layer illite-smectite clay form coatings on detrital clay minerals and framework grains (e.g. H-K1, A13-D11). Authigenic illite-smectite clay outlines intergranular pore regions which may have originated from dissolution of framework grains (at top center and lower right center of this view). Authigenic illite-smectite inhibited crystals growth of authigenic potassium feldspar (center at G-H6.5). Authigenic illite crystals have nucleated over mixed-layer illite-smectite (B6, B-C7, C7, C9, E8, G8), and over authigenic pyrite crystal aggregates (C4.5). Note that euhedral, authigenic pyrite crystals have nucleated over authigenic mixed-layer illite-smectite and potassium feldspar in this view (D6-6.5, D-E7.5, J5-7).

Plate 14B

A 4500X magnification photomicrograph of the matrix in this sandstone. Authigenic mixed-layer illite-smectite clay forms coatings on detrital chlorite (A-B5 to C6.5) and framework grains. Irregular crystal aggregates of illite-smectite form coatings on the pyrite framboid at lower left center of this view. This pyrite framboid, which is composed of irregular, anhedral to subhedral crystals, does not exhibit intercrystalline porosity. This pyrite framboid may have formed prior to the pyrite crystal aggregates of Plate 14A.

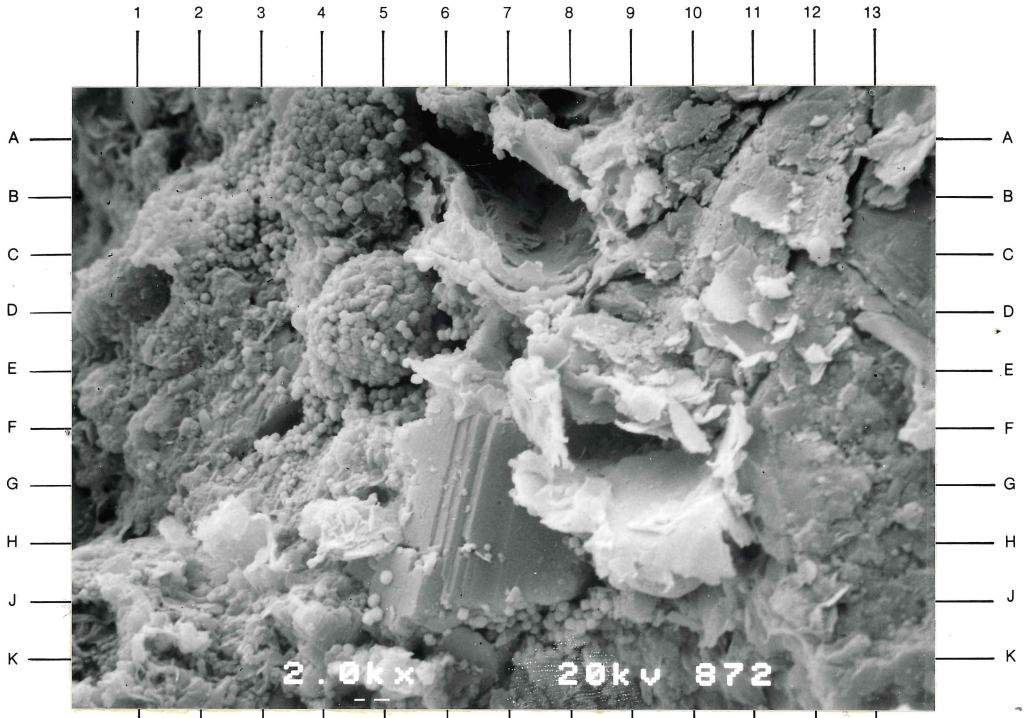
1 2 3 4 5 6 7 8 9 10 11 12 13
A B C D E F G H J K
2.0kx 20kv 872

A

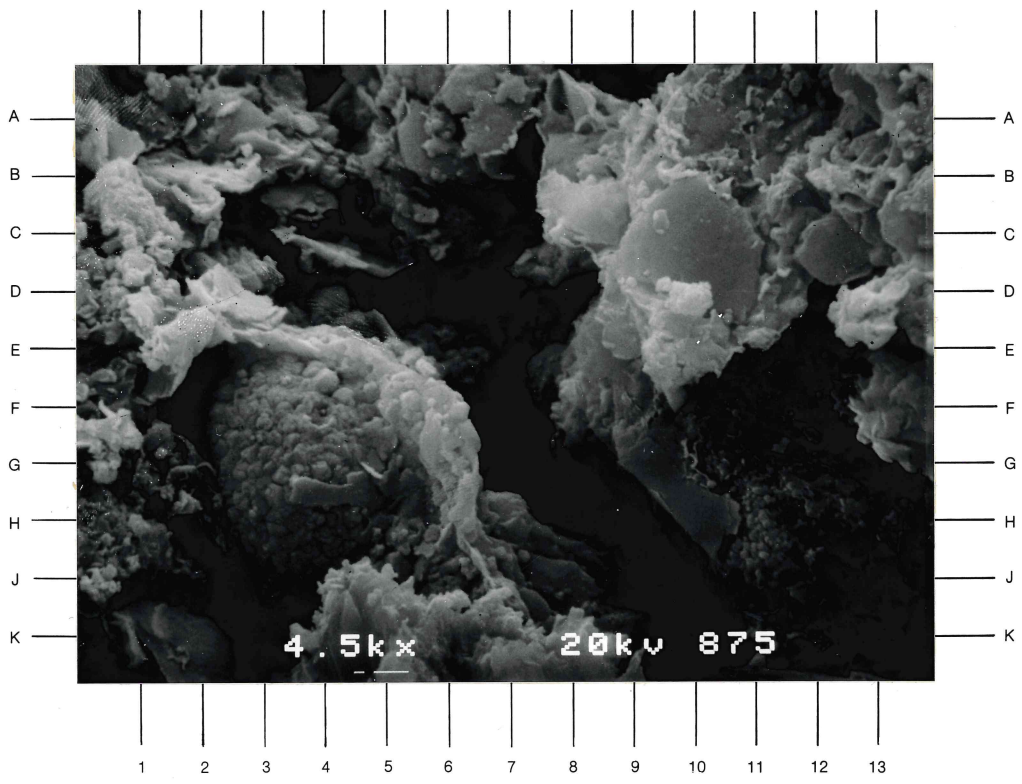
1 2 3 4 5 6 7 8 9 10 11 12 13
A B C D E F G H J K
4.5kx 20kv 875

B

Amoco Production Company
Nancy No. 1 O.C.S. Y-0719 Well

File Number: PD-85074

Sample Depth: 6652 feet

Plate 15A

A 40X magnification view of a poorly sorted, very fine-grained sandy siltstone. Angular grains of quartz (D10, E-F4, E-F11.5), plagioclase (H9, H-J7.5, K7.5), and mica (G0.5), and subrounded lithic fragments (e.g. H7) occur in clay matrix. The apparent disaggregation occurred during sample retrieval.

Plate 15B

A 160X magnification photomicrograph of the texture of this sandy siltstone (refer to H-J12, Plate 15A). Authigenic clay forms coatings on the framework grains and detrital clay matrix, and has occluded most of the intergranular porosity of this sample. Minor intragranular porosity is present due to partial dissolution of detrital plagioclase or rock fragments (e.g. A-B5, B-C6.5, D8).

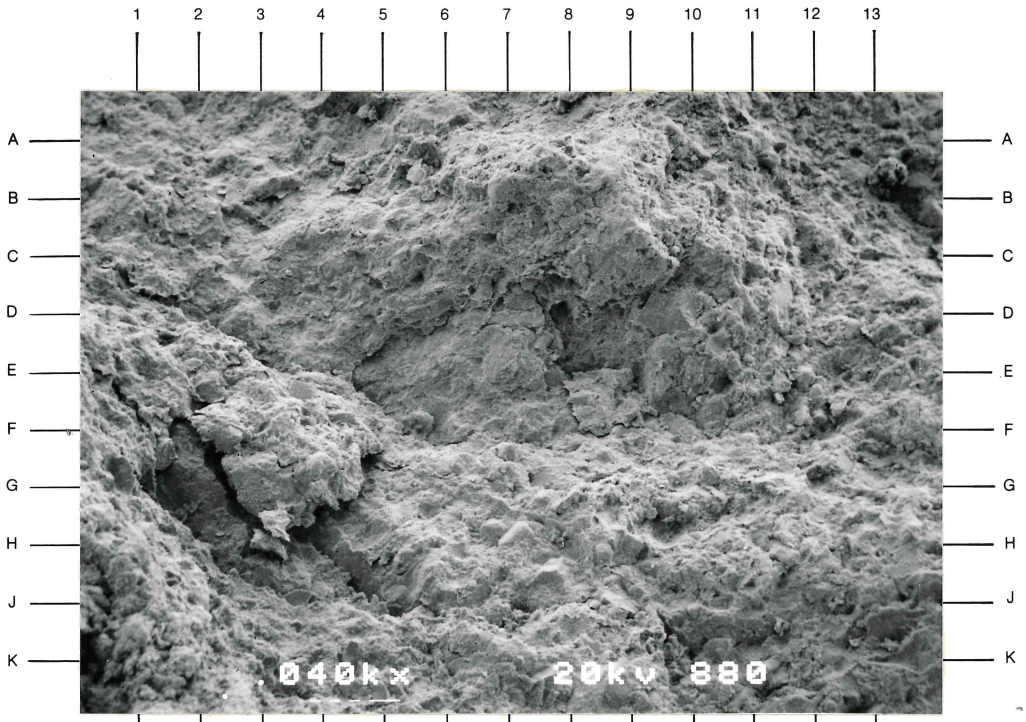

A

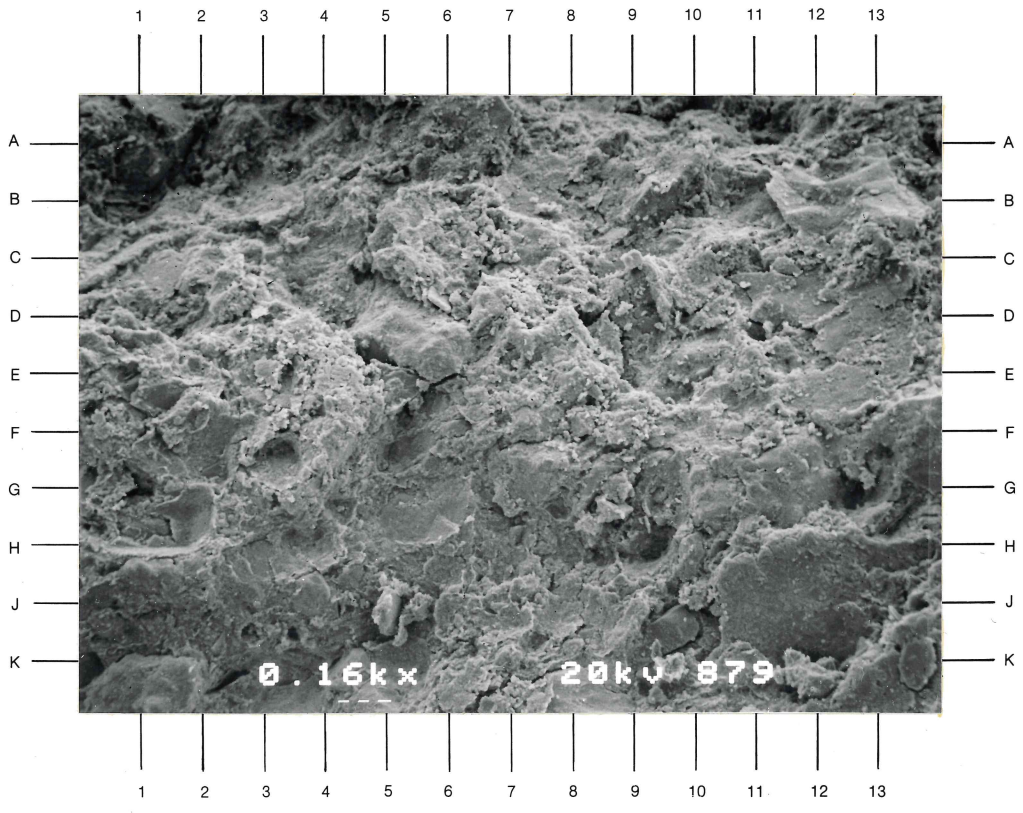

B

CORE LABORATORIES, INC.

Reservoir Geology/Petrographic Services

Amoco Production Company
Nancy No. 1 O.C.S. Y-0719 Well

File Number: PD-85074

Sample Depth: 6652 feet

Plate 16A

A 900X magnification view of an intergranular area in this sandy siltstone (refer to C6.5, Plate 15B). Dissolution of a detrital plagioclase grain resulted in the apparent intragranular porosity at A-B7, B5, C6, and D6-F6.5 of this view. Authigenic mixed-layer illite-smectite clay coats the framework grain constituents (e.g. A0.5-C3). A detrital mica fragment is visible at H-J2 of this view.

Plate 16B

A 3000X magnification photomicrograph of the intragranular porosity in a partially dissolved plagioclase grain (refer to E-F7, Plate 16A). Pore-lining and grain-coating aggregates of authigenic illite-smectite crystals (A5-D7, B8.5-D9, B-C2-E-F2, H-J5) host hair-like fibers or irregular fibrous masses of illite (A-B9.5, F12.5, H11, H6.5). Intragranular pore pathways exhibit complex geometry and not be well interconnected due to authigenic clay occlusion.

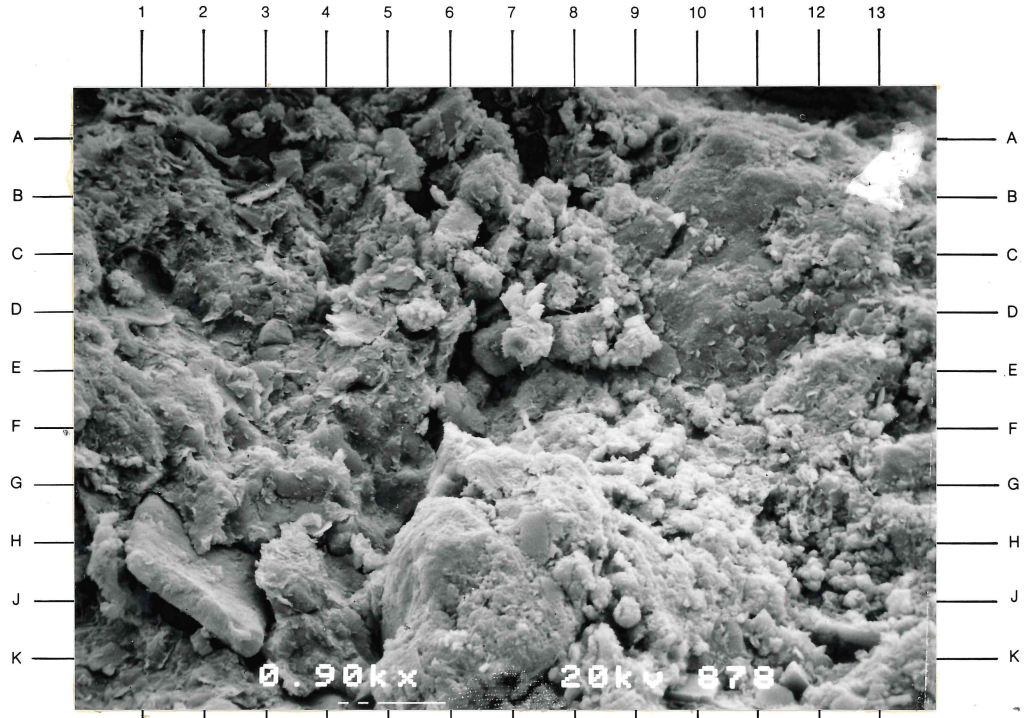

A

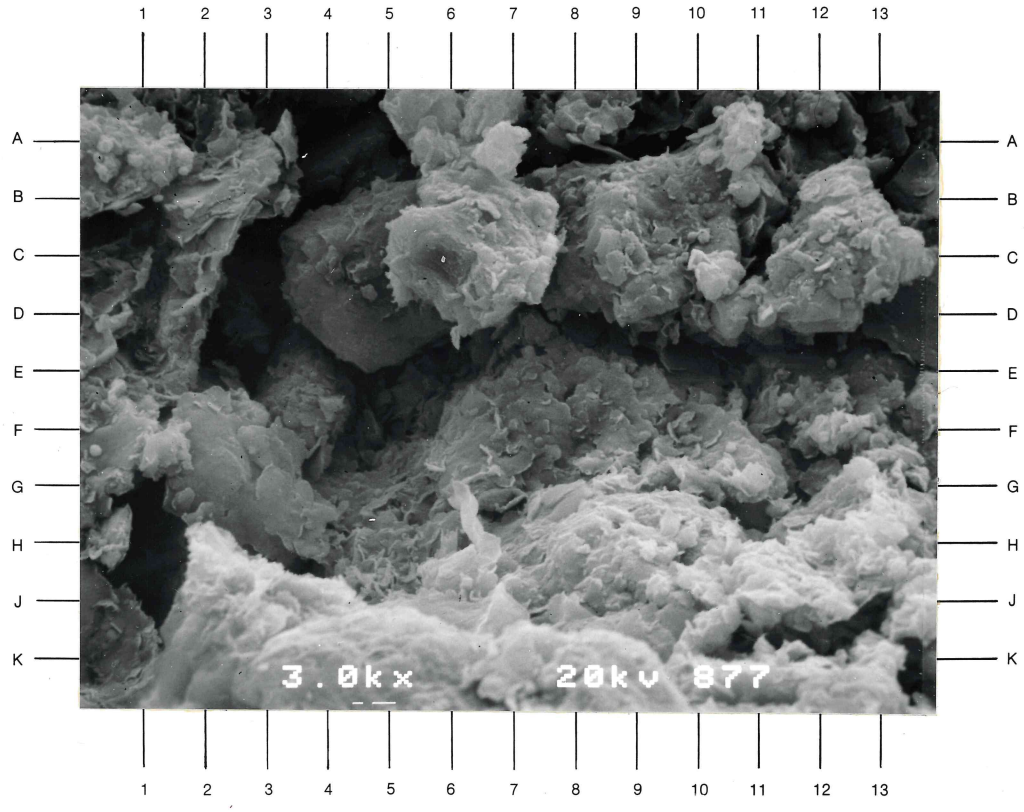

B

CORE LABORATORIES, INC.

Reservoir Geology/Petrographic Services

Amoco Production Company
Nancy No. 1 O.C.S. Y-0719 Well

File Number: PD-85077

Sample Depth: 7229 feet

Plate 17A

A 40X magnification view of a poorly to very poorly sorted, fine-grained sandy siltstone that exhibits indistinct wavy lamination (G1.50F13) and possible cross lamination (G0-J11). Traces of intergranular porosity are visible in rare locations (D4, E7). Angular detrital grains of plagioclase are visible at C-D3 and C9 of this view.

Plate 17B

A 1000X magnification photomicrograph of a partially cemented porous region in this sandy siltstone (refer to E-F7, Plate 17A). Intergrowths of euhedral gypsum crystals (Spectrum 7) have partially (A-C4, D10-G7) to almost totally (E13.5-K9) occluded the visible pore pathways at this location. The optically continuous, gypsum crystal intergrowths may have crystallized in a dissolution void or fissures of this sample. Gypsum crystals exhibit partial dissolution in this open pore region (e.g. A2.5, C1-E2, H-J1.5), and exhibit crystal coatings of authigenic clay (C2-D2.5, E2.5, C3).

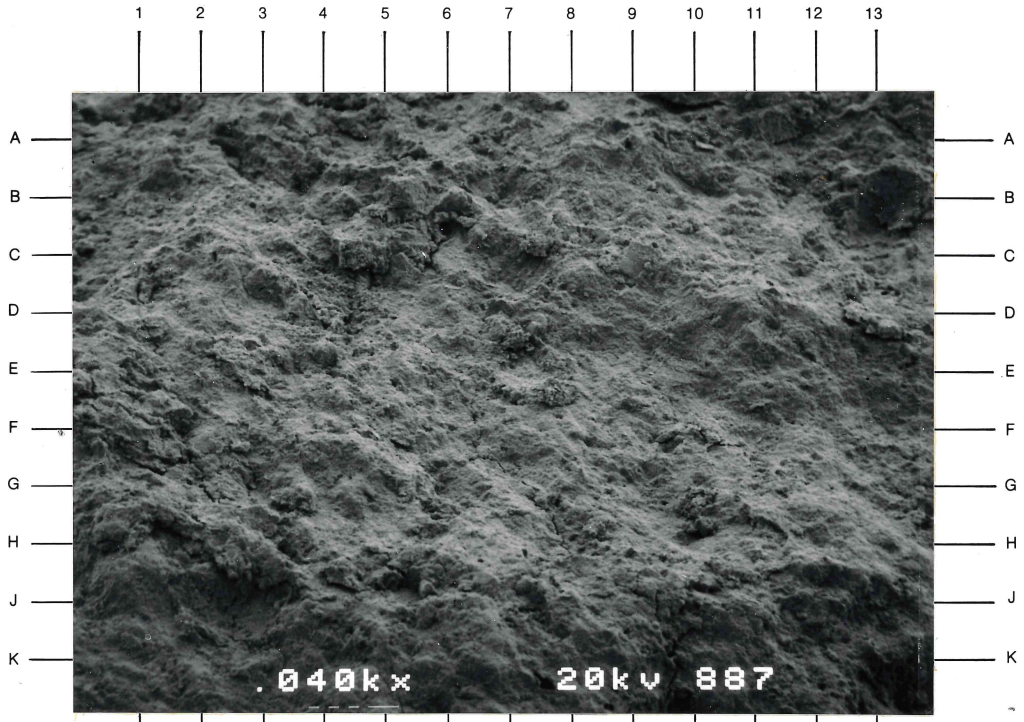

A

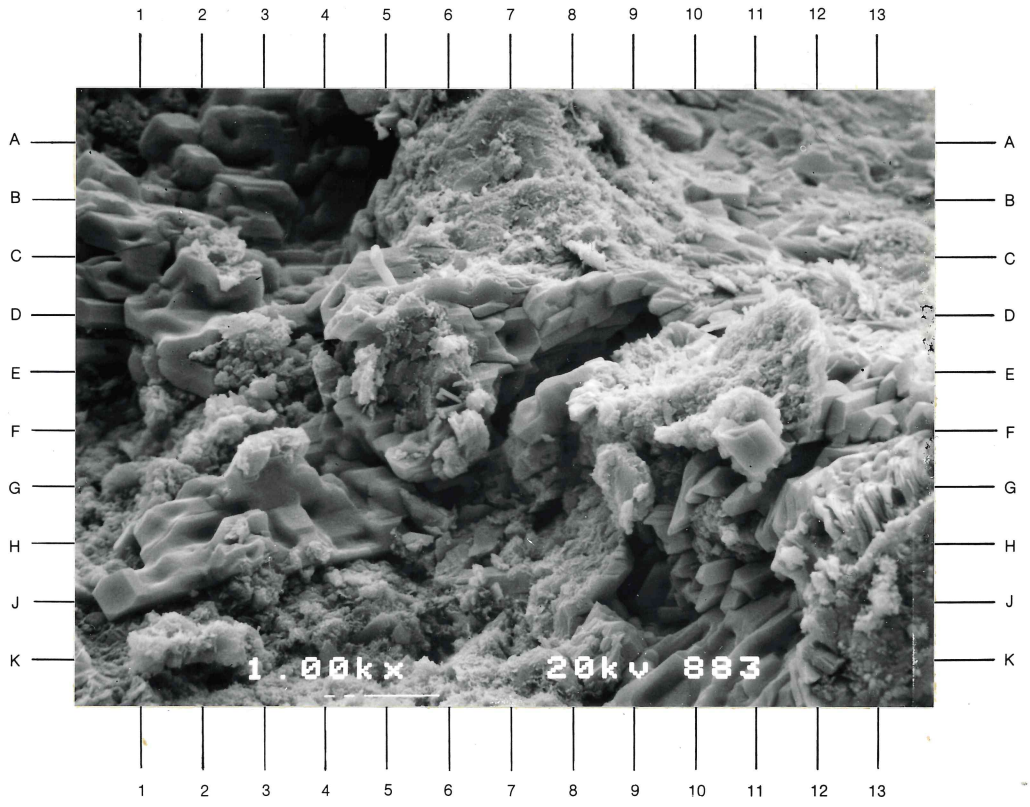

B

CORE LABORATORIES, INC.

Reservoir Geology/Petrographic Services

Amoco Production Company
Nancy No. 1 O.C.S. Y-0719 Well

File Number: PD-85077

Sample Depth: 7229 feet

Plate 18A

A 4000X magnification view of an intercrystalline area of this gypsum-cemented pore region (refer to F12, Plate 17B). An aggregate of detrital chlorite plates (E4.5) exhibits coatings of authigenic mixed-layer illite-smectite (E3). The irregular crystal masses of illite-smectite (A0-F7) and the crystal aggregate of chlorite host wire- or hair-like fibers of authigenic illite (A-B8.5, D5.5). Note the aggregate of stacked, detrital chlorite plates at J13 of this view.

Plate 18B

A 5000X magnification photomicrograph of the authigenic minerals in this pore region (refer to E-F6.5, Plate 17B). Partially dissolved gypsum cement exhibits coatings of irregular, flake-like crystal aggregates of mixed-layer illite-smectite clay (left half of view). Rod-shaped crystals of zeolite (var. Heulandite; Spectrum 5) have crystallized in a dissolution cavity of the gypsum cement (F-G5).

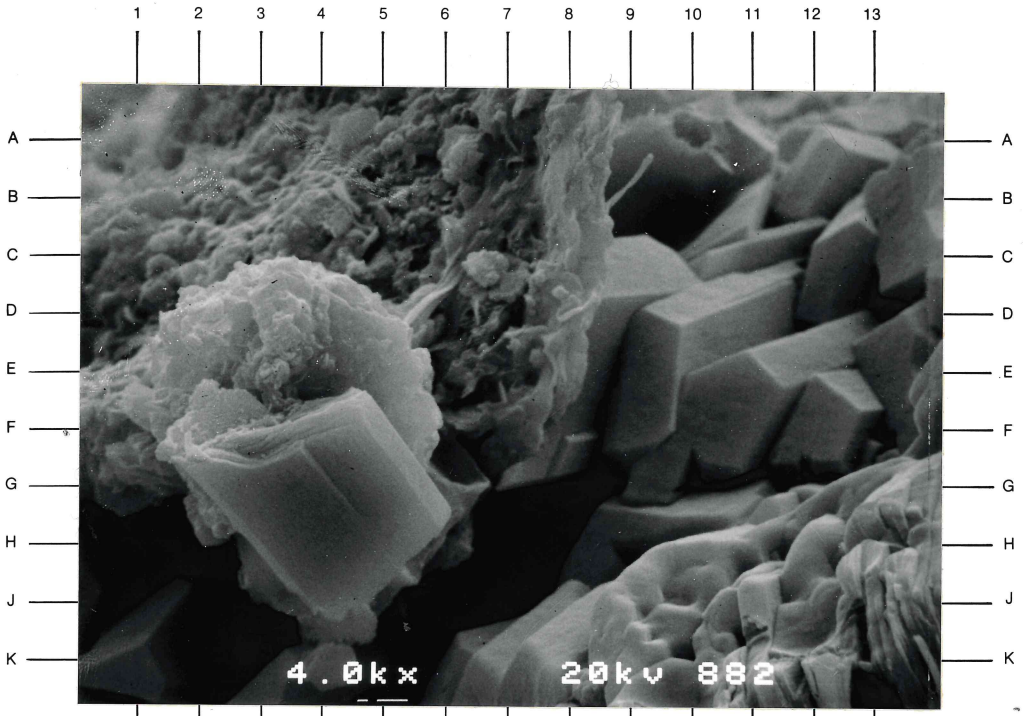

A

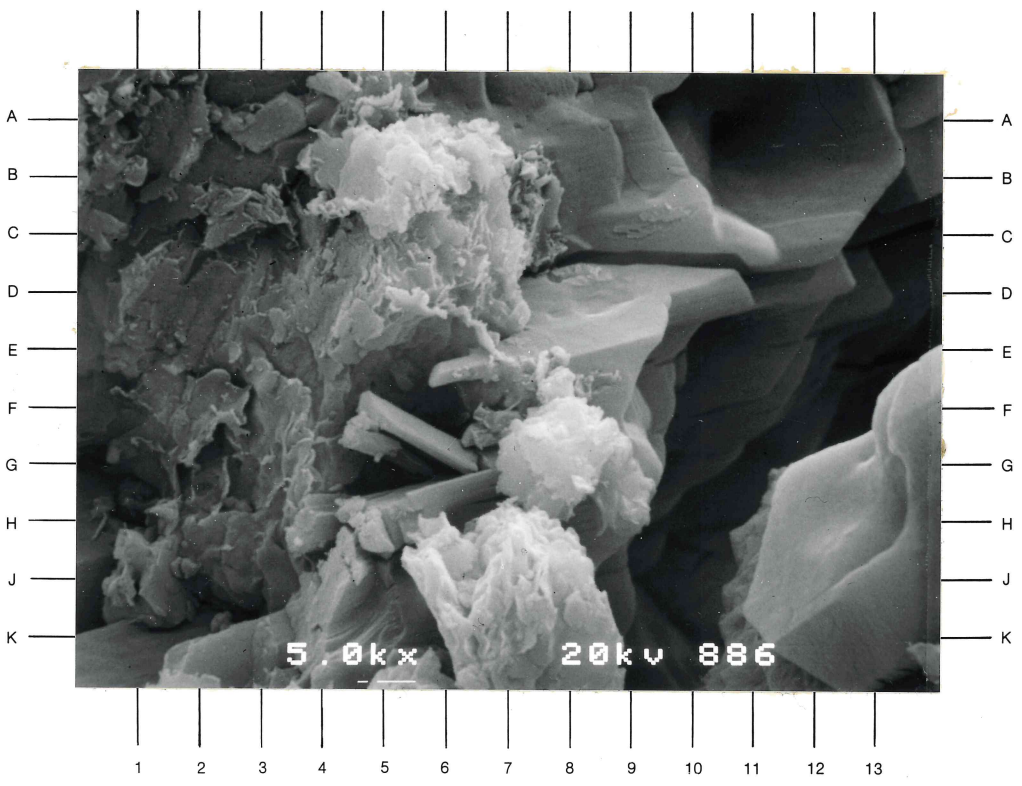

B

CORE LABORATORIES, INC.

Reservoir Geology/Petrographic Services

Amoco Production Company
Nancy No. 1 O.C.S. Y-0719 Well

File Number: PD-85077

Sample Depth: 7413 feet

Plate 19A

A 40X magnification view of a very poorly sorted, medium-grained lithic sandstone that is composed dominantly of subrounded detrital rock fragments (e.g. B-C6.5, B-C9, C-D11, J-K1). Note the broad, framework grain size distribution of this view (B-C6.5, A-B11, E6.5). This sample contains traces of visible porosity (e.g. G3, H9, J11).

Plate 19B

A 160X magnification photomicrograph of the texture of this lithic sandstone. Detrital rock fragments form the principal framework grain constituent of this sample (centers at A-B12.5, D-E9.5, F5, J-K12.5). Partial dissolution of a rock fragment (at B-C2 of this view) has caused development of intragranular porosity. Note the prominent grain-coatings of authigenic clays.

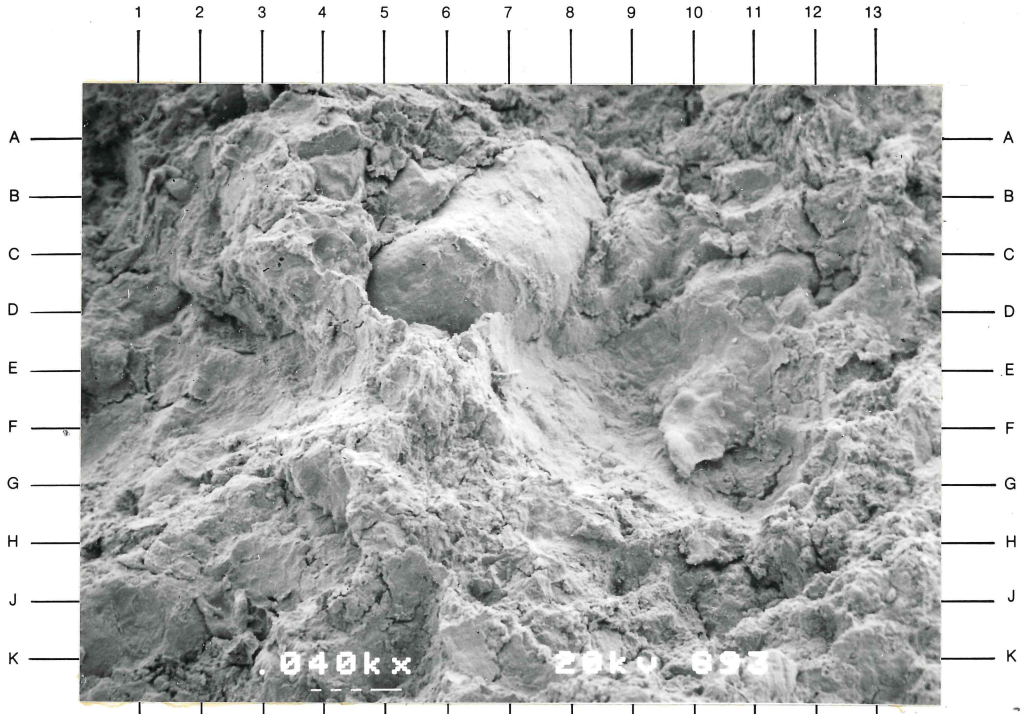

A

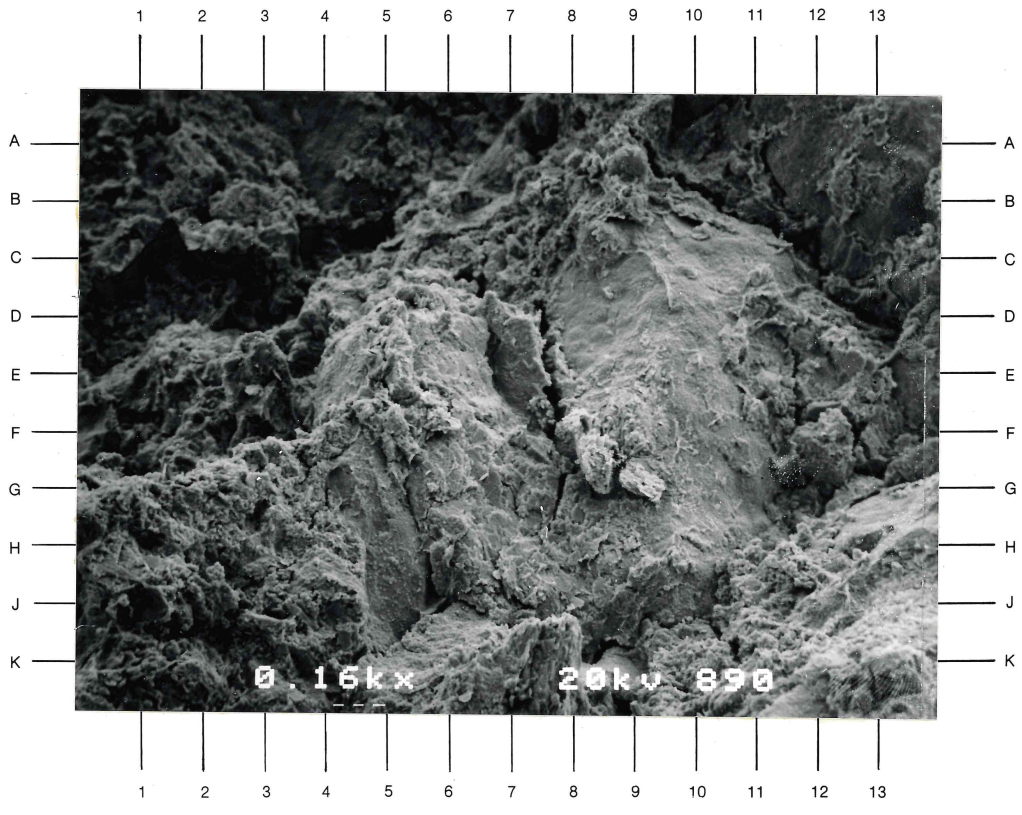

B

CORE LABORATORIES, INC.

Reservoir Geology/Petrographic Services

Amoco Production Company
Nancy No. 1 O.C.S. Y-0719 Well

File Number: PD-85077

Sample Depth: 7413 feet

Plate 20A

A 1500X magnification view of an intragranular pore region in a partially dissolved rock fragment (refer to B-C0.5, Plate 19B). Pore-lining to pore-bridging intergrowths of flake-like authigenic mixed-layer illite-smectite clay have reduced significantly the intragranular porosity of this rock fragment. Visible porosity is dominantly ineffective microporosity among the aggregates of clay crystals. Note that the chlorite plates at J-K4 of this view are not coated with authigenic mixed-layer illite-smectite clay.

Plate 20B

A 4500X magnification view of grain-replacing authigenic mineral constituents (refer to J7, Plate 19A). A relict detrital grain of calcic plagioclase (E-J13.5) exhibits authigenic overgrowths of euhedral sodic plagioclase (A14.5-J8.5). The authigenic albite and the grain-coating aggregates of mixed-layer illite-smectite crystals (G1.5-K6.5) host vermicular stacks of authigenic ferroan chlorite crystals (Spectrum 8; C-D1-H9). The irregular shapes of the authigenic chlorite and albite crystals is relict from sample preparation.

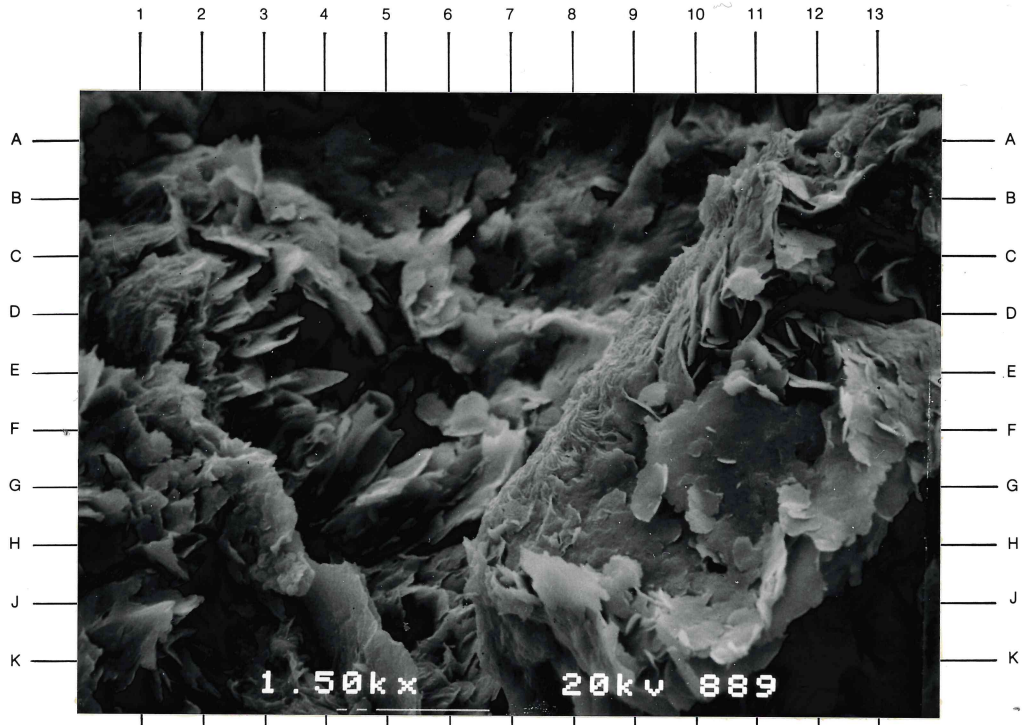

A

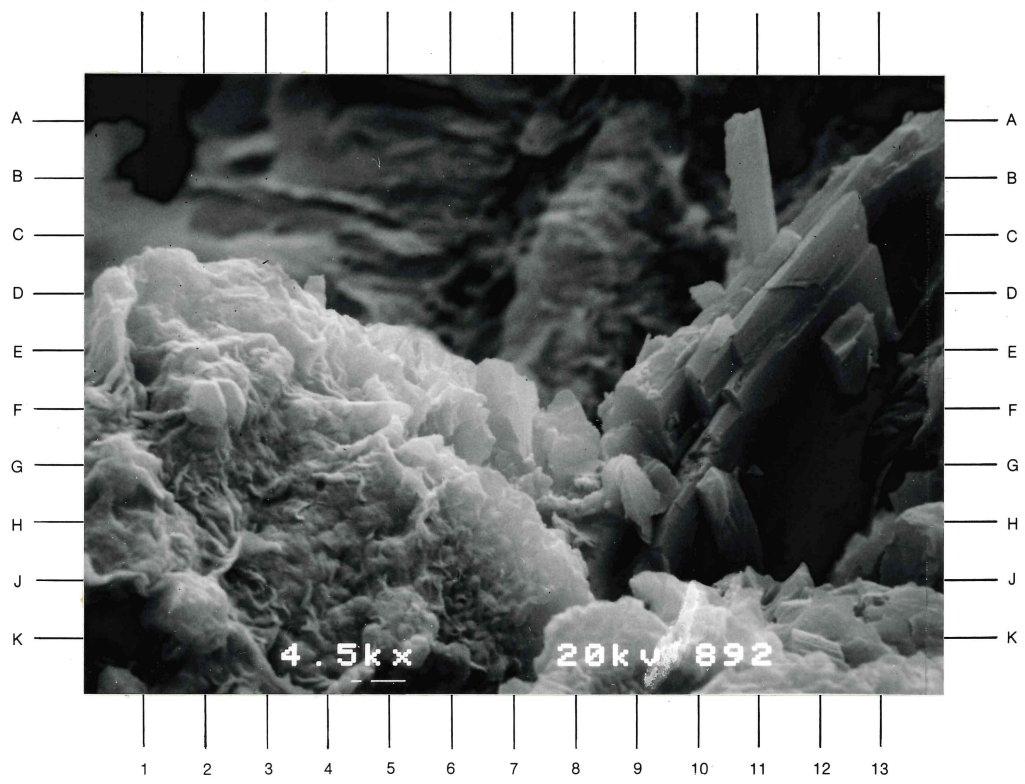

B

CORE LABORATORIES, INC.

Reservoir Geology/Petrographic Services

Amoco Production Company
Nancy No. 1 O.C.S. Y-0719 Well

File Number: PD-85077

Sample Depth: 8051 feet

Plate 21A

A 40X magnification view of a very poorly sorted, fine-grained lithic sandstone that is composed dominantly of irregular-shaped rock fragments (e.g. A2.5, B1.5, C2.5, D1.5, E-F0.5). The lithic fragments exhibit a broad range of framework grain size (center at D3.5, C7.5). Note that sample fracturing follows the boundaries of these deformed rock fragments (e.g. K4-H13).

Plate 21B

A 500X magnification view of intragranular porosity in partially dissolved rock fragments (refer to E6, Plate 21A). Three rock fragments (centers at B7, H6, H-J12.5) exhibit minor to extensive dissolution and partial replacement by authigenic clay minerals. Note that the highly irregular grain boundaries of these rock fragments may be attributed to grain deformation during compaction (e.g. E-J10 to F-G13.5).

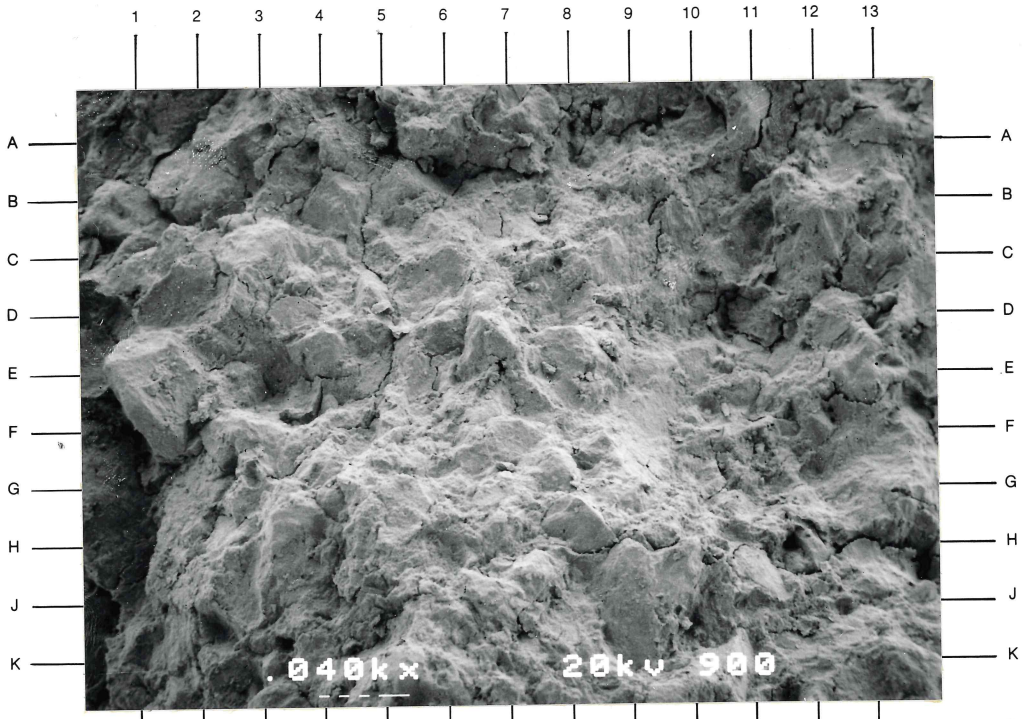
1 2 3 4 5 6 7 8 9 10 11 12 13
A B C D E F G H J K
.040kx 20kv 900

A

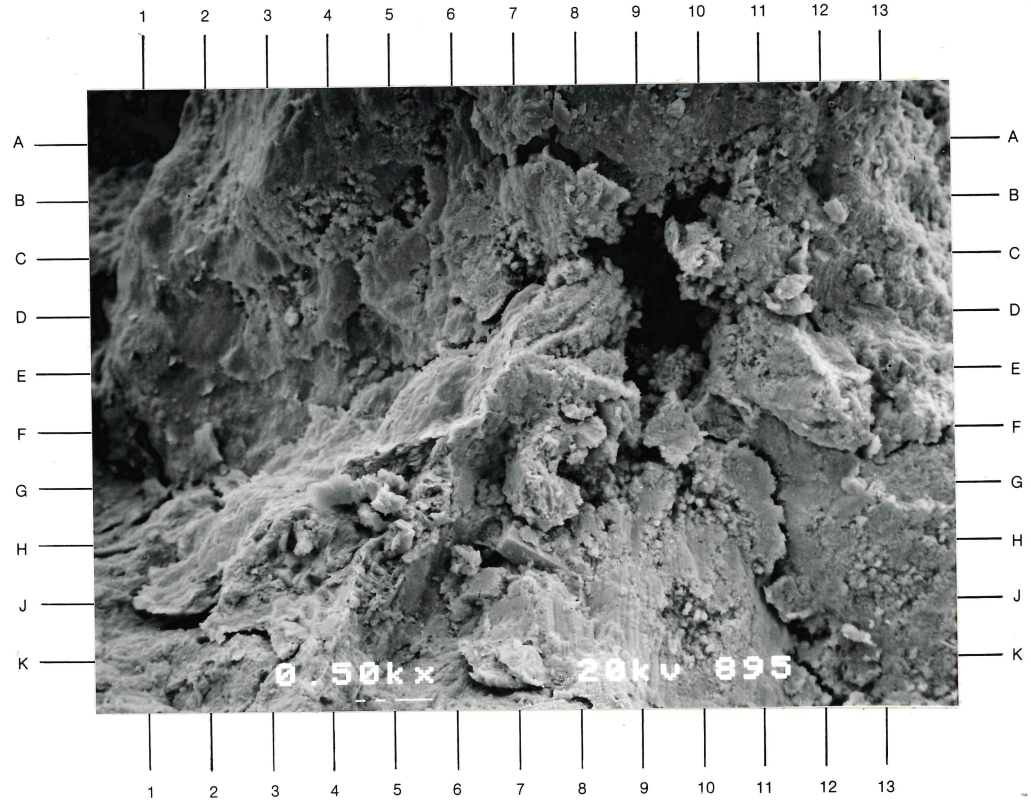
1 2 3 4 5 6 7 8 9 10 11 12 13
A B C D E F G H J K
0.50kx 20kv 895

B

Amoco Production Company
Nancy No. 1 O.C.S. Y-0719 Well

File Number: PD-85077

Sample Depth: 8051 feet

Plate 22A

A 1500X magnification view of an intragranular pore region in a partially dissolved rock fragment (refer to D9, Plate 21B). Irregular flake-shaped crystals and crystal aggregates of mixed-layer illite-smectite form coatings on the relict detrital rock fragment (e.g. C5 to G-H0.5, H4-5). Vermicular crystal aggregates of ferroan chlorite have nucleated along pore walls and in pore pathways. Note the small diameters (less than 5 microns) of the multiple pore throats in this dissolution pore area (B4.5, B6.5, G7, J9). The effective interconnection of pore pathways is reduced significantly by the authigenic chlorite.

Plate 22B

A 2000X magnification photomicrograph of the authigenic mineral constituents in a dissolution pore area (refer to G8, Plate 21B). Relict calcic plagioclase crystals exhibit minor (J3) to extensive (E4) dissolution and replacement by authigenic mixed-layer illite-smectite and illite clay minerals (e.g. E2-G3) and authigenic sodic plagioclase crystals (A-B7, B4, G-H2). The relict plagioclase crystals may have originated as phenocrysts in this partially dissolved rock fragment. Note the partial pore occlusion by the vermiform aggregates of ferroan chlorite crystals. Vermiform chlorite is the latest authigenic mineral in this sample.

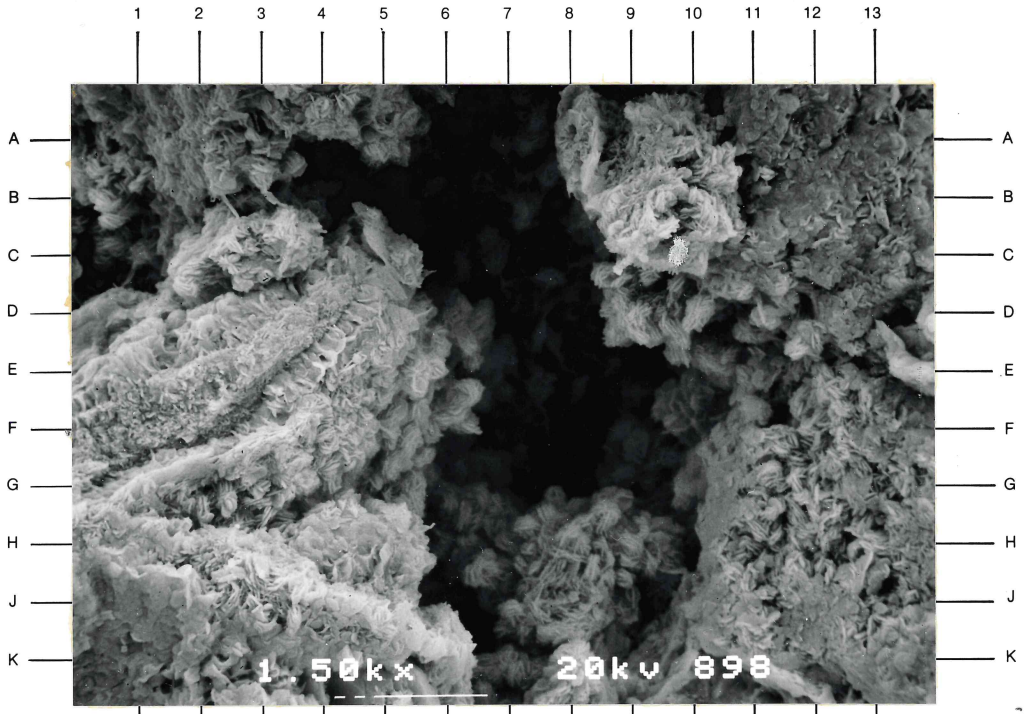
1 2 3 4 5 6 7 8 9 10 11 12 13
A B C D E F G H J K
1.50kx 20kv 898

A

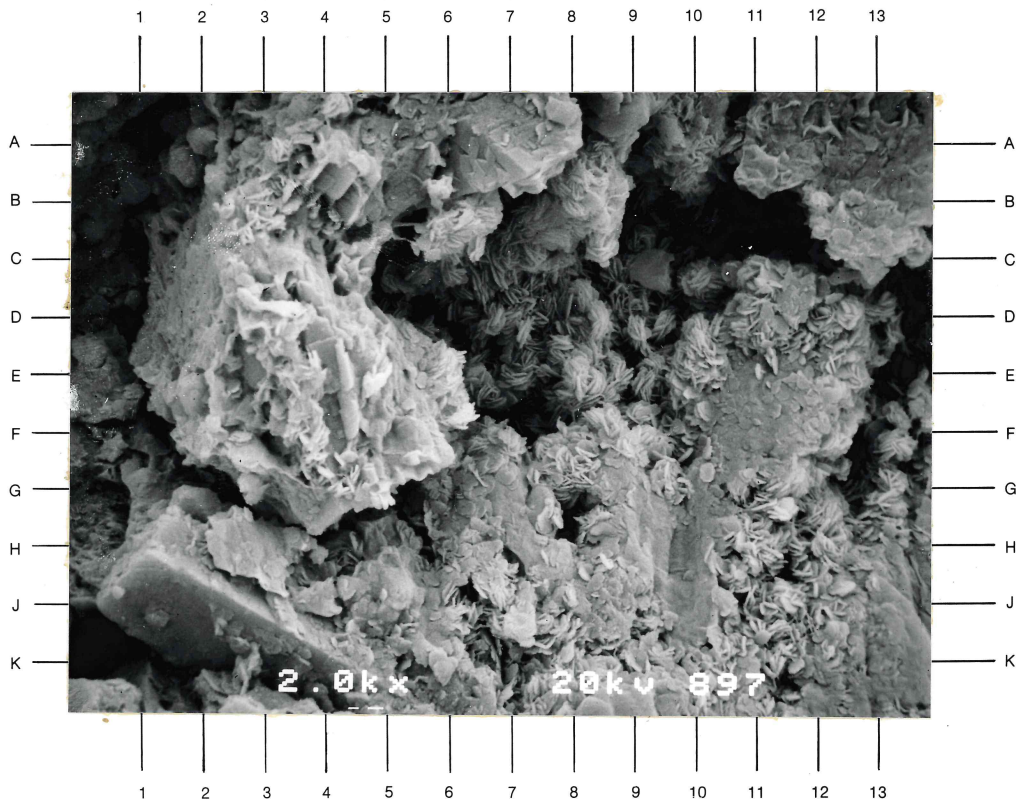
1 2 3 4 5 6 7 8 9 10 11 12 13
A B C D E F G H J K
2.0kx 20kv 897

B

Amoco Production Company
Nancy No. 1 O.C.S. Y-0719 Well

File Number: PD-85066

Sample Depth: 2462 feet

Plate 23A

A 40X magnification, plane polarized light view of a moderately to poorly sorted, diatomaceous siltstone. Framework grains are composed of silt- to sand-size quartz (E11-12), plagioclase (A12-13), carbonate (F-G13-14), mica (K-10) and volcanic rock fragments (G-H13). The lighter colored region in the left half of the view is the original (undisrupted) matrix; the microporous region (blue color) of the right half of the view is bioturbated. Crystalline aggregates of pyrite (C8, F8, G8) and glauconite (A15.5) are present in the bioturbated areas.

Plate 23B

A 160X magnification, plane polarized light photomicrograph of the region from E-G8-9 of Plate 23A (rotated 90° to the left). Two large crystalline aggregates of pyrite (black) are present in the center of the view. Some of the intraskeletal porosity (A15, C6) is occluded by pyrite. Diatom fragments are very abundant. Devitrified volcanic rock fragments (J-K 3-4, B-C 11-12), detrital plagioclase (H8), quartz grains, and clay minerals form lesser percentages of this sample.

TN-5400 Core Labs Aurora,CO. MON 23-DEC-85 11:03

Cursor: 0.000keV = 0

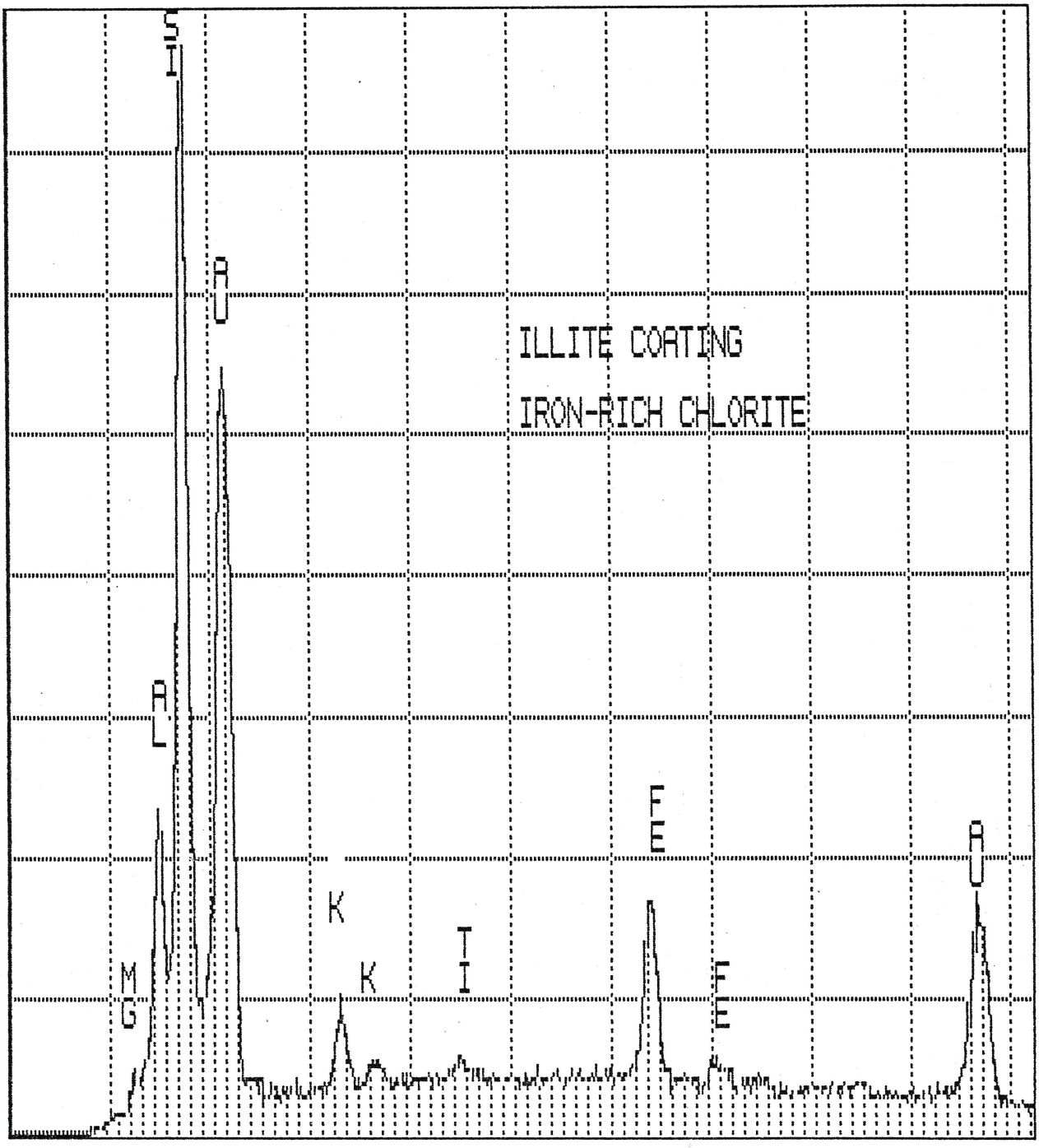

0.000 VFS = 1024 10.240

75 AMOCO PROD.; PD-85066; SAMPLE DEPTH: 2462 FT

Spectrum 1

TN-5400 Core Labs Aurora,CO. MON 23-DEC-85 15:06

Cursor: 0.000keV = 0

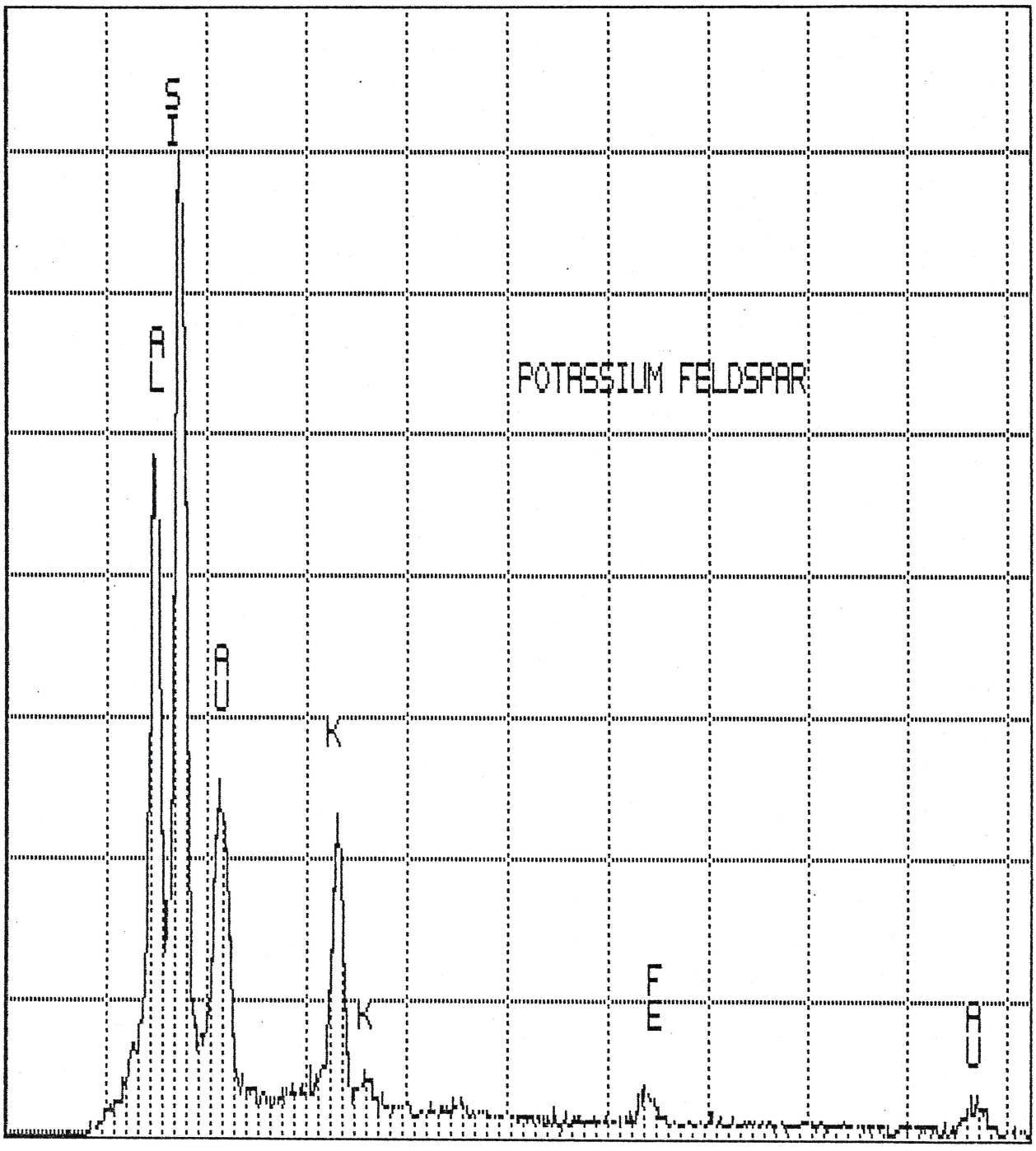

0.000 VFS = 512 10.240

30 AMOCO PROD.; PD-85066; SAMPLE DEPTH: 2950 FT

Spectrum 2

TN-5400 Core Labs Aurora,CO. THU 26-DEC-85 16:07
Cursor: 0.000keV = 0

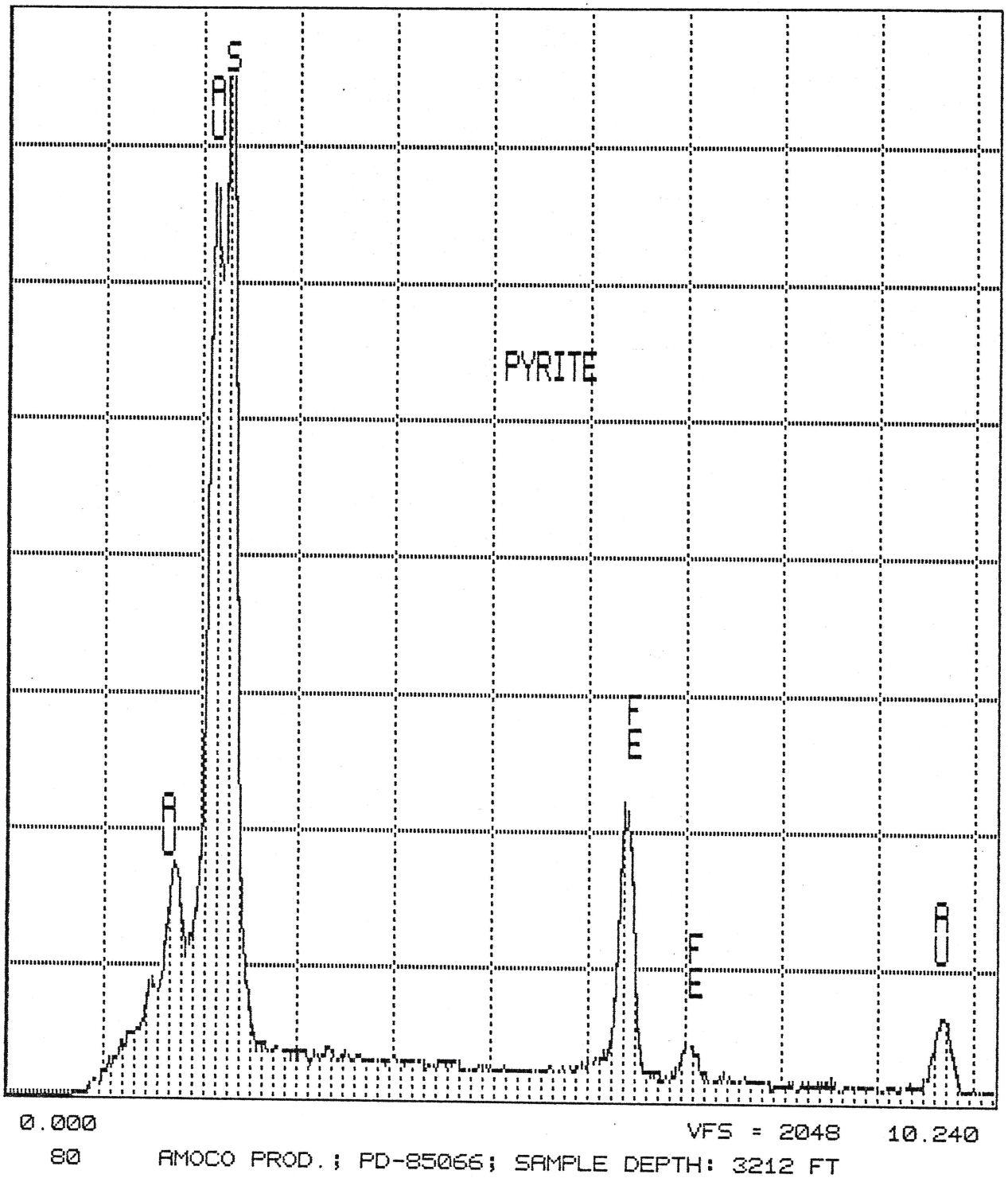

Spectrum 3

TN-5400 Core Labs Aurora,CO. FRI 27-DEC-85 16:03

Cursor: 0.000keV = 0

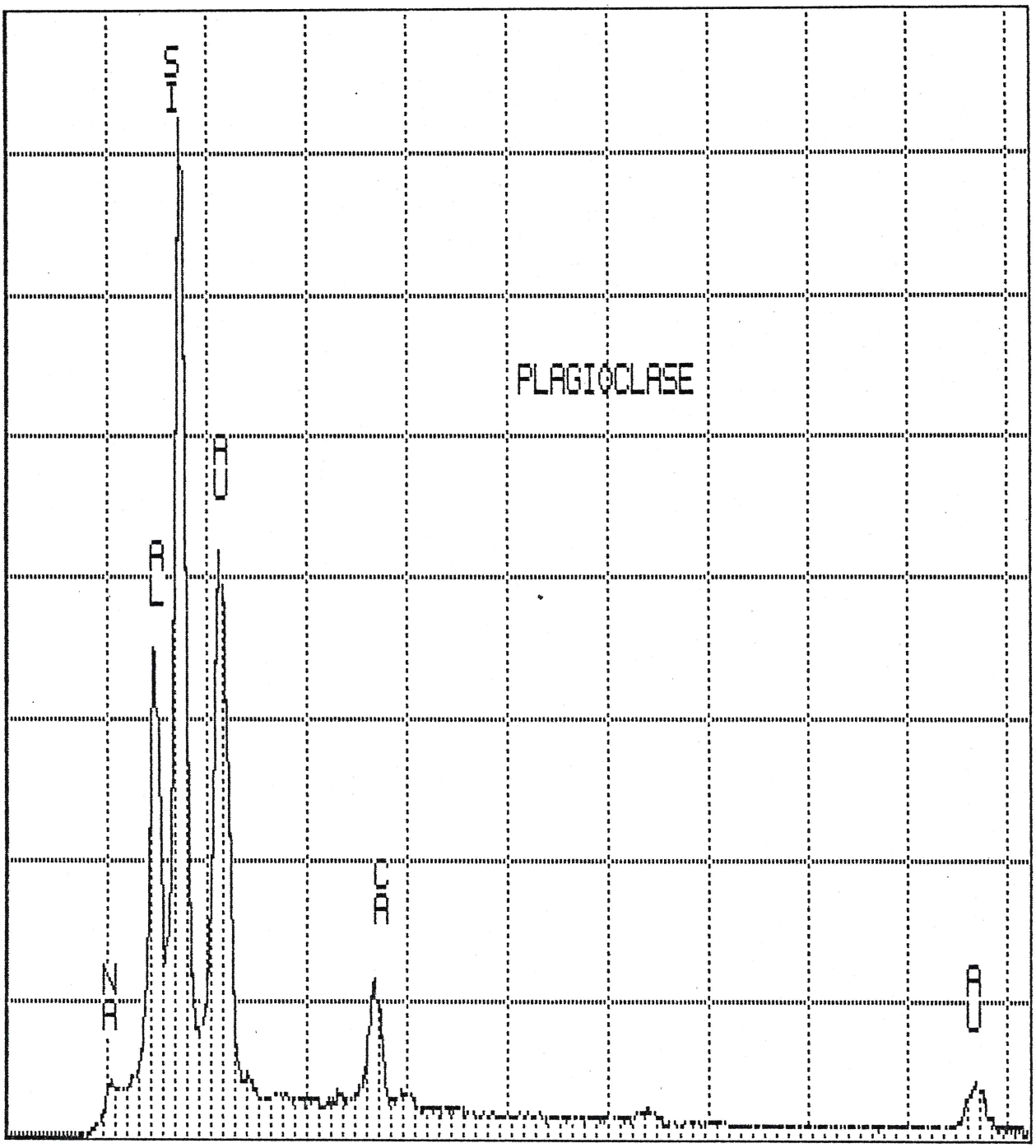

65 AMOCO PROD.; PD-85066; SAMPLE DEPTH: 4104 FT

Spectrum 4

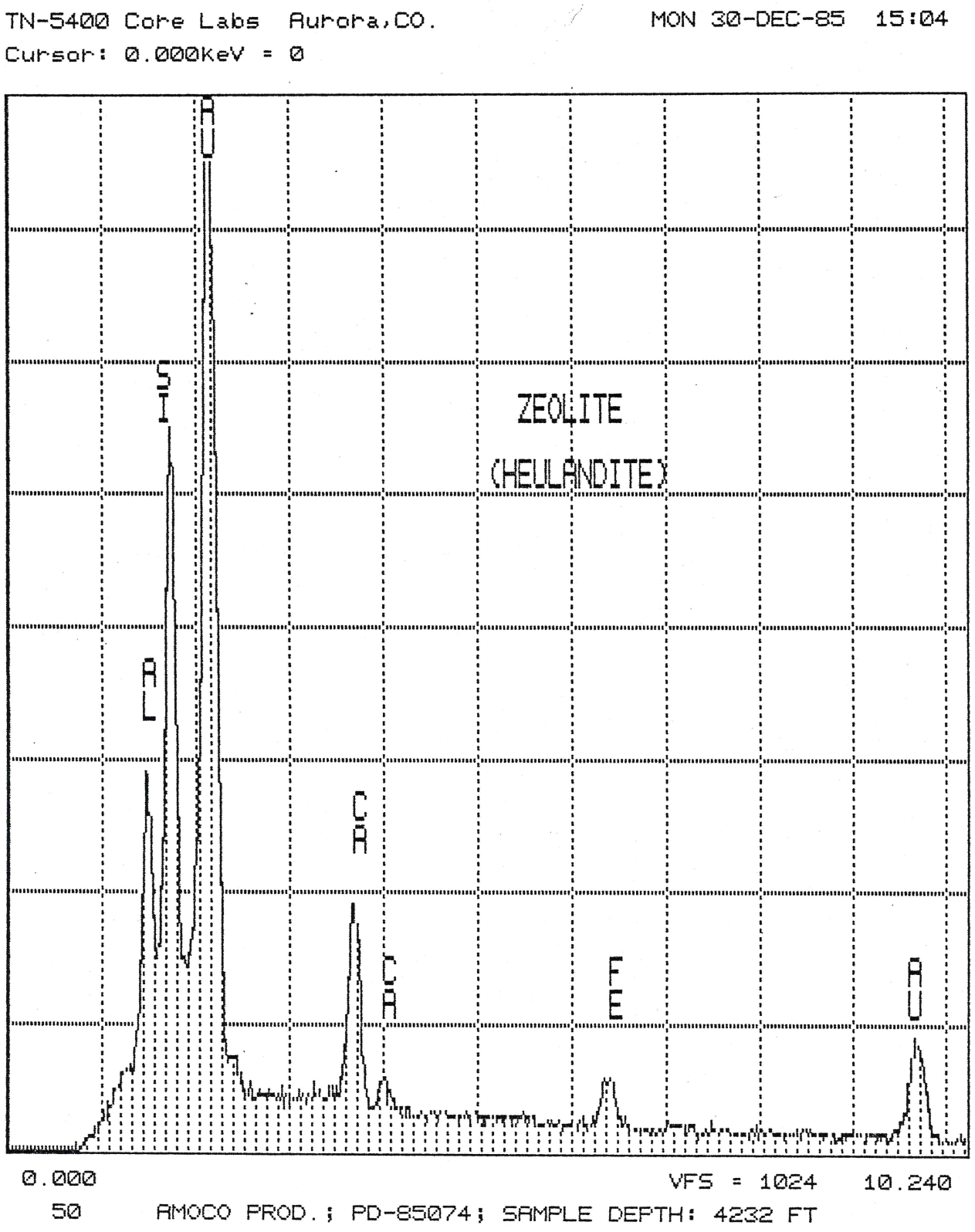
TN-5400 Core Labs Aurora,CO.
MON 30-DEC-85 15:04
Cursor: 0.000keV = 0
AU
SI
AL
CA
CA
FE
AU
ZEOLITE
(HEULANDITE)
0.000
VFS = 1024
10.240
50
AMOCO PROD.; PD-85074; SAMPLE DEPTH: 4232 FT

Spectrum 5

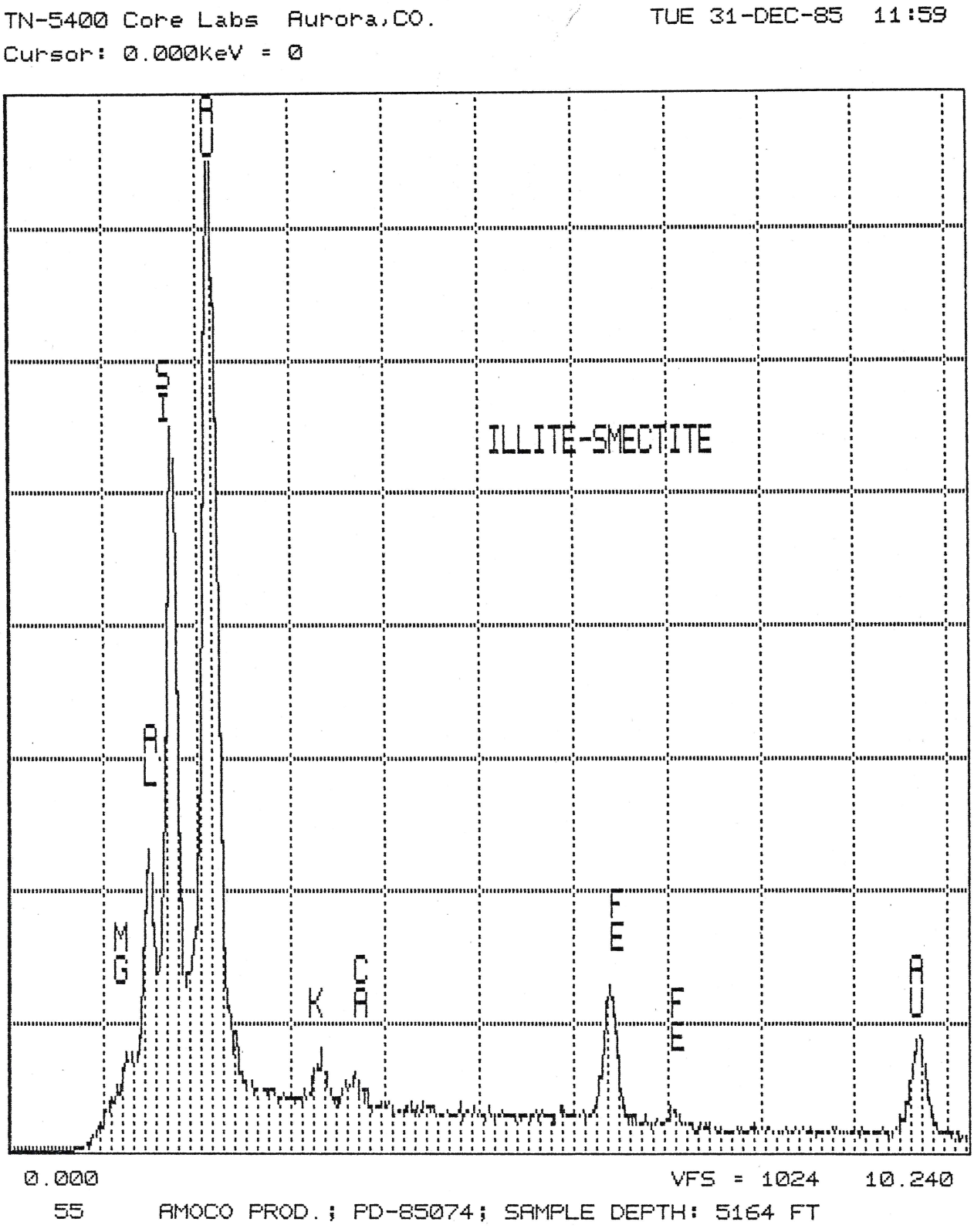
TN-5400 Core Labs Aurora,CO.
TUE 31-DEC-85 11:59
Cursor: 0.000KeV = 0
ILLITE-SMECTITE
0.000
VFS = 1024
10.240
55 AMOCO PROD.; PD-85074; SAMPLE DEPTH: 5164 FT

Spectrum 6

TN-5400 Core Labs Aurora,CO. THU 02-JAN-86 10:40

Cursor: 0.000KeV = 0

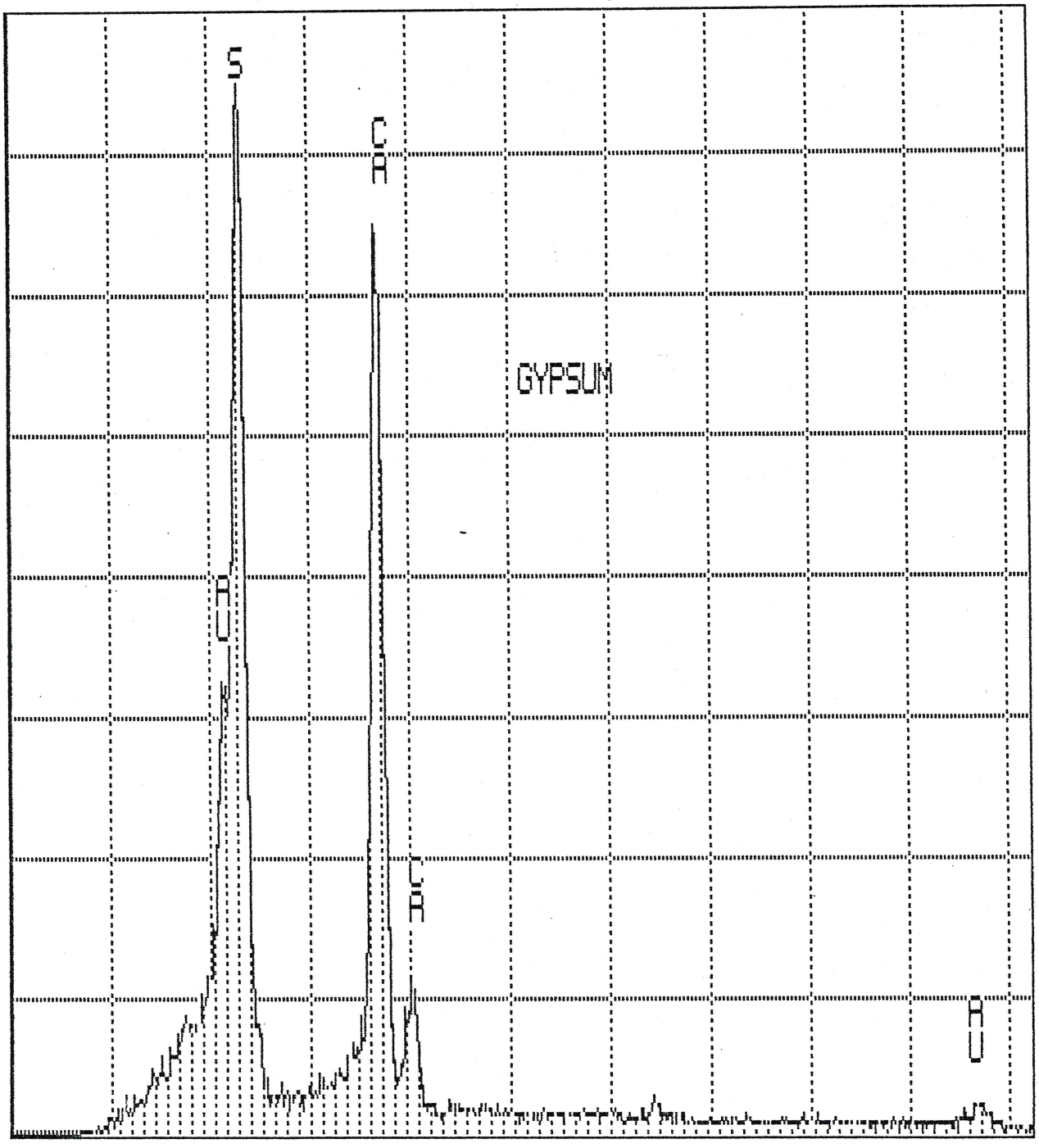

0.000 VFS = 512 10.240

35 AMOCO PROD.; PD-85077; SAMPLE DEPTH: 7229 FT

Spectrum 7

TN-5400 Core Labs Aurora,CO. THU 02-JAN-86 15:57

Cursor: 0.000keV = 0

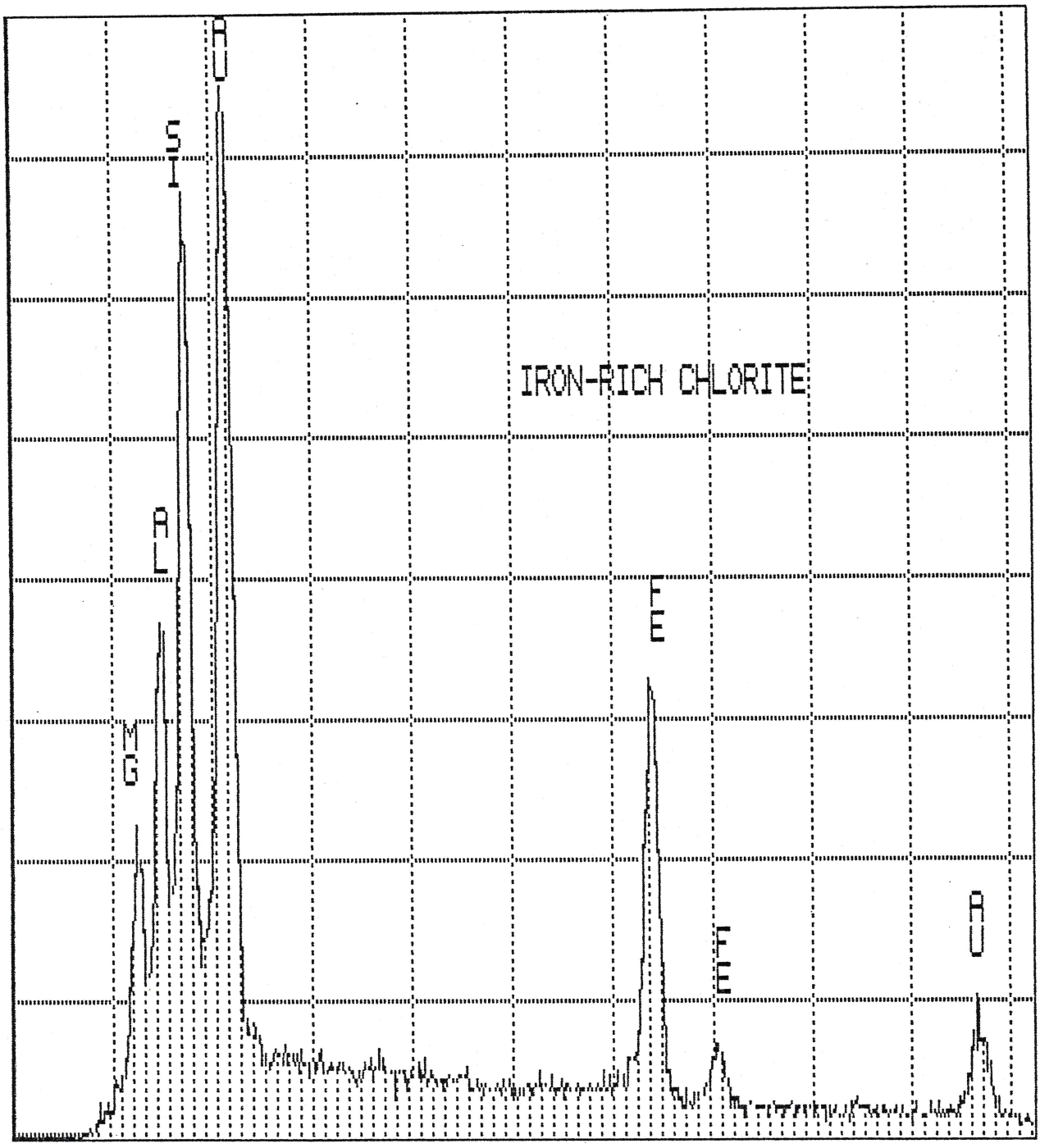

0.000 VFS = 512 10.240

35 AMOCO PROD.; PD-85077; SAMPLE DEPTH: 7413 FT

Spectrum 8

TN-5400 Core Labs Aurora,CO. FRI 03-JAN-86 09:39

Cursor: 0.000keV = 0

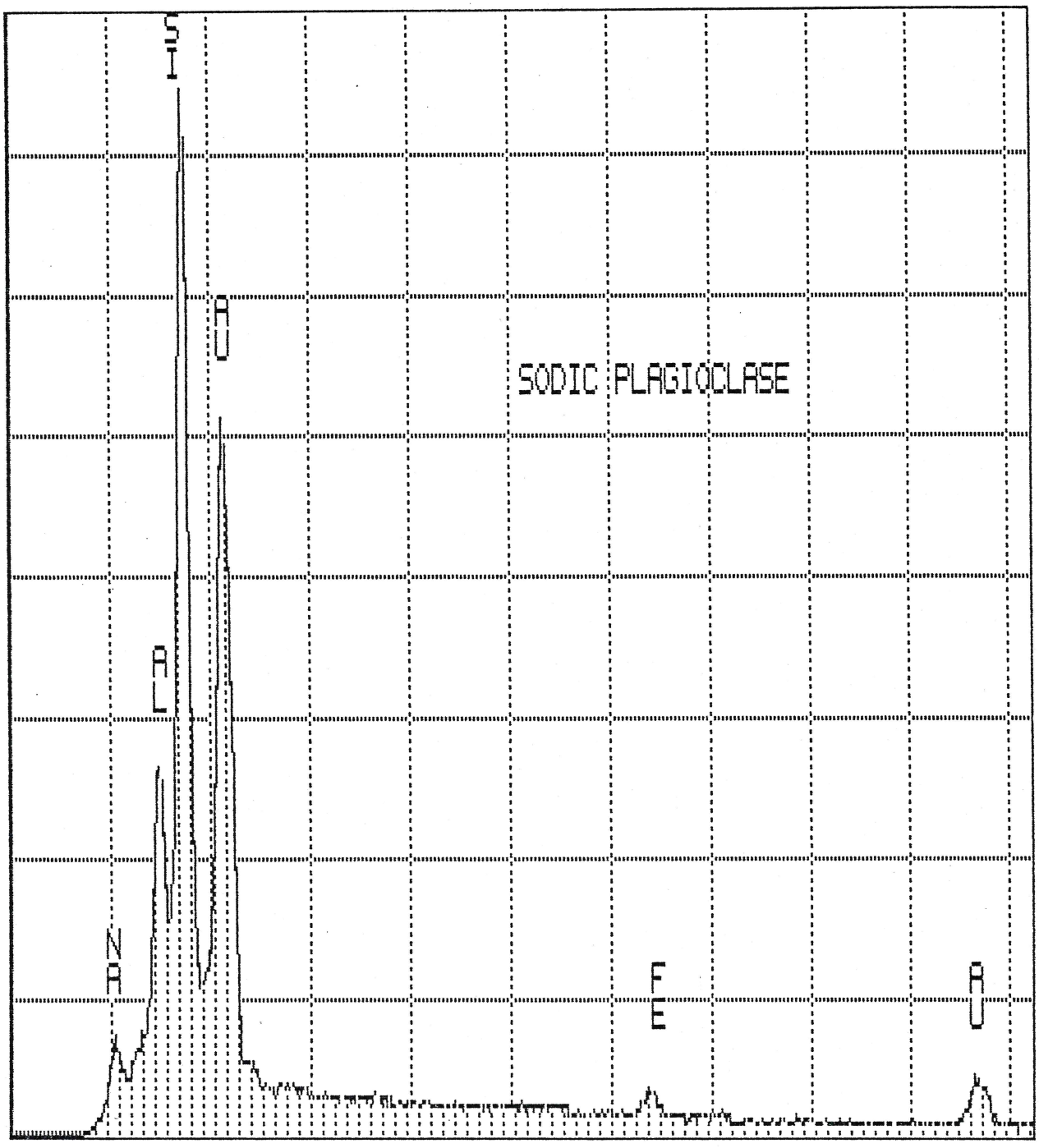

0.000 VFS = 2048 10.240

70 AMOCO PROD.; PD-85077; SAMPLE DEPTH: 7413 FT

Spectrum 9

TN-5400 Core Labs Aurora,CO. FRI 03-JAN-86 11:25

Cursor: 0.000keV = 0

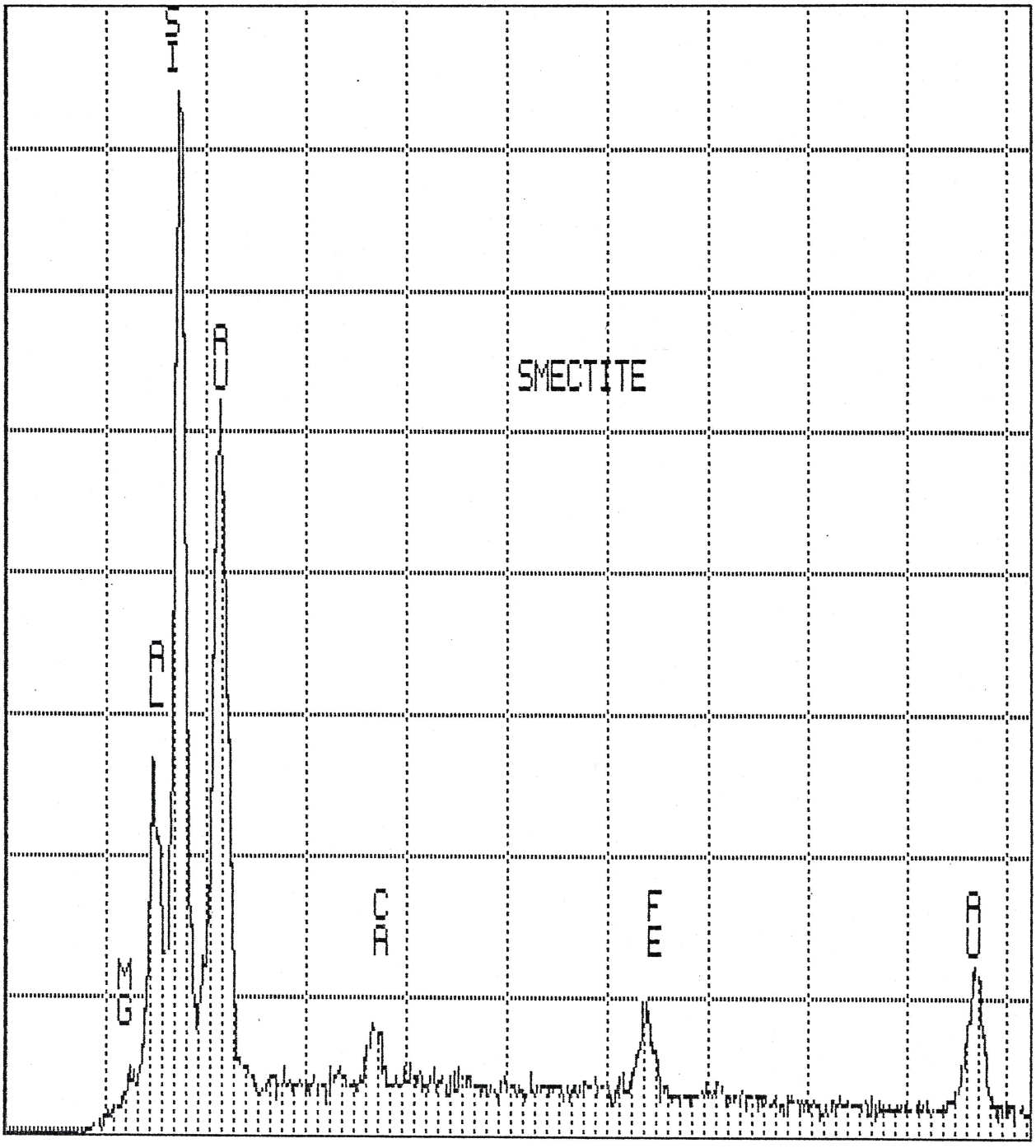

0.000 VFS = 512 10.240

40 AMOCO PROD.; PD-85077; SAMPLE DEPTH: 8051 FT

Spectrum 10

AMOCO PRODUCTION COMPANY
Nancy No. 1 O.C.S. Y-0719 Well

File Number: PD-85066
File Number: PD-85074
File Number: PD-85077

THIN SECTION PHOTOMICROGRAPH SCALES

At 20X magnification, the horizontal width of the photomicrograph represents 6.0 mm.

At 40X magnification, the horizontal width of the photomicrograph represents 3.0 mm.

At 160X magnification, the horizontal width of the photomicrograph represents 0.75 mm.

At 640X magnification, the horizontal width of the photomicrograph represents 0.19 mm.

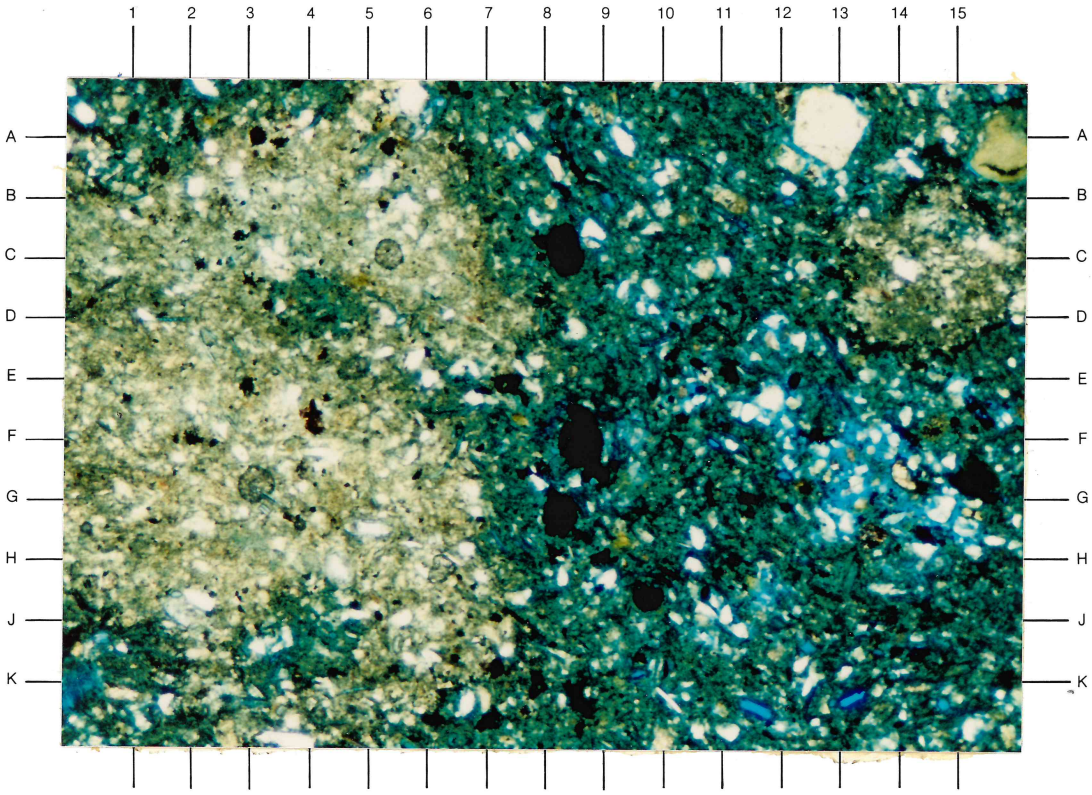

A

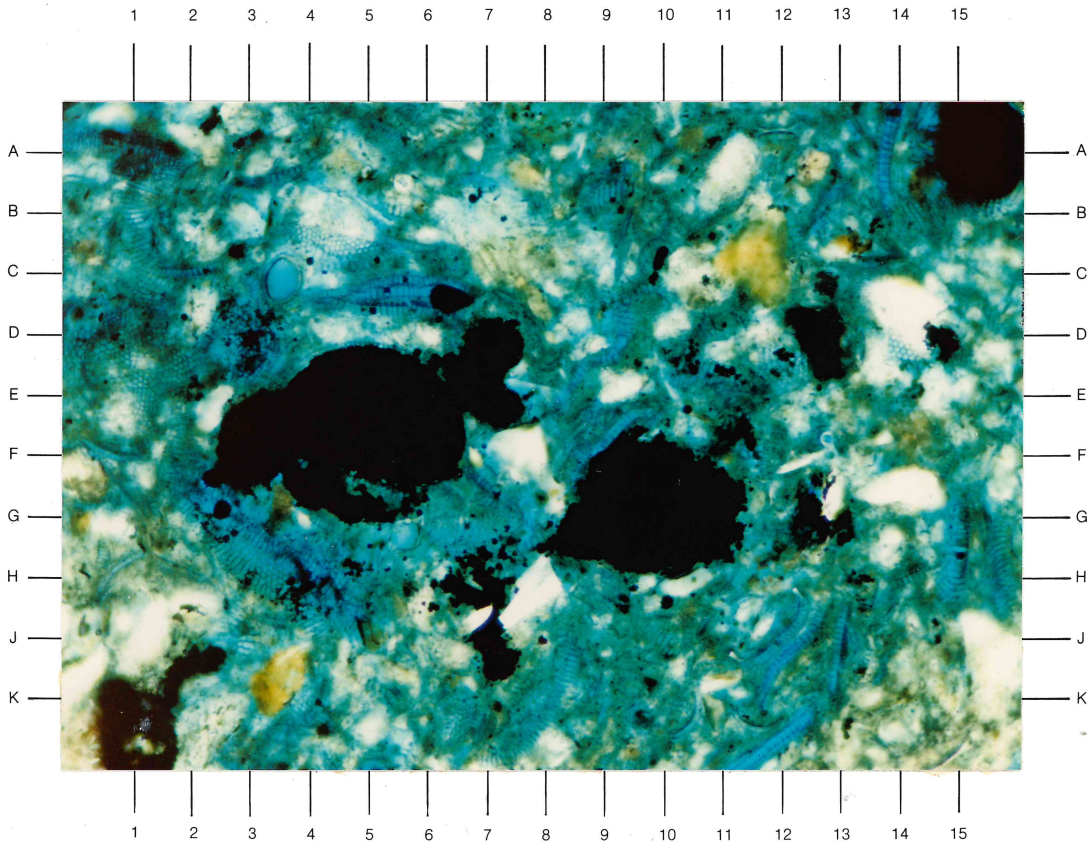

B

CORE LABORATORIES, INC.

Reservoir Geology/Petrographic Services

Amoco Production Company
Nancy No. 1 O.C.S. Y-0719 Well

File Number: PD-85066

Sample Depth: 2950 feet

Plate 24A

A 40X magnification, plane polarized light view of a moderately to poorly sorted, diatomaceous siltstone. Framework grains are composed of quartz, plagioclase (B15.5), mica, glauconite (C-D9-10), and volcanic rock fragments. Floating grains are very abundant. Pyrite has healed the margins of the regions of original (undisturbed) matrix (E2-5, A-B7-8). Note the large variance in grain size of the silt-rich region (lower left) as compared to the clay-rich regions of the rest of this view. The sample exhibits extreme bioturbation.

Plate 24B

A 160X magnification, plane polarized light photomicrograph of the region C-E8-11 of Plate 24A. Skeletal diatom fragments (E-F14-15, J1-2, C2), and detrital grains of plagioclase and glauconite (B11) are common in the clay matrix (green color). Authigenic aggregates of pyrite (black) are common. Intraskeletal microporosity forms the major percentage of the visible porosity in this sample.

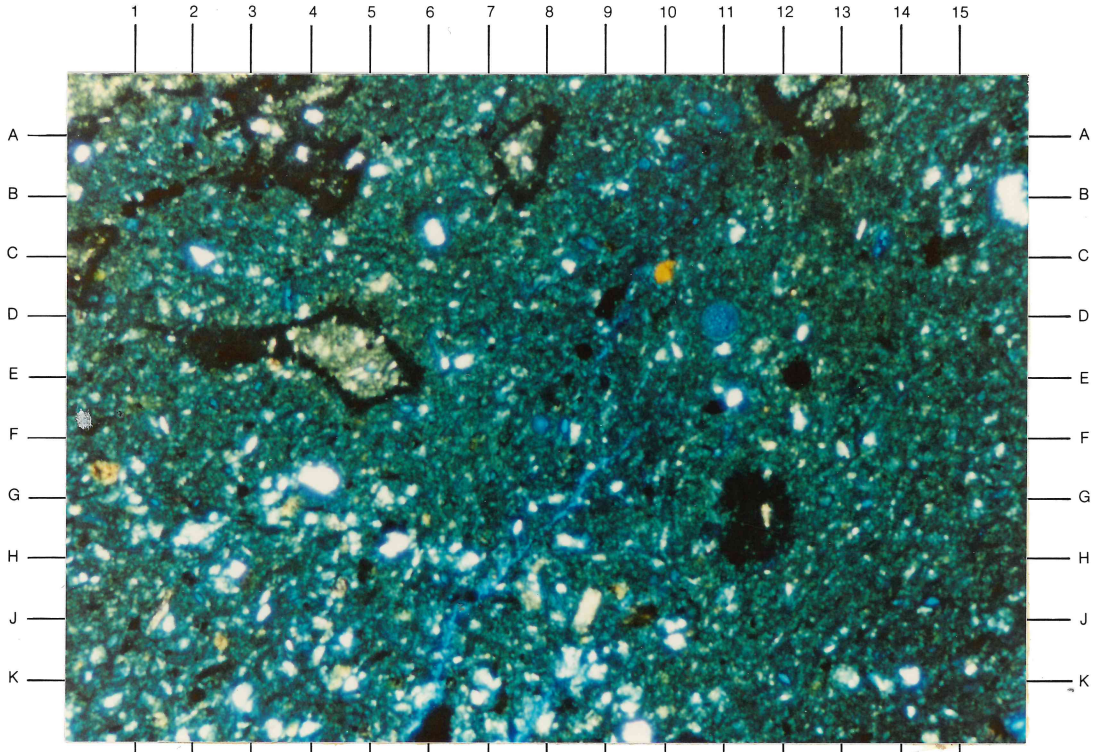

A

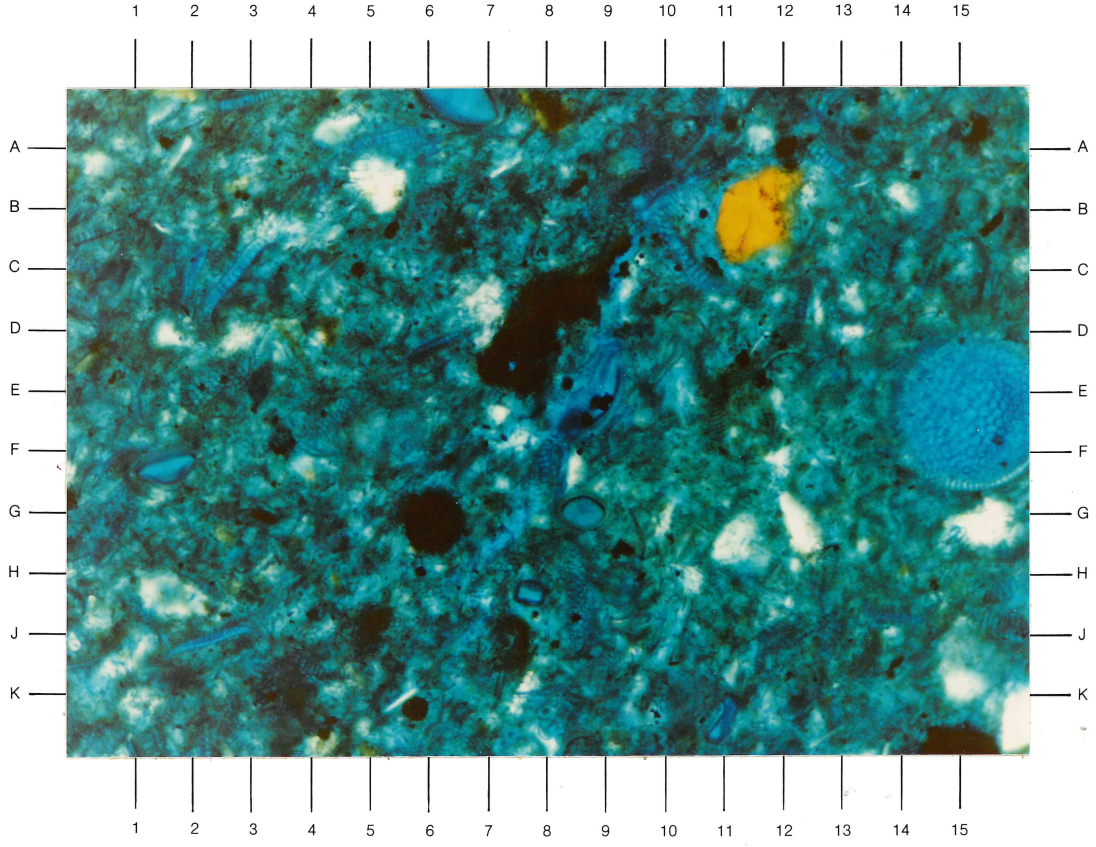

B

CORE LABORATORIES, INC.

Reservoir Geology/Petrographic Services

Amoco Production Company
Nancy No. 1 O.C.S. Y-0719 Well

File Number: PD-85066

Sample Depth: 3212 feet

Plate 25A

A 40X magnification, plane polarized light view of a poorly sorted, sandy diatomaceous siltstone. The majority of this view is heavily bioturbated. Framework grains of quartz, glauconite, plagioclase, mica, and diatom fragments float in a clay-rich matrix (green). The lighter colored region of the bottom right portion of this view is the original undisturbed matrix of the rock. Note that authigenic pyrite (black) has crystallized along the margins of these non-bioturbated regions.

Plate 25B

A 160X magnification, plane polarized light photomicrograph of an area (A-B9-12) from the bioturbated region of Plate 25A. Pennate (K5.5, C12) and centric (E9-10, A13, D3-4) diatom fragments are abundant. Glauconite (F-G14, H11), mica (G-H4), pyrite, plagioclase, and clay minerals form the remainder of this sample. A large, zoned plagioclase grain is visible at the bottom right corner of this view.

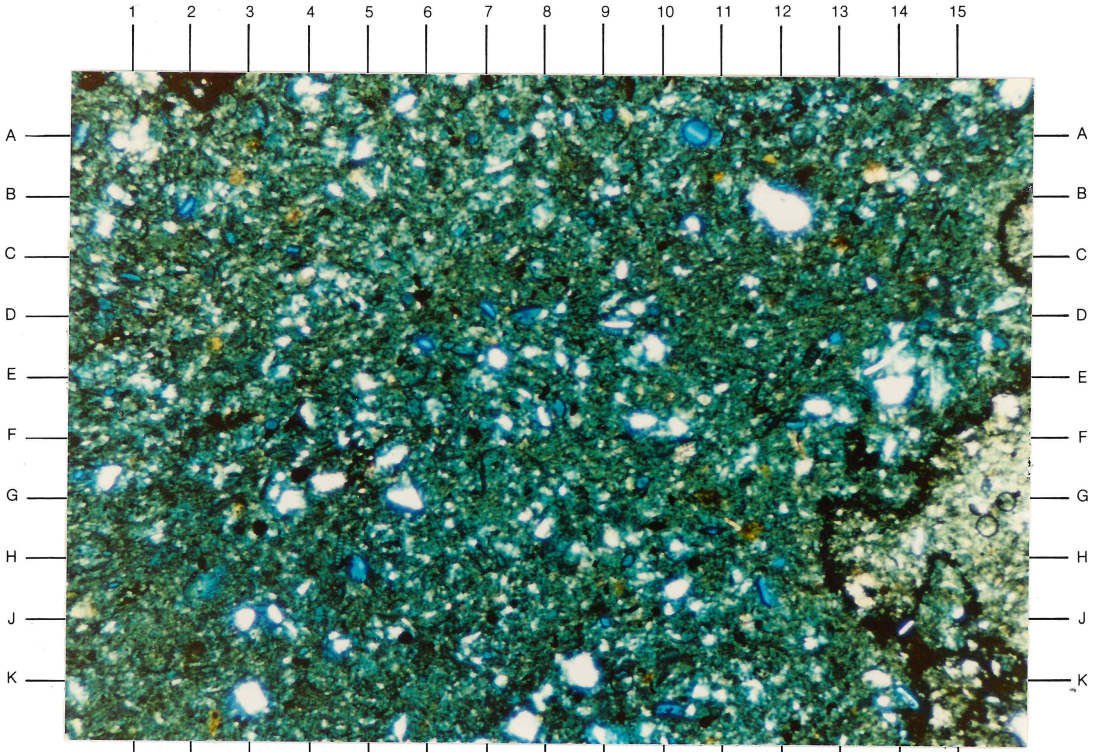
1 2 3 4 5 6 7 8 9 10 11 12 13 14 15
A B C D E F G H J K

A

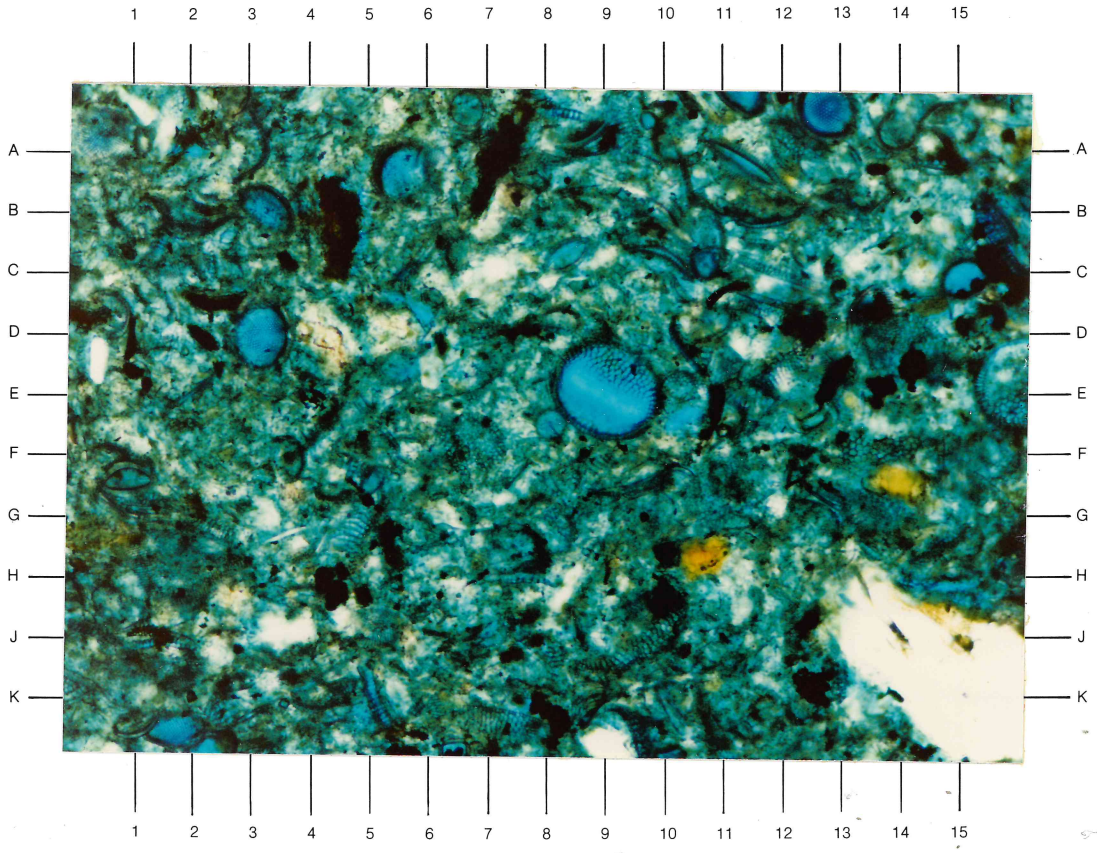
1 2 3 4 5 6 7 8 9 10 11 12 13 14 15
A B C D E F G H J K

B

Amoco Production Company
Nancy No. 1 O.C.S. Y-0719 Well

File Number: PD-85066

Sample Depth: 3742 feet

Plate 26A

A 40X magnification, plane polarized light view of a moderately sorted, bioturbated, diatomaceous siltstone. Framework grains are composed of plagioclase, quartz, diatom fragments, glauconite (G3-4), and volcanic rock fragments (B-C12-14, J10-11). Individual grains are angular to rounded and are free-floating in the matrix. Note the pyrite-rimmed, undisturbed region of this sample at the bottom right corner of this view.

Plate 26B

A 160X magnification, plane polarized light photomicrograph from E-H10-12 of Plate 26A. Most of the visible porosity occurs as intraskeletal microporosity in diatom fragments. Minor intragranular porosity has developed due to partial dissolution of plagioclase (B-C2, J3).

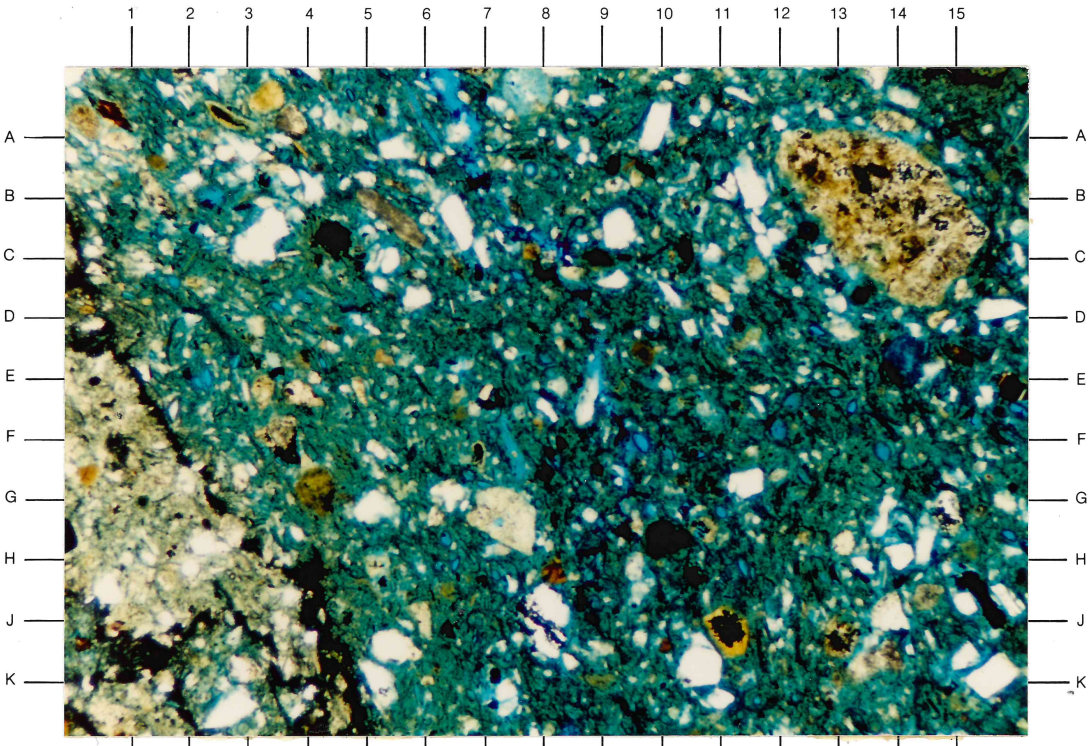
1 2 3 4 5 6 7 8 9 10 11 12 13 14 15
A B C D E F G H J K

A

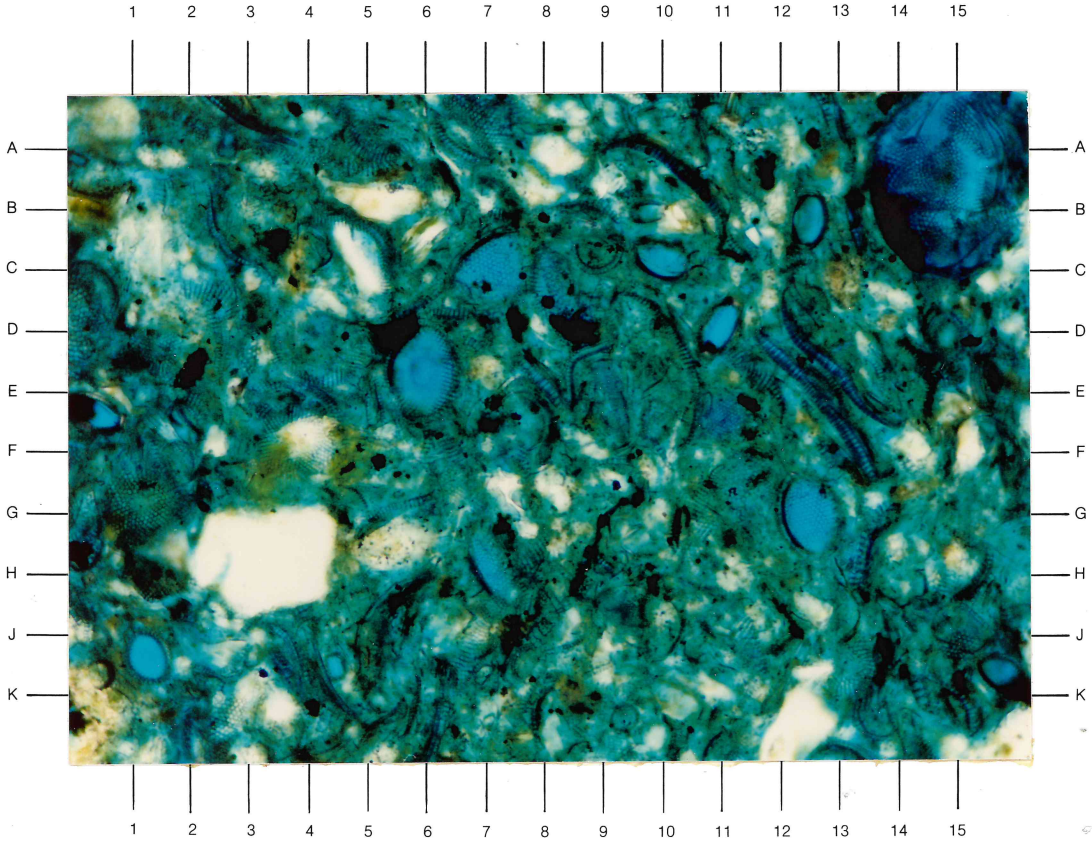
1 2 3 4 5 6 7 8 9 10 11 12 13 14 15
A B C D E F G H J K

B

Amoco Production Company
Nancy No. 1 O.C.S. Y-0719 Well

File Number: PD-85066

Sample Depth: 4104 feet

Plate 27A

A 40X magnification, plane polarized light view of a moderately to poorly sorted, diatomaceous siltstone. This view exhibits the general boundary between the bioturbated areas (center, green color) and the undisturbed regions of this sample (top and far right, lighter green to brown color). Frequently, pyrite (black) occurs along the margins of this contact. Quartz, plagioclase, rock fragments, glauconite (F4), and devitrified volcanic rock fragments (G3, K4.5) form the framework grain constituents.

Plate 27B

A 160X magnification, plane polarized light photomicrograph of the region F-H1-4.5 from Plate 27A. Plagioclase, devitrified volcanic glass (D8, F10-11), glauconite (A-B13-14), pyrite (black) and zircon (H3, D10) are featured in this view. Traces of intergranular porosity are visible locally (blue colored regions). Trace to minor intragranular porosity has developed due to dissolution of plagioclase (F3, G-H1.5, K15) and, possibly, of volcanic rock fragments.

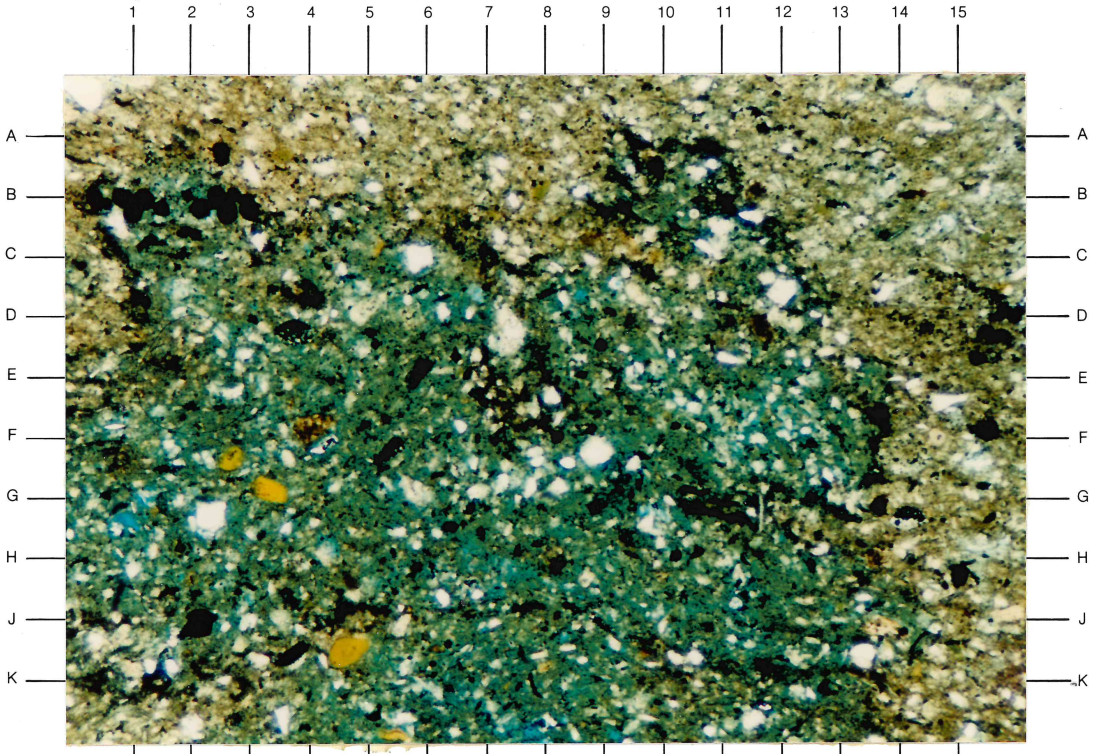
1 2 3 4 5 6 7 8 9 10 11 12 13 14 15
A B C D E F G H J K

A

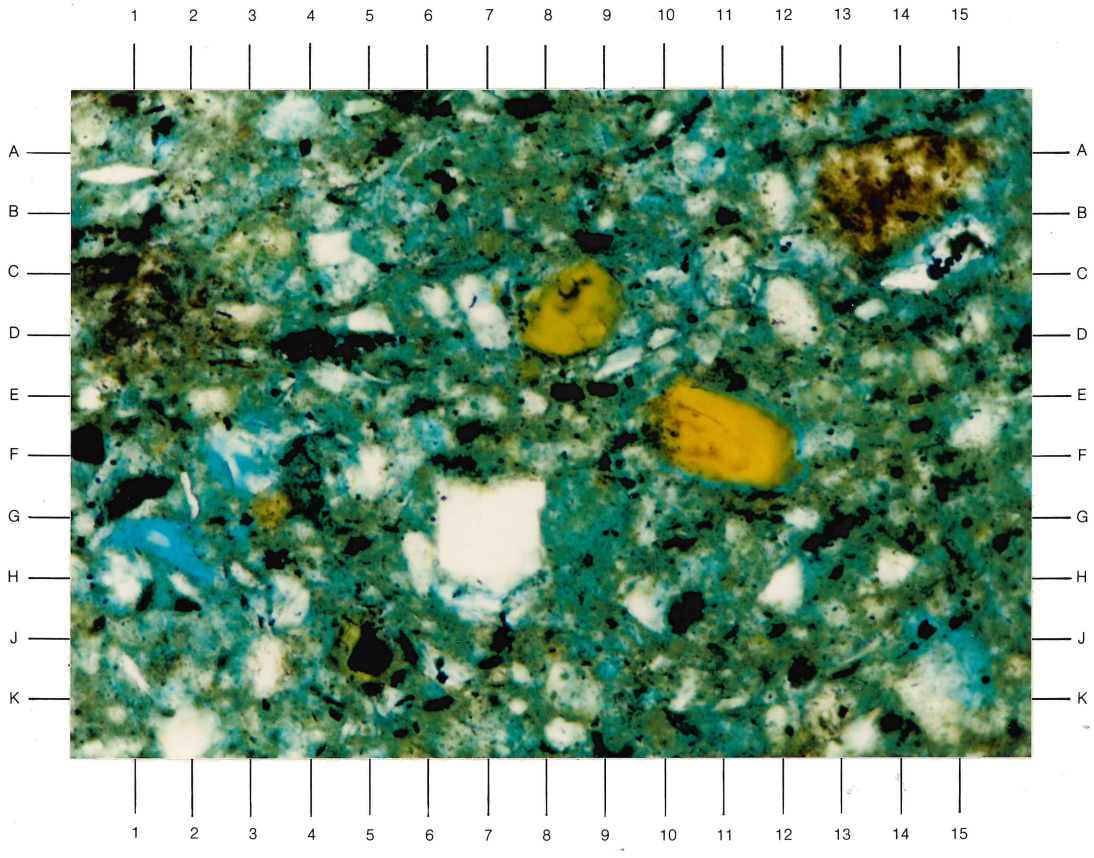
1 2 3 4 5 6 7 8 9 10 11 12 13 14 15
A B C D E F G H J K

B

Amoco Production Company
Nancy No. 1 O.C.S. Y-0719 Well

File Number: PD-85074

Sample Depth: 4232 feet

Plate 28A

A 20X magnification, plane polarized light view of a poorly to very poorly sorted, silty sandstone. Framework grains are composed of quartz, plagioclase, glauconite (F14, J-K5.5), and plutonic rock fragments (C-D14-15). This plutonic rock fragment is a granodiorite or quartz monzonite in composition. Large, angular to subrounded detrital grains are concentrated in the microporous, bioturbated regions of this sample.

Plate 28B

A 640X magnification, plane polarized light photomicrograph of an intragranular pore area in this sample. Authigenic zeolite has partially occluded a dissolution pore of a detrital plagioclase grain (center of view). Note that authigenic pyrite (black) and authigenic clay had crystallized in the dissolution pore prior to growth of the zeolite. Crystallization of zeolite was impeded by these constituents. Detrital grains of glauconite (center at D-E1) and quartz (center at C-D15), and a detrital volcanic rock fragment (top left center) surround the relict plagioclase grain at bottom center of this view.

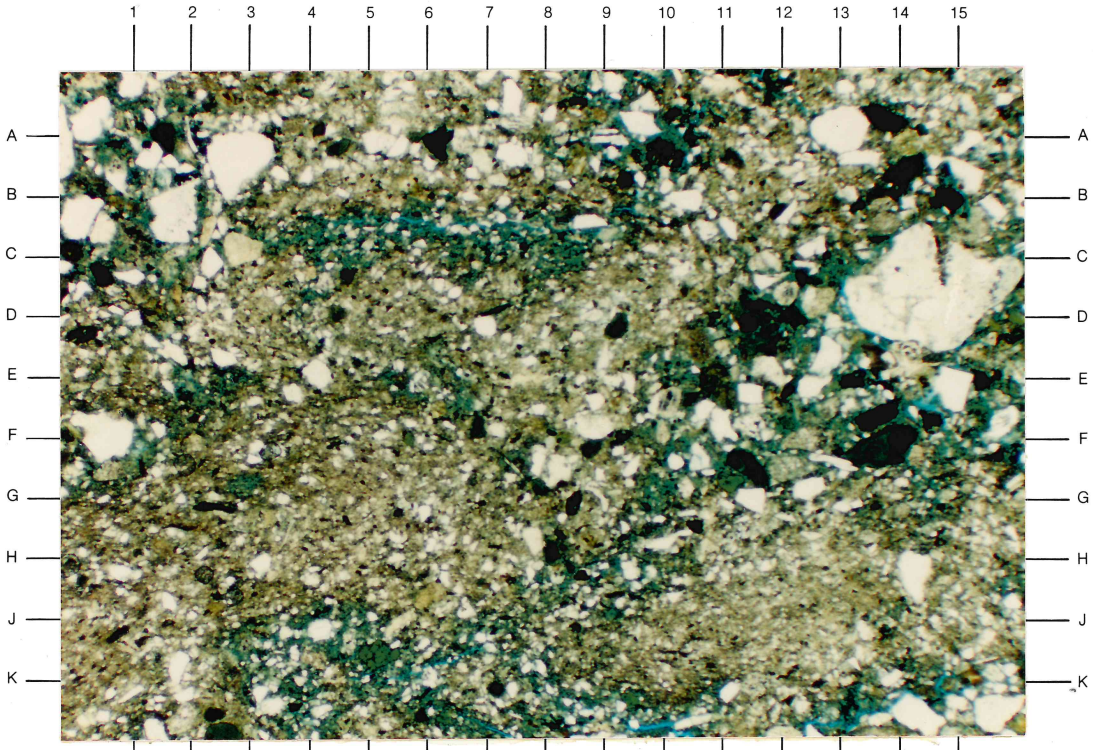

A

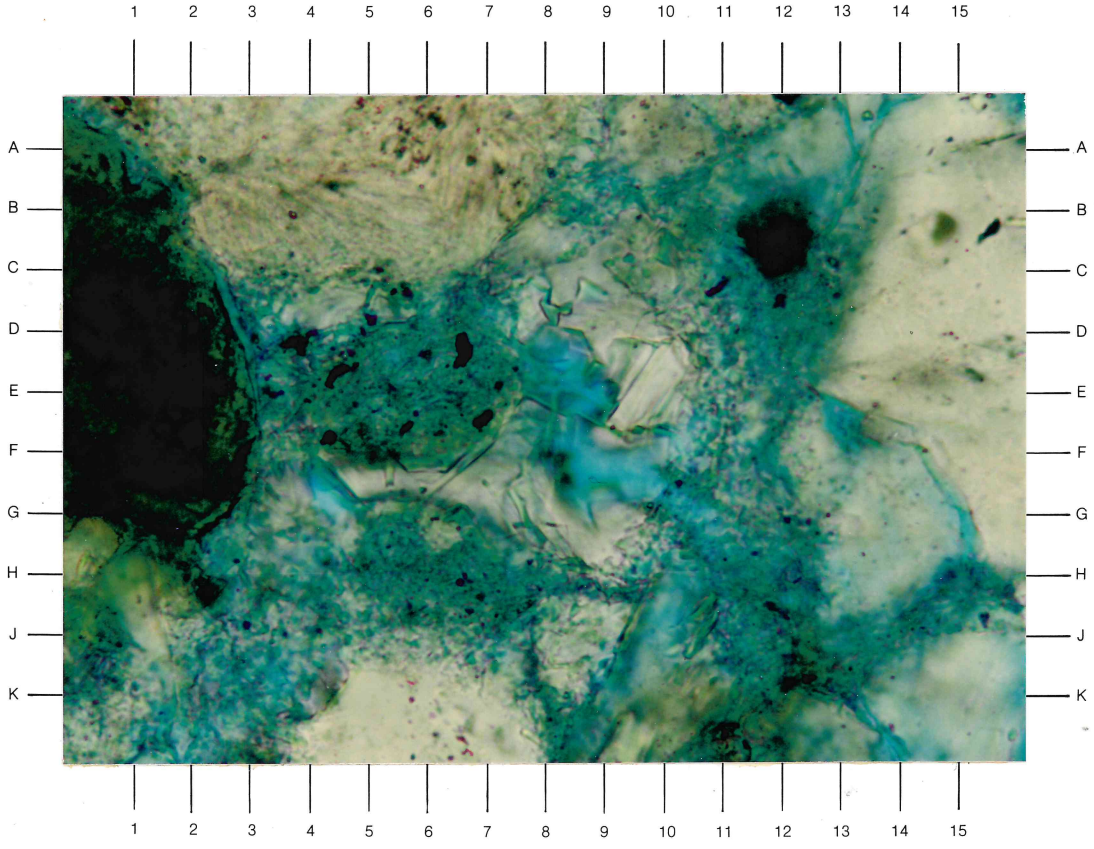

B

CORE LABORATORIES, INC.

Reservoir Geology/Petrographic Services

Amoco Production Company
Nancy No. 1 O.C.S. Y-0719 Well

File Number: PD-85074

Sample Depth: 5164 feet

Plate 29A

A 40X magnification, plane polarized light view of a poorly to moderately sorted, silty sandstone. Note the textural change from a laminar silty claystone to a massive sandy siltstone (from bottom to top of view). The coarser, more porous zones have undergone some bioturbation. Some laminae of the lower portion of the view have been filled with discontinuous stringers of pyrite. Note the large, detrital plagioclase grains of this view (D-E6-7, A9).

Plate 29B

A 160X magnification, plane polarized light photomicrograph of a silty sandstone. Framework grains are composed of quartz, plagioclase (E-F1-2, H9), hornblende (A14-15), glauconite (D15, E12.8, K1), plutonic rock fragments (B14), and muscovite (H7, E1-2, C10). Grains are angular to rounded, and intergranular pore regions are filled with clay minerals and pyrite.

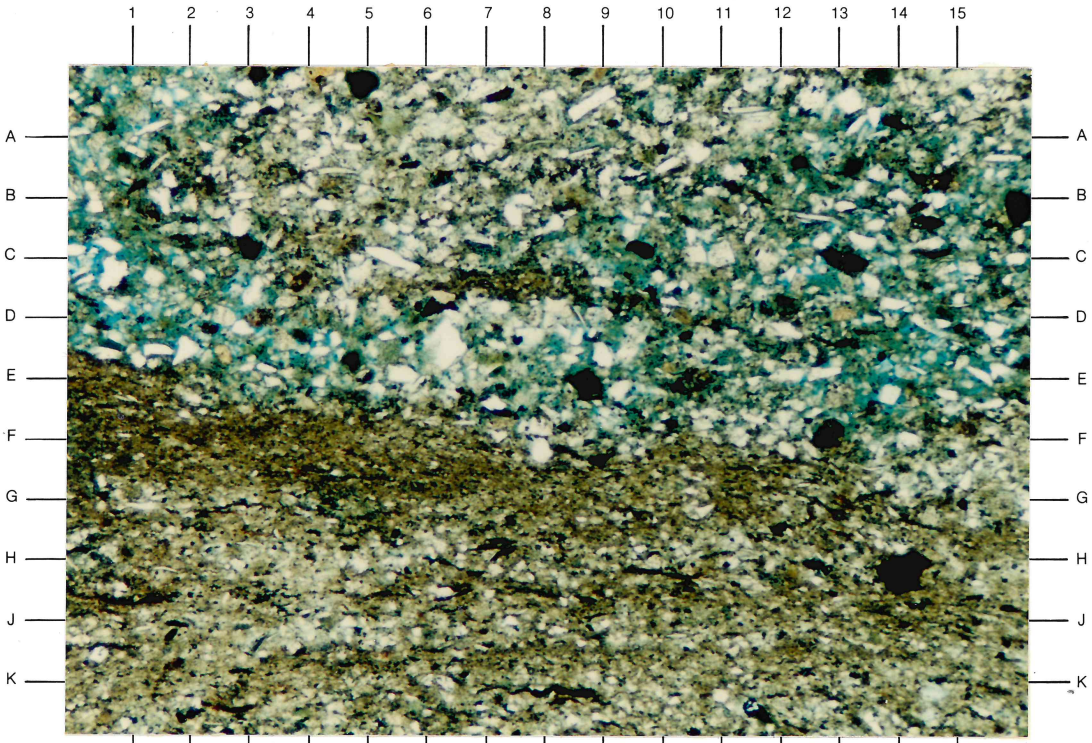

A

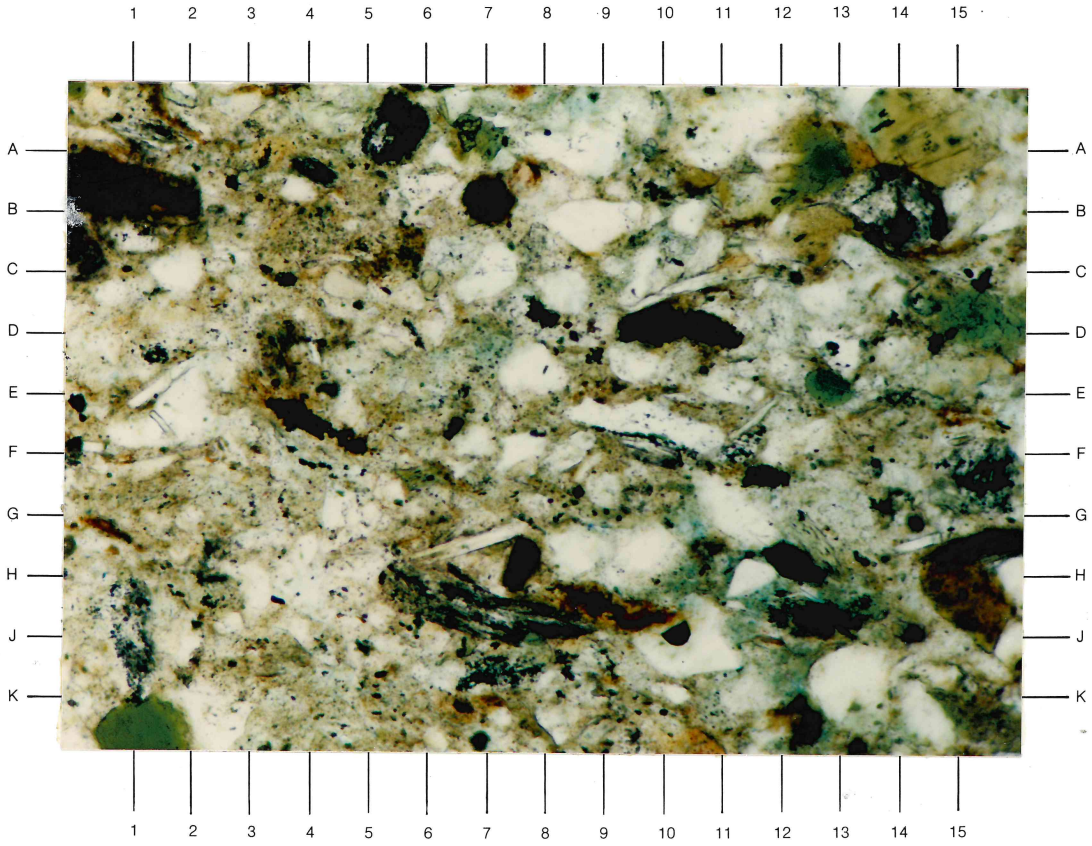

B

CORE LABORATORIES, INC.

Reservoir Geology/Petrographic Services

Amoco Production Company
Nancy No. 1 O.C.S. Y-0719 Well

File Number: PD-85074

Sample Depth: 6652 feet

Plate 30A

A 20X magnification, plane polarized light view of a poorly to moderately sorted, silty sandstone. Note the healed horizontal fracture system at C1-12 of this view. Truncated angular layering is apparent in the upper right corner of this view. Some of the lensoidal sand-rich regions of this sample exhibit indistinct size grading of framework grains (e.g. D-J 1-7).

Plate 30B

A 160X magnification, plane polarized light photomicrograph of a poorly to moderately sorted, sandy siltstone. Framework grains are composed of quartz (B-D12-14), plagioclase, glauconite (E-F3-5, K11), muscovite (A-B2), and volcanic rock fragments (A2-3, B-C6-7). The volcanic rock fragment at A2-3 is a pyritized crystal tuff, and the grain at B-C 6-7 is a porphyritic dacite or rhyodacite. Zircon is present at D-E1, D-E2, and B-11. Intergranular porosity is occluded by clay minerals and pyrite. Some secondary intragranular porosity is caused by dissolution of plagioclase (F2-3, F-G6-7).

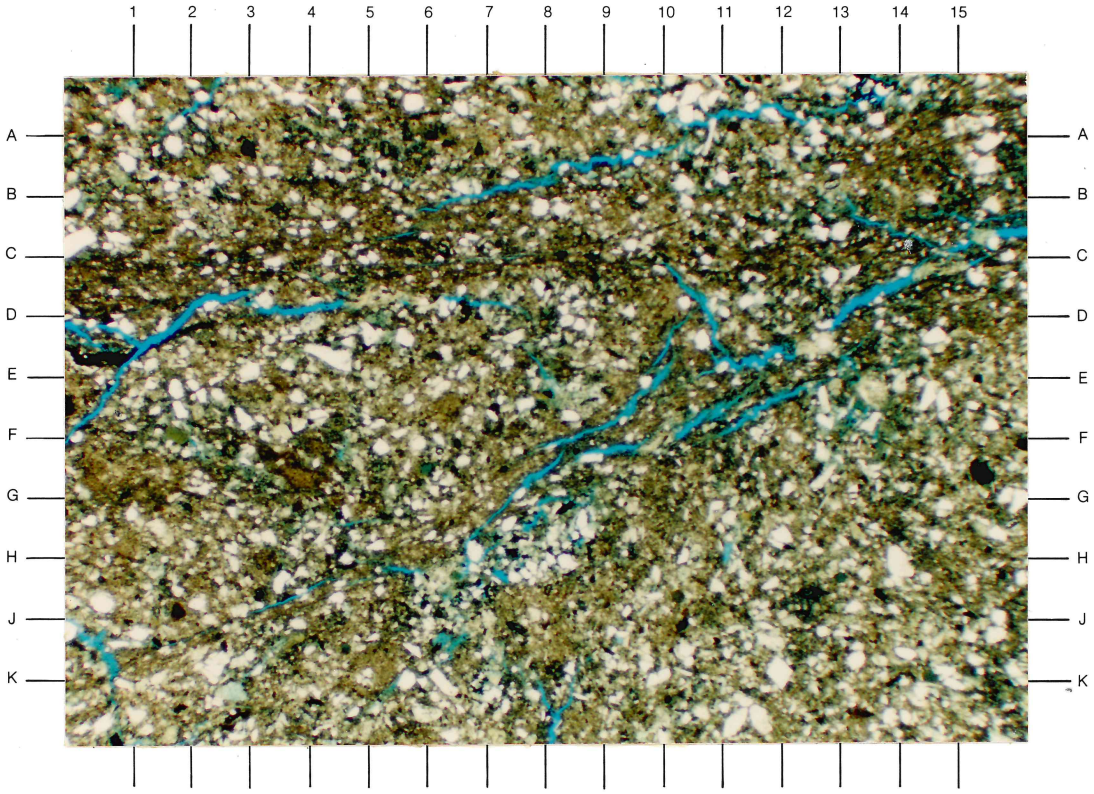

A

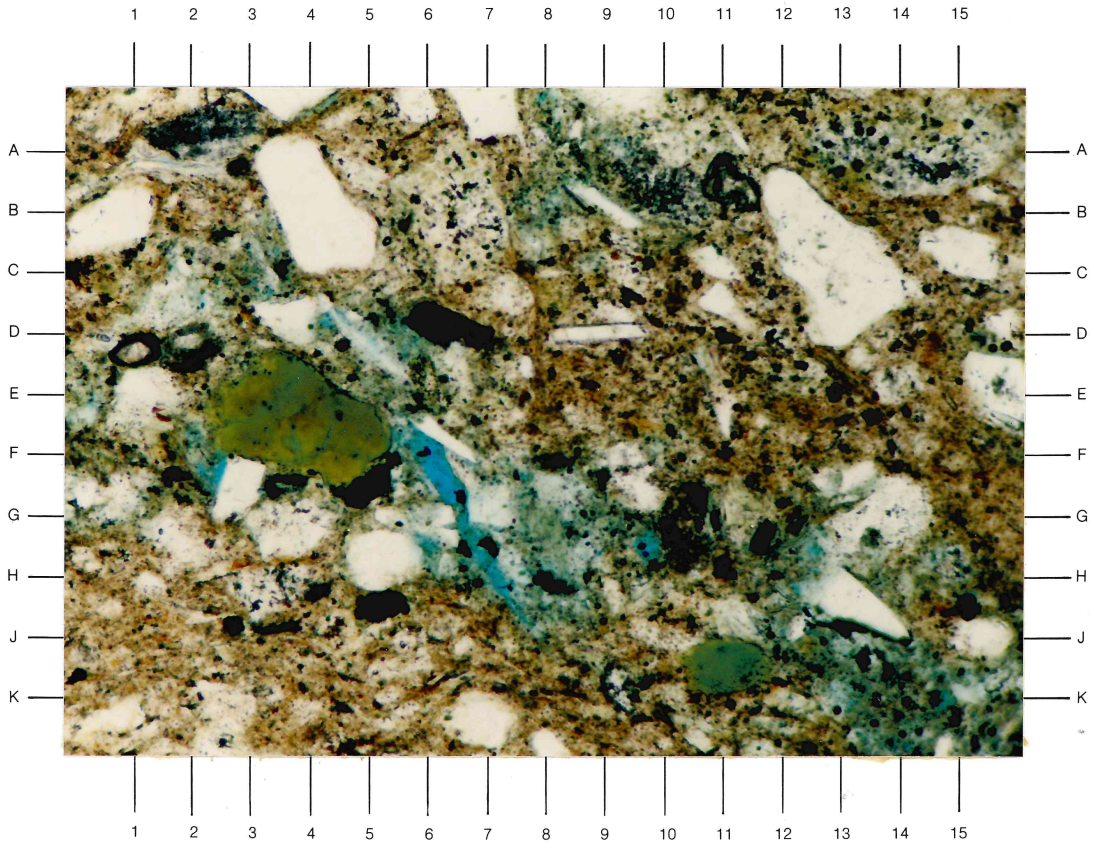

B

CORE LABORATORIES, INC.

Reservoir Geology/Petrographic Services

Amoco Production Company **File Number: PD-85077**
Nancy No. 1 O.C.S. Y-0719 Well

Sample Depth: 7229 feet

Plate 31A

A 40X magnification, plane polarized light view of a poorly sorted, volcaniclastic sandy siltstone. This view exhibits the diversity of grain sizes and lithologies that are present in adjacent regions of this sample. The bottom half of this view is a plagioclase-rich, clayey siltstone. The top half of the view is a volcanic rock fragment-rich, coarse- to very coarse-grained sandstone. Volcanic rock fragments consist of: porphyritic andesite with a pyrite-replaced groundmass (A-D4-9); chert-replaced crystal tuff (A-C1-4); pyrite-replaced crystal tuff (D-E1-2); and a clay-altered and pyrite-replaced, porphyritic dacite or rhyodacite (B-D10-13).

Plate 31B

A 160X magnification, plane polarized light photomicrograph of a sandstone fragment that occurs in a poorly sorted, volcaniclastic sandy siltstone. Authigenic clay alteration and pyrite replacement of plagioclase is apparent in this strain-recrystallized (mosaic intergrowth) sandstone fragment. Some intergranular porosity is developed due to partial dissolution of the plagioclase grains (E-F3-5, C13-14). Glauconite is present at A3-4 of this view.

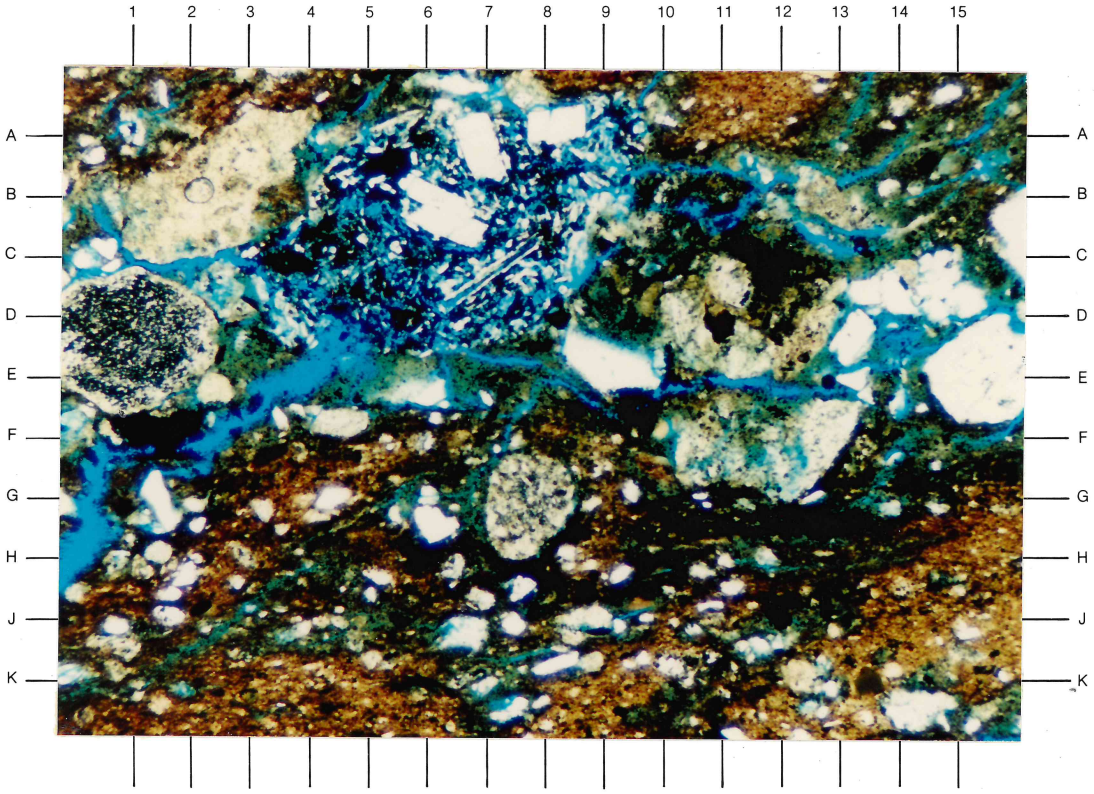
1 2 3 4 5 6 7 8 9 10 11 12 13 14 15
A B C D E F G H J K

A

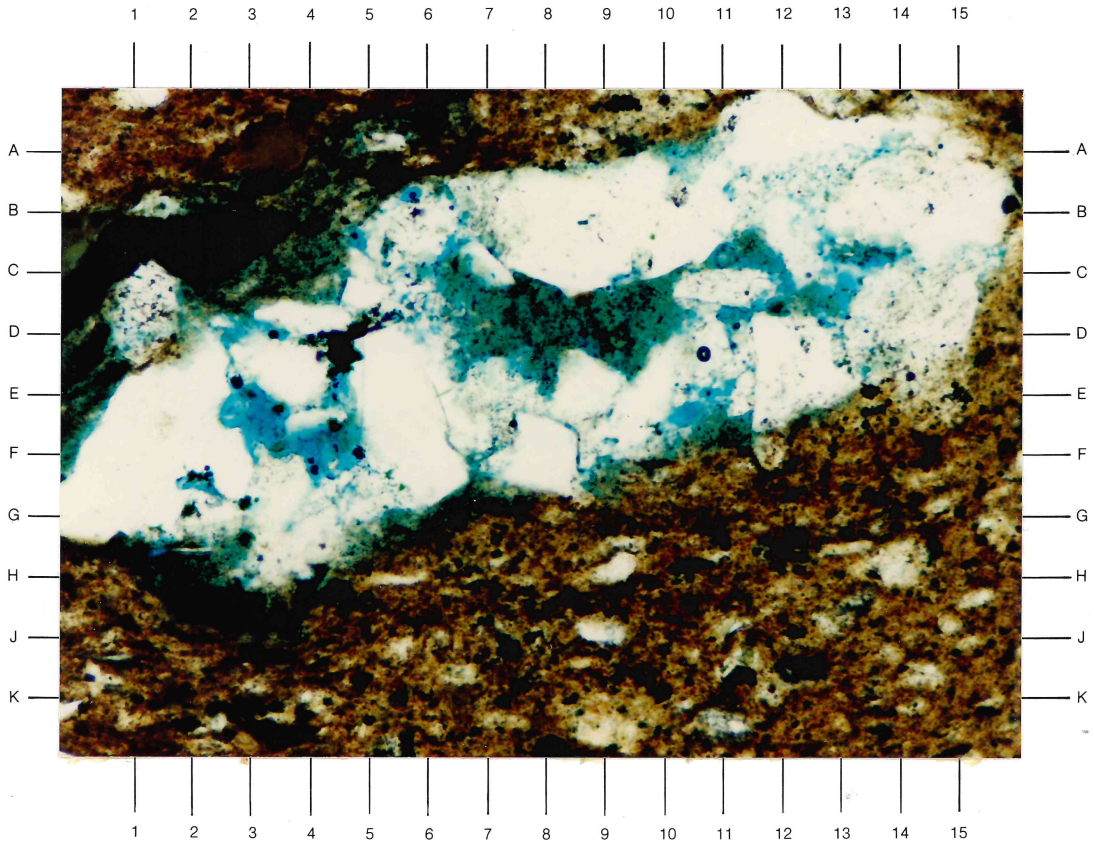
1 2 3 4 5 6 7 8 9 10 11 12 13 14 15
A B C D E F G H J K

B

Amoco Production Company
Nancy No. 1 O.C.S. Y-0719 Well

File Number: PD-85077

Sample Depth: 7413 feet

Plate 32A

A 40X magnification, plane polarized light view of a very poorly sorted, volcaniclastic sandstone. This view highlights the coarse-grained nature of the volcanic rock fragments and the broad range of lithotypes that occur in this sample. The volcanic rock fragments are composed of: porphyritic dacite/rhyodacite (B-E9-11), microlitic to porphyritic dacite/rhyodacite (E-K3-10), porphyritic andesite (J-K12-15), andesitic lithic tuff (F-H11-13), rhyolitic crystal tuff (A-C13-15; A-B10), and a plutonic rock fragment of granodiorite/quartz monzonite composition. Partial dissolution of the groundmass in these rock fragments caused minor development of intragranular porosity. Intragranular porosity is well developed in the dissolved plagioclase grain at A-D4-6. Pore-lining and pore-filling authigenic chlorite (green) is evident at the top right portion of this view.

Plate 32B

A 160X magnification, plane polarized light photomicrograph of the region E-H 9.5-12 of Plate 32A (rotated 90° to the left). This view shows the vermiform texture of authigenic chlorite in this intergranular pore region (green colored mineral at center of view). The andesitic lithic tuff (bottom) and the porphyritic dacite/rhyodacite (right margin) fragments have undergone partial dissolution, which has formed intragranular porosity. These pore regions are partially replaced by authigenic clay minerals and pyrite. Zircon is present in the intergranular pore region at C-D12 of this view.

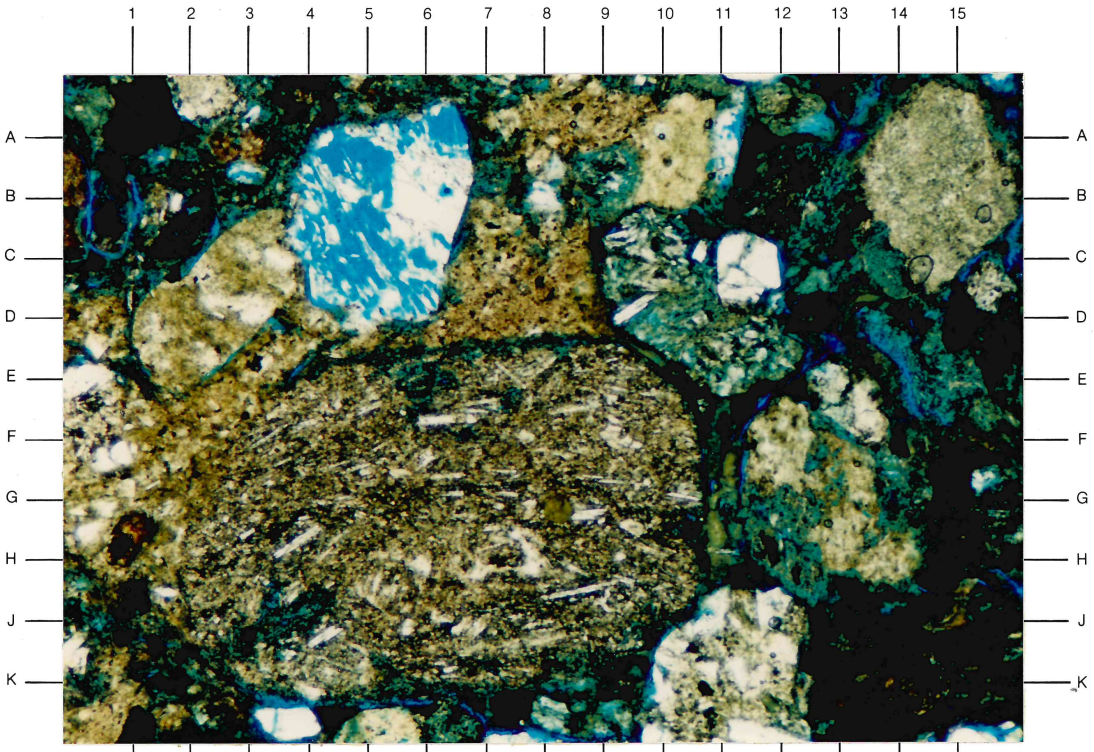

A

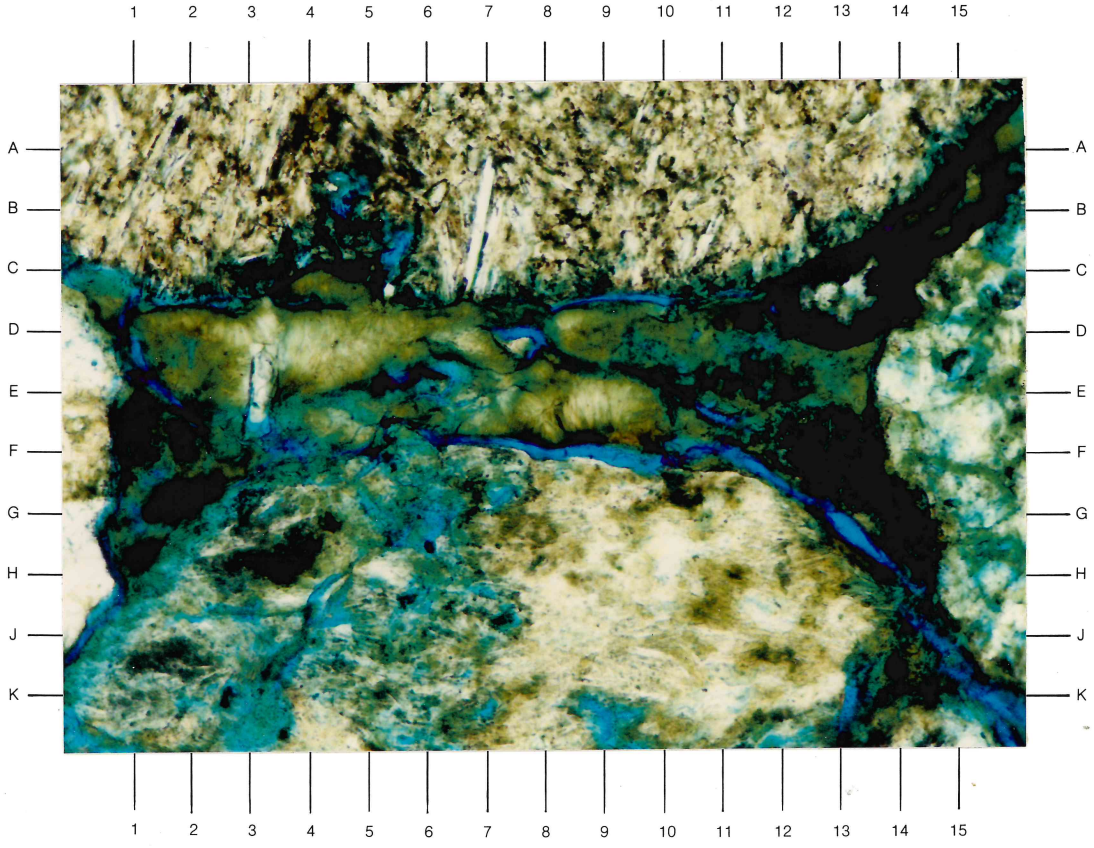

B

CORE LABORATORIES, INC.

Reservoir Geology/Petrographic Services

Amoco Production Company
Nancy No. 1 O.C.S. Y-0719 Well

File Number: PD-85077

Sample Depth: 8051 feet

Plate 33A

A 40X magnification, plane polarized light view of a very poorly sorted, volcaniclastic sandstone. Framework grains are composed of quartz (E8), plagioclase (white), and volcanic rock fragments. The rock fragments at E-10, E-8, and D-7 are contorted due to plastic deformation during grain compaction. These rock fragments form pseudomatrix at this location. Healed fractures are visible at A1-13 (horizontal) and in the lower left portion of the view (oriented at 45 degrees). Intragranular porosity, from partial dissolution of plagioclase and rock fragments, is present at F3 and G1-2 of this view.

Plate 33B

A 160X magnification, plane polarized light photomicrograph of the region from C-E-11 of Plate 32A. The orange- and brown-colored, elongate and contorted grains are composed of tuffaceous and clay-replaced volcanic rock fragments, and biotite. These lithic fragments form pseudomatrix at this location. Other prominent grains are plagioclase (white), quartz (J3), and microlitic dacite/rhyodacite volcanic rock fragments (F-H11-15). Clay minerals occlude intergranular porosity of this view.

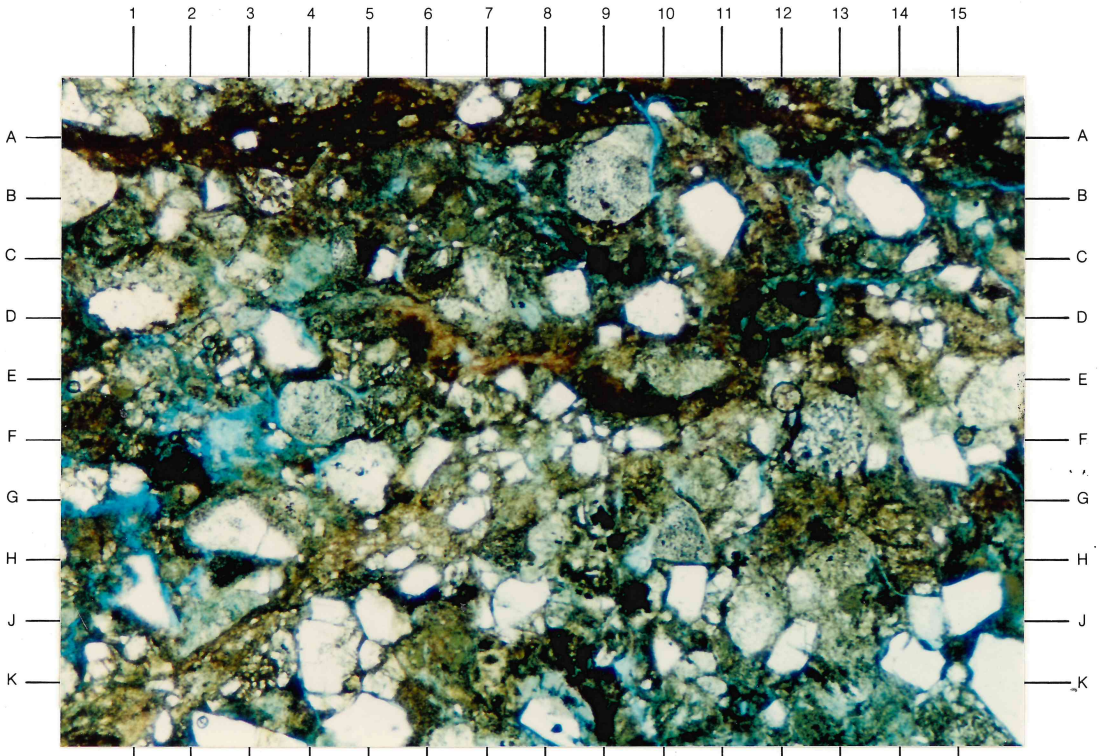

A

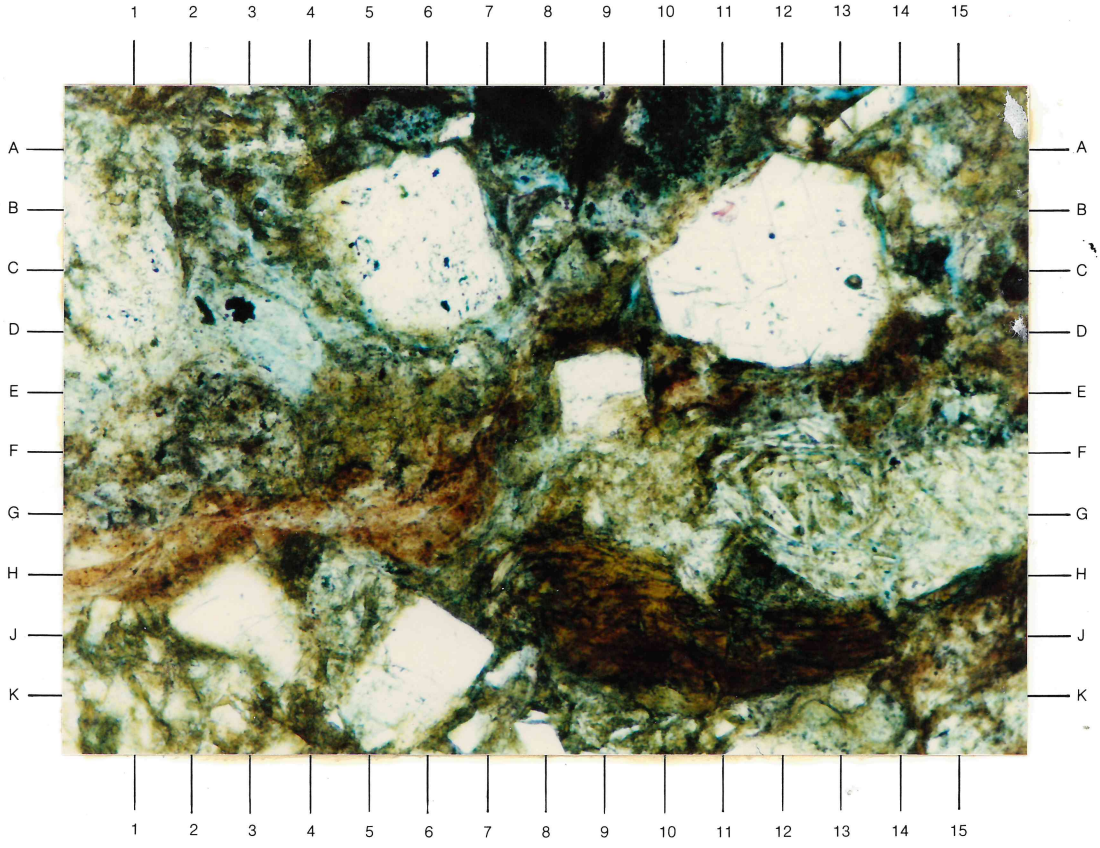

B

CORE LABORATORIES, INC.

Reservoir Geology/Petrographic Services